

# The Electronic Nature of High Temperature Cuprate Superconductors

M. R. Norman<sup>1,2</sup> and C. Pépin<sup>2</sup>

<sup>1</sup>Materials Science Division, Argonne National Laboratory, Argonne, IL 60439, USA

<sup>2</sup>SPhT, L'Orme des Merisiers, CEA-Saclay, 91191 Gif-sur-Yvette, France

E-mail: norman@anl.gov

**Abstract.** We review the field of high temperature cuprate superconductors, with an emphasis on the nature of their electronic properties. After a general overview of experiment and theory, we concentrate on recent results obtained by angle resolved photoemission, inelastic neutron scattering, and optical conductivity, along with various proposed explanations for these results. We conclude by reviewing efforts which attempt to identify the energy savings involved in the formation of the superconducting ground state.

PACS numbers: 74.25.-q, 74.25.Jb, 74.72.-h

Submitted to: *Rep. Prog. Phys.*

**Electronic Nature of HTSC**

<b>1</b>	<b>General Overview</b>	<b>2</b>
1.1	History . . . . .	2
1.2	Crystal Symmetry and Electronic Structure . . . . .	5
1.3	Phase Diagram . . . . .	7
1.4	Inhomogeneities . . . . .	15
1.5	Electron Doped Materials . . . . .	17
<b>2</b>	<b>Theory</b>	<b>18</b>
2.1	BCS . . . . .	18
2.2	Spin Fluctuation Models . . . . .	20
2.3	RVB . . . . .	22
2.4	Marginal Fermi Liquid . . . . .	25
2.5	SO(5) . . . . .	26
2.6	Stripes . . . . .	28
2.7	Pseudogap . . . . .	29
<b>3</b>	<b>Photoemission</b>	<b>31</b>
3.1	General Principles . . . . .	31
3.2	Normal State . . . . .	34
3.3	Superconducting State . . . . .	37
3.4	Pseudogap Phase . . . . .	45
<b>4</b>	<b>Inelastic Neutron Scattering</b>	<b>50</b>
4.1	LSCO . . . . .	51
4.2	YBCO . . . . .	53
<b>5</b>	<b>Optical Conductivity</b>	<b>58</b>
<b>6</b>	<b>Condensation Energy</b>	<b>61</b>
6.1	Optics . . . . .	63
6.2	ARPES . . . . .	67

**1. General Overview***1.1. History*

As with all endeavors in science, there is a prehistory involved, and cuprates are no exception. Research in superconductivity was not the languishing field that it is often portrayed as being prior to the Bednorz-Muller “revolution” of 1986. What had begun to be diminished, though, was the hope that a truly high temperature superconductor would ever be discovered. At the time of the Bednorz-Muller discovery, the highest temperature superconductor known was Nb<sub>3</sub>Ge (23K). That material had been known

since 1973, and was not much of an improvement over NbN (15K) which had been discovered all the way back in 1941 [1]. This pessimistic outlook was best articulated by Bernd Matthias in a number of papers which still make interesting reading today [2]. Such pessimism was not confined to experiment, as witnessed by the famous paper of Cohen and Anderson [3]. As was well appreciated by that time, the A15 materials with highest  $T_c$  were on the verge of a structural transition, and thus it was anticipated that one could not push  $T_c$  much higher before the lattice became unstable [4].

Despite this, a number of new classes of superconductors had been discovered in the period before 1986, including the ternary magnetic superconductors such as  $\text{ErRh}_4\text{B}_4$  and  $\text{HoMo}_6\text{S}_8$ , and various uranium based superconductors such as  $\alpha\text{-U}$  and  $\text{U}_6\text{Fe}$ , many of these discovered by Matthias and his various associates. Matthias' speculation that something really different was going on in f electron superconductors was spectacularly confirmed with the discovery by Frank Steglich in 1979 of "heavy fermion" superconductivity in  $\text{CeCu}_2\text{Si}_2$  [5], followed by the discovery of superconductivity in  $\text{UPt}_3$  and  $\text{UBe}_{13}$  [6].

Heavy fermion superconductivity was one of the main research topics in fundamental physics prior to 1986, and its history has had some impact on the cuprate field. Unlike the magnetic superconductors such as  $\text{ErRh}_4\text{B}_4$  where the magnetic moments are confined to the rare earth site and the superconductivity to the ligand sites, in heavy fermion superconductors, the f electrons themselves become superconducting. This is known from the extremely high effective mass of the superconducting carriers. More properly, the carriers should be thought of as composite objects of conduction electron charge and f electron spin [7]. The fascinating thing about these materials, though, is that their superconducting ground states do not appear to have the  $L=0$ ,  $S=0$  symmetry that Cooper pairs exhibit in normal superconductors [8, 9].

As with cuprates, heavy fermion superconductivity had its own prehistory as well, that being the field of superfluid  $^3\text{He}$ .  $^3\text{He}$  had been speculated in the 1960s to possibly be a paired superfluid with non-zero orbital angular momentum, in particular  $L=2$  pairing [10]. The idea was that the hard core repulsion of the atoms would prevent  $L=0$  pairing, but that longer range pairs could be stabilized by the attractive van der Waals interaction between the He atoms. Subsequently, Layzer and Fay [11] showed that for nearly ferromagnetic metals, and  $^3\text{He}$  as well, spin dependent interactions instead could stabilize  $L=1$ ,  $S=1$  pairs, leading to the concept of paramagnon mediated pairing.

At that time, experimentalists were beginning to push  $^3\text{He}$  to low temperatures, with the idea of searching for magnetic order under pressure. This was subsequently discovered by Bill Halperin. But along the way, Doug Osheroff found superfluidity, and various experiments did indeed confirm the  $L=1$ ,  $S=1$  nature of the pairs [12]. More interestingly, two paired states were found, the so-called A and B phases. Anderson and Brinkman later proposed that the stabilization of the anisotropic A phase relative to the isotropic B phase could be understood by feedback of the pair formation on the spin fluctuation interactions which supposedly gave rise to the pairs to begin with [13]. Such feedback effects are much in vogue lately in regards to spin fluctuation mediated

theories of cuprates [14].

What does this imply for the lattice case? Early theories for heavy fermions were indeed based on the  $^3\text{He}$  paradigm, but with the discovery of antiferromagnetic correlations by inelastic neutron scattering [15], people turned away from these nearly ferromagnetic models (though they have seen a resurgence of late, with the discovery of superconductivity in  $\text{UGe}_2$  [16] and  $\text{ZrZn}_2$  [17]). Rather, theoretical work published in 1986 led to the concept of  $L=2, S=0$  pairs in the nearly antiferromagnetic case [18]. This d-wave model is still one of the leading candidates to describe superconductivity in  $\text{UPt}_3$ , though a competing model based on f-wave pairs has been proposed by Norman [19] and Sauls [20]. The problems with determining the pair symmetry in heavy fermions are the multiple band nature of the problem (orbital degeneracy), along with the effects of non-trivial crystal structures ( $\text{UPt}_3$  has a non symmorphic lattice, for instance) and spin-orbit (which destroys  $L$  and  $S$  as good quantum numbers), not to mention the complications of dealing with three dimensions. (Fortunately none of these problems exist in the cuprates.) One of the interesting observations of these early calculations was the prediction that for a simple cubic lattice, the d-wave pairs should be of the form  $(x^2 - y^2) \pm i(3z^2 - r^2)$  [18]. If one simply eliminates the third dimension, one obtains the order parameter now known to be the pair state of the cuprates. In some sense, the prediction of  $d_{x^2-y^2}$  pairing in the cuprates was the ultimate one liner.

The above path, though, is not what led to the discovery of cuprate superconductors. The history of this is rather lucidly described in Bednorz and Muller's Nobel lecture [21]. Of particular interest to them was the case of doped  $\text{SrTiO}_3$ . This material had a  $T_c$  of less than 1K, but as it had such an incredibly low carrier density, it shouldn't have been superconducting at all, at least according to what people thought at the time. In fact, the properties of this material led to a speculation by Eagles about the possibility of Bose condensation [22], with pairs existing above the superconducting transition temperature, a forerunner of the pseudogap physics currently being discussed for the cuprates. Although Binning and Bednorz did some work on this material, it never led to much, so Binning got bored and moved on to the discovery of the scanning tunneling microscope, which he later got the Nobel prize for.

After this, Bednorz began to work under Alex Muller, who was also interested in the possibility of oxide superconductors. Alex was particularly intrigued by the role that Jahn-Teller effects played in the perovskite structure; that is, in the distortions of the oxygen octahedra surrounding the transition metal ions which lead to the lifting of the degeneracy of the 3d crystal field levels. While searching around, they became aware of work that Raveau's group had done on  $\text{LaBaCuO}$ , and in the course of reproducing this work, they discovered high temperature superconductivity. The story subsequently circulated was that Raveau took his samples off the shelf, and found that they too were superconducting. It is on such twists of fate that careers in science are often decided.

After the original discovery, several groups got in the act, and by use of pressure, Paul Chu's group was able to drive the initial transition temperature of 35K up to 50K. The real quest, though, was to find a related structure with a higher transition

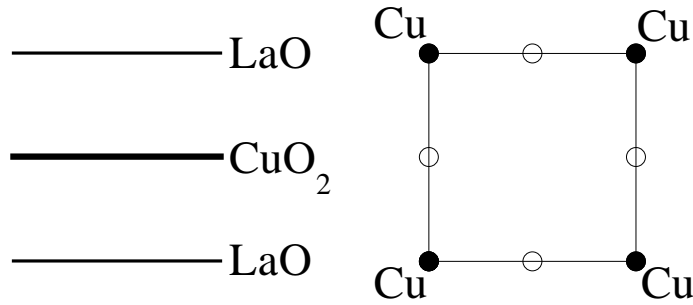


**Figure 1.** Crystal structure of  $La_2CuO_4$ . Left panel shows the layer structure along the  $c$ -axis, the right panel the structure of the  $CuO_2$  plane.

temperature, and this was rapidly discovered in early 1987, when Chu and collaborators found 90K superconductivity in YBCO [23]. The liquid air barrier (77K) had finally been breached, and true high temperature superconductivity had at last been discovered. By varying the crystal structure and again exploiting pressure, transition temperatures up to 160K have been achieved, again by Chu's group. Matthias must have been smiling from on high.

### 1.2. Crystal Symmetry and Electronic Structure

The crystal structures of the cuprates were one of the first things elucidated, which is obvious because of the patent rights involved (after a very long struggle, Bell Labs eventually won that one [24]; for an illuminating account of those heady days, the reader is referred to the book by Hazen [25]). Though they come in many variants, the basic structure is quite simple (Fig. 1). The material consists of  $CuO_2$  planes, where each Cu ion is four fold coordinated with O ions, separated by insulating spacer layers. The exception to this is YBCO, which has metallic CuO chain layers as one of the spacer layers. The original LBCO material had two apical oxygens (the standard perovskite structure, where the transition metal ion is in the center of an octahedron formed from six surrounding oxygen ions), but in YBCO, one of these oxygens is absent, and in other structures, such as that formed by electron doped cuprates, the apical oxygens are totally missing. What this means is that despite all of these complications, the essential structure to worry about are the  $CuO_2$  planes, which was understood early on, particularly by Anderson [26]. Of course, the superconducting transition temperature varies a lot from structure to structure, and is generally higher the more  $CuO_2$  planes per unit cell that there are, but after years of study, most researchers have come to the conclusion that the main  $c$ -axis effect is simply to tune the electronic structure of the  $CuO_2$  planes.

When considering these planes, one immediately comes across a basic fact. Most transition metal oxides are insulators with a particular electronic structure. This is due to the fact that the transition metal 3d level and oxygen 2p level are separated by a greater energy than the energy spread of these levels from band formation. The

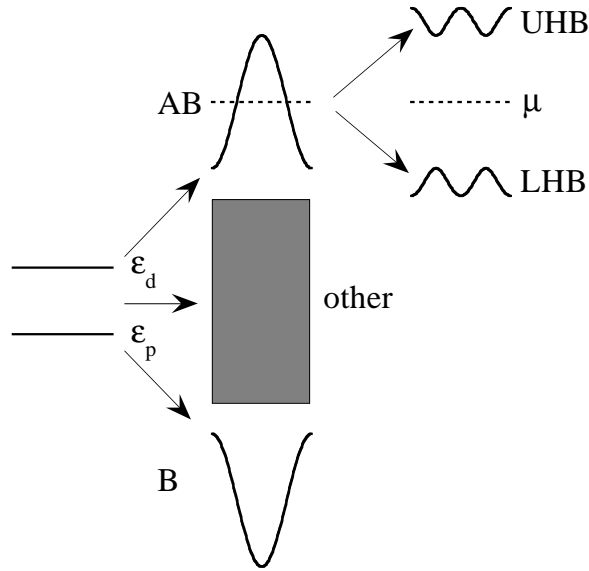


**Figure 2.** Electronic structure of the undoped cuprates. Left panel shows the atomic Cu d and O p levels, middle panel the band structure of the solid (where B is the bonding combination of the atomic levels, AB the antibonding one), and right panel the effect of correlations (Mott-Hubbard gap) on the AB band (LHB and UHB are the lower and upper Hubbard bands).

net result is one gets separate 3d and 2p energy bands. The Coulomb repulsion on the transition metal site is so large that the 3d band “Mott-Hubbardizes”, splitting into upper and lower Hubbard bands separated by this energy scale,  $U$  (typically 8-10 eV in the solid). The true energy gap then becomes of the charge transfer type, separating the filled oxygen 2p valence band from the empty 3d conduction (i.e., upper Hubbard) band [27].

The cuprate case is different, though (Fig. 2) [28]. In the solid, the Cu ion is in a  $d^9$  configuration ( $Cu^{++}$ ) and the O ion in a  $p^6$  configuration ( $O^{--}$ ), with the Cu 3d energy level above but relatively close to the O 2p energy level. In the layered perovskites, the tetragonal environment of the Cu ion leads to the single 3d hole having  $d_{x^2-y^2}$  symmetry. In this case, the dominant energy is the bonding-antibonding splitting involving the quantum mechanical mixture of the Cu 3d  $x^2 - y^2$  orbital and the planar O  $2p_x$  and  $2p_y$  orbitals (with an energy of 6 eV). The net result is that in the parent (undoped) structure, one is left with a half filled band which is the antibonding combination of these three orbitals, with the bonding, non-bonding, and the rest of the Cu and O orbitals filled. As Anderson speculated early on [26], it is this copper-oxygen antibonding band which “Mott-Hubbardizes”, forming an insulating gap of order 2 eV in the parent compound (the effective  $U$  being reduced because of the Cu-O orbital admixture).

Therefore, in the end, the complicated electronic structure leads to a single 2D energy band near the Fermi energy, which is what makes the cuprates so attractive from a theoretical perspective [29]. But one can even reduce this “one band Hubbard model” further by taking the limit of large  $U$ . In this case, the upper Hubbard band is

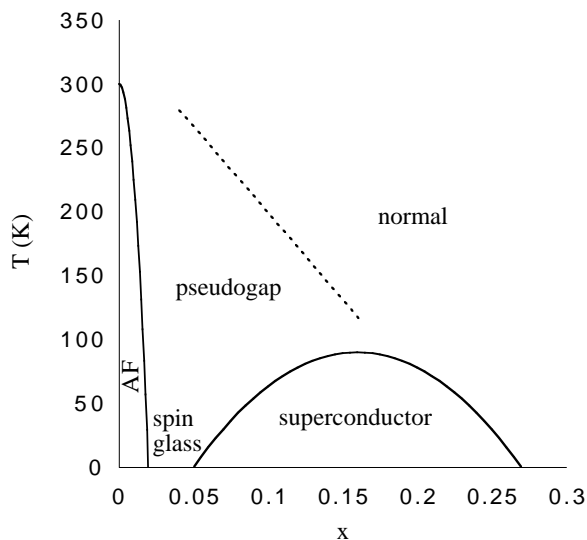


**Figure 3.** Phase diagram of the cuprates ( $x$  is the hole doping). AF is the antiferromagnetic insulator. The dotted line is a crossover line between the normal metal phase and the pseudogap phase.

projected out (assuming we are considering hole doping the insulator), and the effect of  $U$  becomes virtual, leading to a superexchange interaction between the Cu spins,  $J$  ( $t^2/U$ , where  $t$  is the effective Cu-Cu hopping mediated by intervening O sites). This is easily understood by noting that two parallel spins are not allowed to occupy the same Cu site because of the Pauli exclusion principle, but antiparallel spins can, leading to an energy savings of  $t^2/U$  from second order perturbation theory. This so-called “ $t$ - $J$ ” model is the minimal model for the cuprates. Despite the success of motivating this model from first principles calculations [30], it is not generally agreed upon. For instance, Varma has advocated that one must consider the full three band Hubbard model (one band from each of the three states, Cu  $3d x^2 - y^2$ , O  $2p_x$ , and O  $2p_y$ ). His claim is that upon projection to the low energy sector, non-trivial phase factors between the three bands become possible, which can lead to an orbital current state which he associates with the pseudogap phase [31].

### 1.3. Phase Diagram

The original hope of Anderson was that the insulating phase of the cuprates would turn out to be a spin liquid [26]. The issue here is that most Mott insulators exhibit broken symmetry, such as antiferromagnetism. This means that such insulators can be adiabatically continued to an ordinary band insulator with magnetic order, as originally proposed by Slater [32]. The cuprates would be another example of this, since the half filled band discussed above would become one full and one empty band upon magnetic ordering due to the unit cell doubling (in this picture, the lower Hubbard band would correspond to the up spin band of the band insulator, the upper Hubbard band to the down spin band). Anderson believed, though, that the Mott phenomenon

should be unrelated to this argument, and that the cuprates would be the ideal place to demonstrate this. Since there is only one d hole per Cu site (and thus,  $S=1/2$ ), and given the 2D nature of the material, he felt that quantum fluctuations would be sufficient to destroy the order, leading to a spin liquid ground state, which he called a resonating valence bond (RVB) state (harking back to the theory of benzene rings, where each C-C link resonates between a single bond and a double bond state).

As was discovered soon after, though, the undoped phase is indeed magnetic, though the moment is reduced by  $1/3$  from the free ion value due to fluctuations [33]. On the other hand, magnetic order is rapidly destroyed upon hole doping, so in fact the magnetic phase only takes up a small sliver (Fig. 3) of the phase diagram (in the electron doped case, though, the magnetism exists over a much larger doping range). So, in that sense, Anderson's intuition was quite good.

For dopings beyond a few percent, the system either enters a messy disordered phase exhibiting spin glass behavior (as in LSCO) before superconducting order sets in, or immediately goes to the superconducting phase (as in YBCO). The superconducting transition monotonically rises with doping, reaching a maximum at about 16% doping, after which  $T_c$  declines to zero. The net effect is to form a superconducting "dome" which extends from about 5% to 25% doping.

At first sight, the superconducting phase is not so different from that of classical superconductors. We know that it exhibits a zero resistance state with a Meissner effect. Experiments show that the superconducting objects are charge  $2e$ , and thus pairs are formed. What is unusual, though, are the short coherence lengths. For typical superconductors, the coherence length is quite long, usually several hundred  $\text{\AA}$  or more. This is in contrast to magnets, which have quite short coherence lengths. Therefore, for most superconductors we know, mean field theory works extremely well, as opposed to magnets where it almost always fails. But cuprates exhibit short coherence lengths, of order  $20\text{\AA}$  in the plane, and a paltry  $2\text{\AA}$  between planes. The latter is so short, the cuprates are essentially composed of Josephson coupled planes, as has been experimentally verified by a number of groups [34]. Such coupling is necessary, of course, since long range superconducting order cannot occur in two dimensions (except the Kosterlitz-Thouless phase, whose existence in the cuprates is still debated [35]).

Another unusual finding is the symmetry of the order parameter (Fig. 4). For many years, it was felt that the order parameter probably had s-wave symmetry. There was no evidence from thermodynamic measurements for nodes in the gap as in heavy fermion superconductors, except for an early report of a non-exponential temperature dependence of the Knight shift [36]. And the cuprates were viewed as quite disordered (doping being achieved by chemical substitution), which is known to be pair breaking for unconventional superconductors. This was despite the prediction of d-wave pairing from both spin fluctuation models [37] and RVB theory [39, 38]. But this began to change when NMR measurements found a  $T^3$  variation of the spin lattice relaxation rate, as found in heavy fermion superconductors, as opposed to the exponential behavior found in s-wave superconductors [40]. This was soon followed by penetration depth



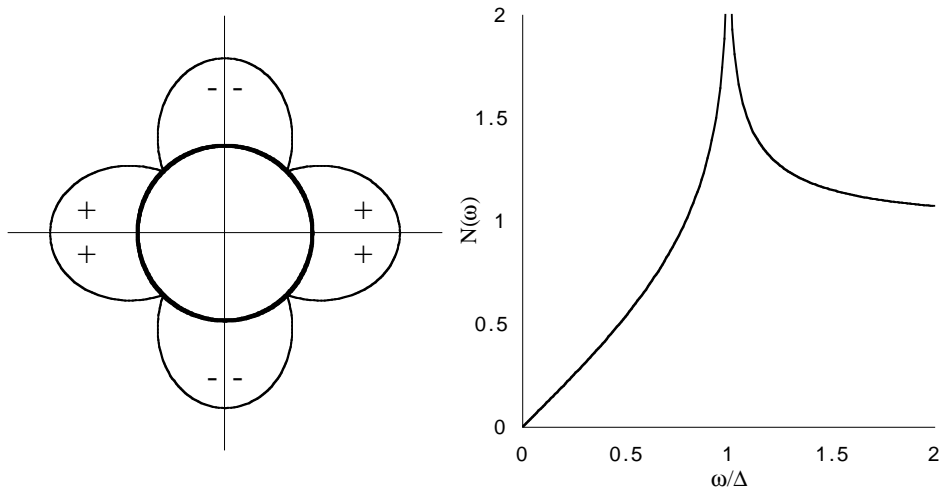


**Figure 4.** Angular variation of the d-wave gap around the Fermi surface is shown in the left panel (with nodes at  $k_x = \pm k_y$ ). The resulting density of states is plotted in the right panel.  $\Delta$  is the maximum superconducting energy gap.

measurements, where a corresponding linear in T behavior was found [41]. At the same time, angle resolved photoemission measurements gave direct spectroscopic evidence for nodes in the gap [42].

Of course, the possibility still remained that the order parameter was s-wave, but with a highly anisotropic gap. These worries were put to rest once and for all by phase sensitive measurements. The first of these was by van Harlingen's group. Following suggestions by Leggett, they formed SIS tunneling junctions on the ac and bc faces of YBCO, using an ordinary s-wave superconductor as the counterelectrode. These two junctions were then connected, and the superconducting phase difference measured from the dependence of the Josephson critical current on applied magnetic field. They found exactly the  $\pi$  phase shift expected for a d-wave state (which differs by a minus sign between the two orthogonal a and b directions) [43]. This was soon followed by the tricrystal grain boundary experiments of Tsuei and Kirtley [44], where three grain boundaries at different orientations were brought together at a point. Thus, about the tricrystal point, there are three junctions. Each junction will act as a "zero" junction or a  $\pi$  junction depending on the superconducting phase difference across the junction. If the number of such  $\pi$  junctions is odd, then a half integral flux quantum will appear at the tricrystal point. The advantage of this method is that by varying the crystallographic orientation of the three grains, the symmetry of the order parameter can be mapped out in detail. The net result was that for only those orientations where d-wave symmetry predicted a half integral flux quantum was one observed. As YBCO is orthorhombic, though, there still remained an out (since s-wave and d-wave are the same group representation in that crystal structure), but the tricrystal experiments were repeated for Tl2201, which has tetragonal symmetry, with the same results [45]. After that, there was no question anymore about the order parameter symmetry, and for these pioneering efforts, four of the researchers were awarded the Buckley prize in 1998.

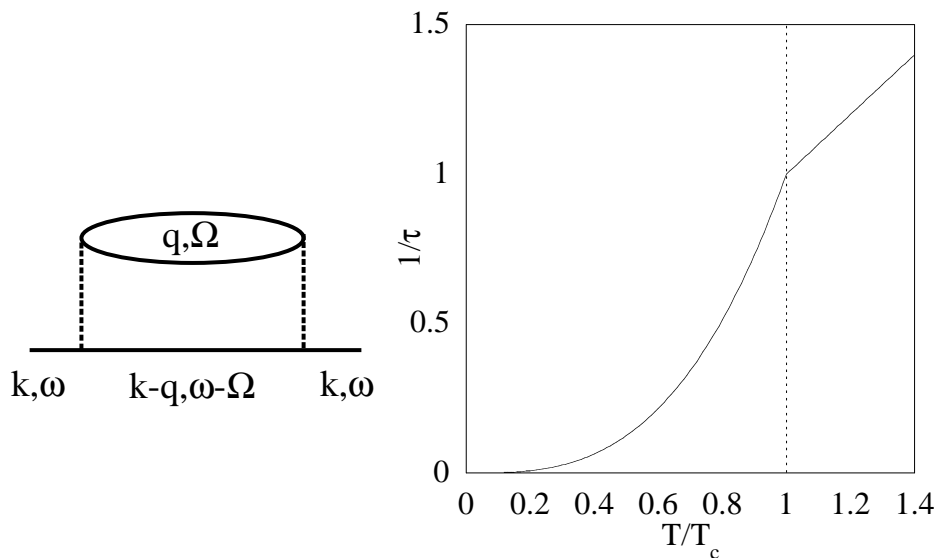


**Figure 5.** Left panel: lowest order Feynman diagram for electron-electron scattering. Right panel: resulting temperature dependence of the zero energy scattering rate.  $T_c$  is the superconducting transition temperature (dotted line).

Perhaps the most unusual finding, though, is the difference of the dynamics between the normal and superconducting states. As will be discussed below, the normal state of the cuprates (away from the overdoped side of the phase diagram) does not appear to be a Landau Fermi liquid. On the other hand, a variety of experiments, first microwave conductivity [46], then thermal conductivity [47], infrared conductivity [48], and photoemission [49], revealed that the scattering rate of the electrons at low energies drops precipitously in the superconducting state (right panel, Fig. 5). At low temperatures in YBCO, mean free paths of the order of microns have been inferred for the electrons, as opposed to the very short mean free paths found in the normal state. This strong loss in inelastic scattering would be unusual for an electron-phonon mediated superconductor, since the phonons are not gapped in the superconducting state. The implication, then, is that the primary scattering is electron-electron like in character, and thus is strongly reduced in the superconducting state since the electrons become gapped. This can be easily seen from the lowest order Feynman diagram (left panel, Fig. 5, showing an electron scattering off a particle-hole excitation), since every internal line in the diagram is gapped by  $\Delta$  (a point first noted by Nozieres in his famous book[50]). This obviously points to an electron-electron origin to the pairing as well.

This brings us to a consideration of the rest of the phase diagram. As discussed above, cuprates should be thought of as doped Mott insulators. What this means is that for low doping, the number of carriers is small. As the superconducting phase is conjugate to the number operator, this implies that phase fluctuations could play an important role on the underdoped side of the phase diagram. Again, this was realized early on by Anderson, who proposed that the doped holes would only be phase coherent below a temperature which scaled linearly with doping [51]. This should be

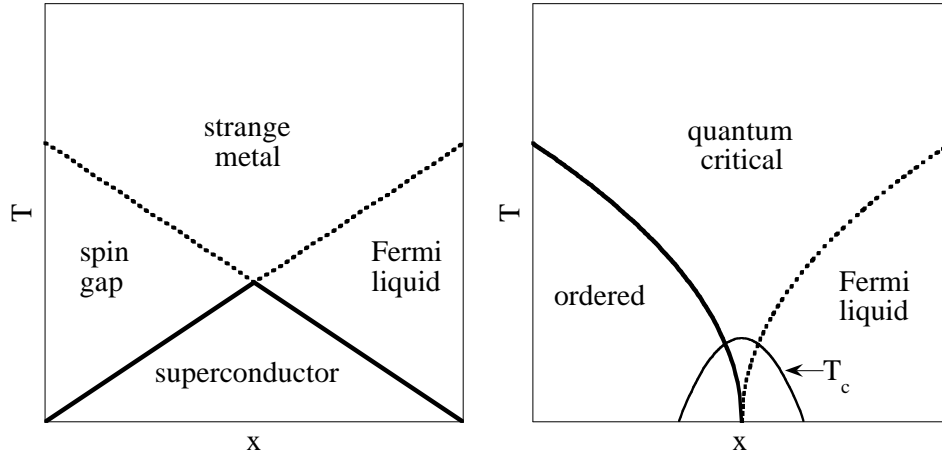


**Figure 6.** Two proposed theoretical phase diagrams for the cuprates: RVB picture (left panel) [53] and the quantum critical scenario (right panel).

contrasted with the “pairing” scale, which within the RVB model would be maximal for the insulator, and then drops to zero on the overdoped side when the bandwidth  $xt$  of the doped holes becomes comparable to the superexchange energy  $J$  [52, 39]. These two crossing lines led to the proposal of a generic “RVB” phase diagram (left panel, Fig. 6) [53] composed of four phases, a superconductor (bottom quadrant), a Fermi liquid (right quadrant), a strange metal phase (upper quadrant), and a spin gap phase (left quadrant, now known as the pseudogap phase). In this picture, only the superconducting phase (which lies below both crossing lines) should be considered as having true long range order, otherwise, these “phase” lines should be considered as crossover lines.

The first of these “phases” which was studied in detail was the strange metal phase. Transport measurements revealed that the resistivity was dead linear in temperature over a large range, the most amazing example of this being in single layer Bi2201, where linearity persisted down to 10K (when superconductivity finally occurred) [54]. No saturation at high temperatures was observed as occurs in A15 superconductors. This behavior was further confirmed by a generalized Drude analysis of infrared data, which shows a scattering rate linear in energy up to half an eV [48]. These striking observations led Varma and colleagues to propose the so-called marginal Fermi liquid phenomenology for the strange metal phase [55]. In this model, the electrons are assumed to be scattering off a bosonic spectrum which is linear in energy up to an energy scale  $T$ , then constant afterwards. Because of this, no energy enters the problem except the temperature (modulo an ultraviolet cut-off), a phenomenon referred to as quantum critical scaling. This in turn has led to the proposal of an alternate (to the “RVB”) phase diagram based on a quantum critical point (right panel, Fig. 6). In such a picture, the ordered phase (to the left of the critical point) would correspond to the pseudogap phase, its disordered analogue (to the right of the critical point) to the Fermi liquid phase, and the quantum critical regime (above the critical point) to the strange metal phase. The superconducting “dome” surrounds the critical point, screening it like an event horizon

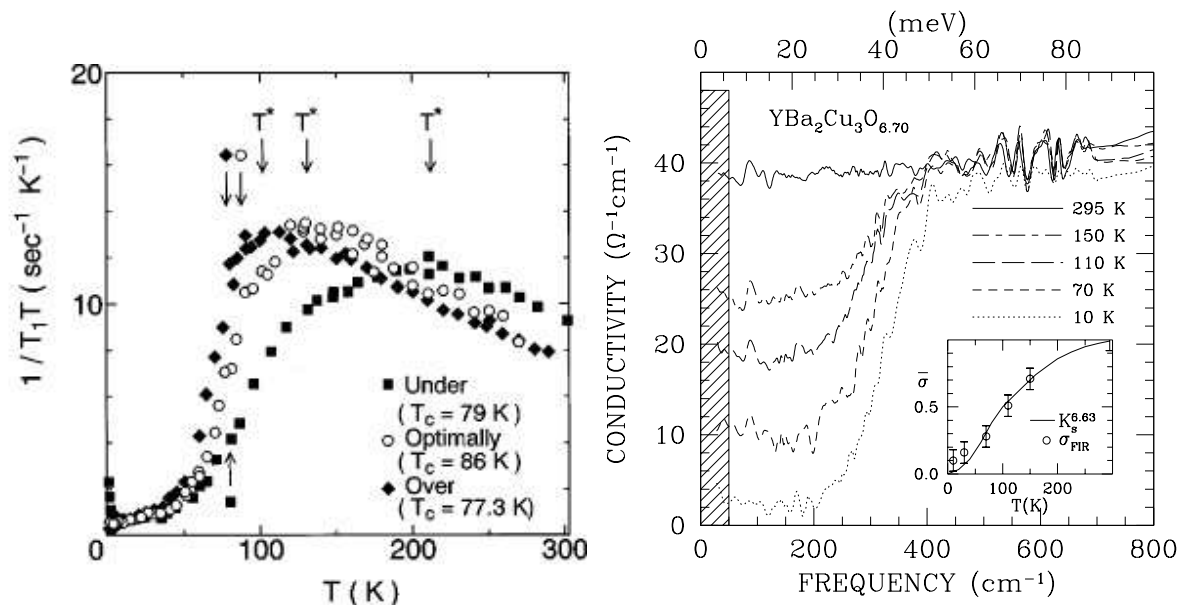


**Figure 7.** Experimental evidence for a pseudogap. Left panel is the NMR relaxation rate for various samples of Bi2212 [64], with a suppression of  $1/T_1T$  (spin gap) starting at  $T^*$  well above  $T_c$  for underdoped samples. Right panel is the c-axis conductivity for underdoped YBCO, with a pseudogap which fills in with temperature [48]. The inset shows that the subgap conductance scales with the Knight shift.

of a black hole. We note that the Fermi liquid/strange metal boundary is a crossover line in both phase diagram scenarios, but the strange metal/pseudogap boundary is a crossover line in the RVB model and a true phase line in the quantum critical model. An exception is in certain antiferromagnetic quantum critical scenarios where the “phase line” corresponds to short range 2D order [14].

This brings us to the most controversial aspect of the cuprate field, the nature of the pseudogap phase [56, 57]. The first experimental indication of such a phase was from NMR measurements by the Bell group, which showed that the spin lattice relaxation rate of underdoped cuprates begins to decrease well above  $T_c$  (left panel, Fig. 7) [58]. A similar decrease is seen in the Knight shift [59], which measures the bulk susceptibility (NMR measuring the zero energy limit of the imaginary part of the dynamic susceptibility divided by the energy). A signature of a gap was also evident in infrared measurements, which showed a dip in the conductance separating the low energy Drude peak from the so-called mid-infrared bump [60, 61], with the temperature dependence of the conductance near the dip energy [61] scaling with the spin lattice relaxation rate [62]. The resulting sharpening of the Drude peak leads to a decrease of the planar resistivity in the pseudogap phase [63]. But the most dramatic effect was in c-axis polarized infrared measurements, which showed a significant gap at low energies (no Drude peak), with the temperature dependence of the subgap conductance [65] tracking the Knight shift (right panel, Fig. 7) [62]. This leads to an insulating up turn below the pseudogap temperature,  $T^*$ , in the c-axis resistivity [66].

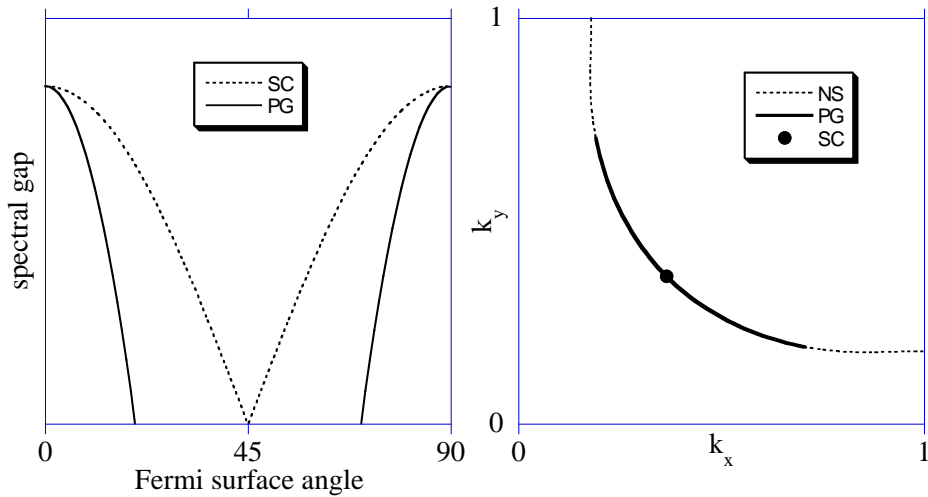


**Figure 8.** Momentum anisotropy of the pseudogap from ARPES. Spectral gap around the Fermi surface is plotted in the left panel (SC is the superconducting state, PG the pseudogap phase), the locus of gapless excitations in the right panel (NS is the normal state Fermi surface, PG the Fermi arc of the pseudogap phase, and SC the node of the d-wave superconducting state).

What brought the pseudogap effect to the forefront, though, was its observation by angle resolved photoemission [67, 68, 69]. These experiments found that although the quasiparticle peak in the spectral function was destroyed above  $T_c$ , the spectral gap persisted to the higher temperature,  $T^*$ . This so-called leading edge gap had a similar magnitude and momentum anisotropy as the superconducting energy gap, leading to the speculation that this gap was a precursor to the superconducting gap, that is, that the pseudogap phase represented pairs without long range phase order [69]. This picture was consistent with the NMR and Knight shift data, in that pair formation is equivalent to singlet formation, and thus the Knight shift and the spin lattice relaxation rate should decrease accordingly [70]. The strong coupling limit of this picture is simply the RVB physics mentioned above, where the pseudogap state corresponds to d-wave pairing of spins. This picture received further support by later ARPES experiments which showed that the pseudogap's minimum gap locus in momentum space coincided with the normal state Fermi surface. That is, the pseudogap is locked to the Fermi surface, as would be expected for a  $Q=0$  instability [71] (in superconductors, pairs have zero center of mass momentum). Later tunneling experiments were found to be in support of this picture as well [72].

Despite this, the situation, even from ARPES, remains controversial. ARPES experiments reveal that the pseudogap turns off at different momentum points at different temperatures, leading to the presence of temperature dependent Fermi arcs (Fig. 8) [73]. These arcs persist to low doping; they have even been observed for LSCO at a 3% doping level, where the system is on the verge of magnetism [74]. Some authors have taken this as evidence that these arcs represent one side of a small hole pocket, the latter picture expected when doping the magnetic insulating phase (the idea being

that SDW coherence factors suppress the intensity on the back side of the pocket). This magnetic precursor scenario is one of the leading alternatives to the preformed pairs picture. Despite much searching, though, no ARPES experiment to date has ever seen a true hole pocket centered about  $(\pi/2, \pi/2)$ .

Another explanation has been put forward that the pseudogap represents an orbital current phase. This was implicit in certain treatments of the RVB model, which predicted at low dopings the presence of a so-called staggered flux phase, which is quantum mechanically equivalent to the d-wave pair state in the zero doping limit [75]. This has been generalized to the d density wave state, first discussed by Heinz Schulz [76], but popularized by Laughlin and colleagues [77]. A related picture has been put forth by Varma, where his orbital current phase is the result of a non-trivial projection of the three band Hubbard model onto the low energy sector [31]. Some experimental evidence for such a state was obtained from inelastic neutron scattering which indicated a momentum form factor inconsistent with simple Cu spins [78], but after studies by several groups, the feeling is that the observed effect may represent an impurity phase (always a problem for neutrons given the large crystals needed for such measurements). The latest evidence, though, has been given again by ARPES, where Campuzano's group has done measurements with circularly polarized light [79]. What they have found is the presence of chiral symmetry breaking below  $T^*$ . The momentum dependence of the effect, though, is not what is expected from the d density wave scenario, though one of the two orbital current states proposed by Varma appears to be consistent with these observations [80].

The main debate, though, is whether the pseudogap phase represents a state with true long range order (which the neutron and circularly polarized ARPES give some evidence for), or simply some precursor phase. If it is the former, then the preformed pairs scenario is probably wrong, unless the ordering is some parasitical effect. Long range order is certainly in line with a quantum critical point scenario. Additional support for such a scenario comes from various measurements by Loram and Tallon (Fig. 9), who claim that the pseudogap phase line passes through the superconducting dome and goes to zero at some critical point within the dome (19% doping) [81]. One of the strongest points given as evidence for their conjecture is that upon impurity doping, the superconducting dome appears to collapse about the pseudogap phase line (right panel, Fig. 9). In their picture, the specific heat data indicate a loss of states in the pseudogap phase. This implies that the pseudogap eats up part of the Fermi surface, leaving a smaller part available for pairing, thus explaining the collapse of  $T_c$  on the underdoped side. This "mean field" picture is in total contrast to the phase fluctuation picture discussed in the context of the precursor pairing scenario [82].

Recently, there has been a new measurement which comes out in support of the precursor pair scenario. Ong's group has measured the Nernst effect, the coefficient of a higher order transport tensor which is very small in normal metals, but is appreciable in superconductors because of the presence of vortices. What they find is a sizable Nernst signal on the underdoped side of the phase diagram which persists well above  $T_c$ , though

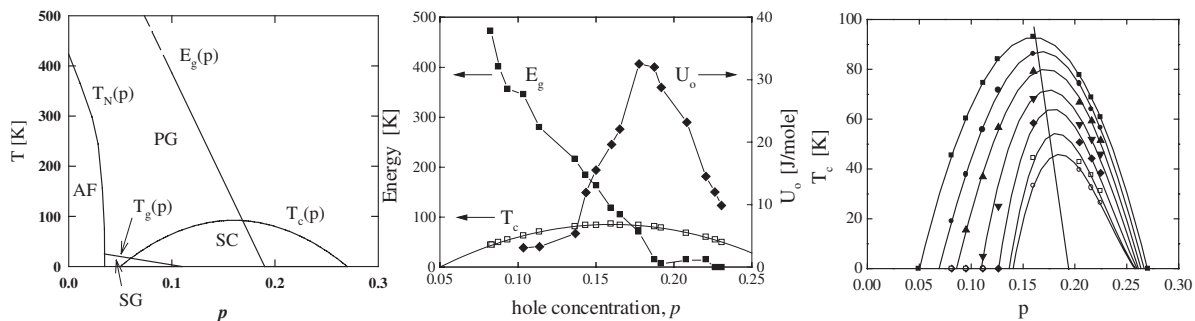


**Figure 9.** Left: Tallon/Loram picture of the phase diagram, with a quantum critical point at  $p=0.19$  where  $E_g$ , the pseudogap energy scale, vanishes ( $p$  is the hole doping).  $SG$  is a spin glass phase. Middle: Variation with doping of  $E_g$  and the superconducting condensation energy  $U_0$  as extracted from specific heat data on YBCO. Right: Collapse of the superconducting dome about the  $E_g$  crossover line with increasing cobalt doping for Bi2212. From Ref. [81].

not as high in temperature as the ARPES pseudogap [83]. The only explanation that has been put forth for this amazing observation is that the pseudogap phase does indeed contain vortices. This may be connected to the results of STM measurements, which reveal that the pseudogap forms in the vortex cores in the superconducting state for underdoped samples [84].

#### 1.4. Inhomogeneities

How one crosses over from the Fermi arc state to the insulator is still an unresolved issue. In one scenario, the chemical potential jumps from the middle of the Mott-Hubbard gap to either the lower Hubbard band upon hole doping, or the upper Hubbard band upon electron doping. There is some evidence of this from photoemission. In particular, the Fermi arc is in a momentum region near the  $(\pi/2, \pi/2)$  point, and the latter is the top of the valence band in the insulator, as seen by photoemission in  $\text{Sr}_2\text{CuO}_2\text{Cl}_2$  [85]. This picture has been bolstered recently by photoemission experiments on the sodium doped version of this insulator, which also find a Fermi arc [86].

The other scenario is that upon doping, one creates new states inside the gap. Shen's group has given evidence that the latter scenario occurs in LSCO, and argues that this is associated with the strong inhomogeneities present in that material [87], though it should be remarked that 3% doped LSCO has the same Fermi arc that is seen in other hole doped cuprates such as Na doped  $\text{Sr}_2\text{CuO}_2\text{Cl}_2$  [74] and underdoped Bi2212 [67, 73].

This brings us to the question of stripes. At low doping, materials can be subject to electronic phase separation. This tendency occurs since each doped hole breaks four magnetic bonds, and thus this magnetic energy loss can be minimized by the holes clumping together. This clumping is opposed by the Coulomb repulsion of the holes. This led to the picture that the doped holes, as a compromise, might form rivers of charge, known as stripes [88, 89].

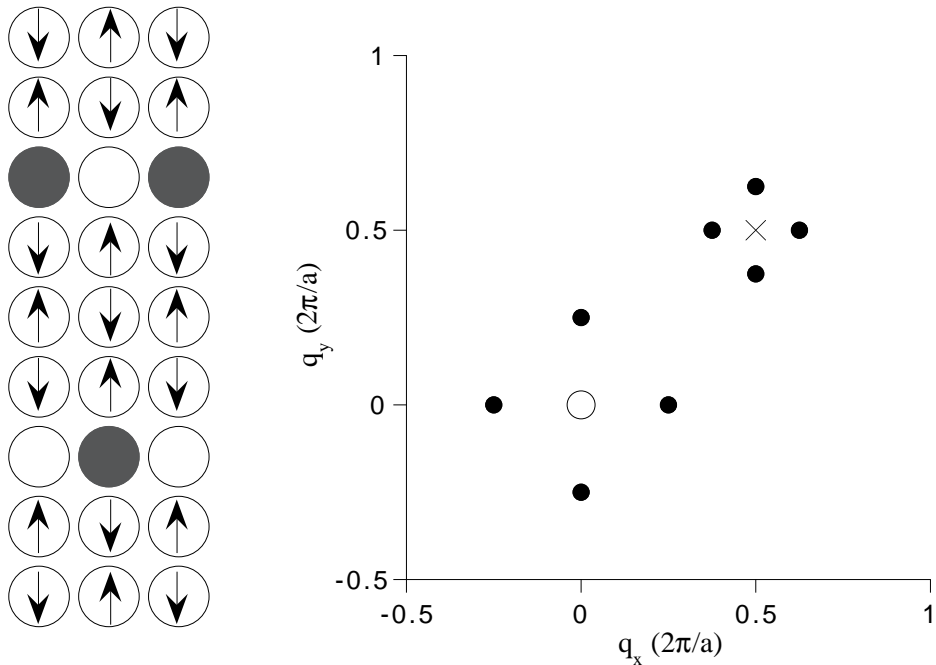


**Figure 10.** Stripe picture. Left panel illustrates stripes for  $\delta=1/8$  doping, arrows represent spins, dark circles doped holes. Right panel plots the resulting neutron scattering peaks (averaged between the x and y directions), with charge peaks at  $\pm 2\delta$  about (0,0) and spin peaks at  $\pm \delta$  about (0.5,0.5). Adapted from Ref. [90].

The first evidence for such stripes was given by Tranquada and co-workers using neutron scattering (Fig. 10) [90]. To understand their result, it should be noted that LSCO has a peculiarity in its phase diagram. LSCO is normally orthorhombic, the tetragonal phase existing either at high temperatures or under pressure. Near 1/8 hole doping, though, LSCO has a tendency to distort from its normal orthorhombic phase to another distorted phase known as low temperature tetragonal, which differs from the high temperature tetragonal phase mentioned above [91]. This LTT phase is stabilized by neodymium doping. What Tranquada and co-workers found was that the LTT phase exhibited long range ordering consistent with the formation of a 1D density wave state. Both charge and spin ordering occurs, but the former sets in at a higher temperature. This stripe formation is consistent with later photoemission [92] and transport [93] measurements, which again indicate 1D behavior.

What remains controversial, though, is whether stripes exist only for this anomalous Nd-doped LSCO compound. Strong incommensurate magnetic spots are seen by inelastic neutron scattering for various dopings in LSCO [94] and YBCO [95], and have been taken as evidence for the existence of dynamic stripes [96], given their resemblance to the static spot pattern of Nd-doped LSCO [90]. On the other hand, these spot patterns can also be reproduced from standard linear response calculations based on the known Fermi surface geometry [97].

What is clear, though, is that there is a definite tendency for underdoped materials to exhibit electronic inhomogeneity. The most dramatic example of this has been



recently provided by STM studies on underdoped Bi2212 by Davis' group [98, 99]. What they find is the existence of large gap regions (which have spectra reminiscent of the pseudogap phase) imbedded in smaller gap regions, with the relative fraction of the larger gap regions increasing with underdoping, similar to earlier results by Roditchev's group [100]. The large gap domains have a size of order  $30\text{\AA}$ . This granular picture would certainly suggest that the pseudogap phase is not a simple precursor to the superconducting phase as has been asserted by previous ARPES and STM studies.

More recently, the same group has seen a charge density wave state associated with the vortex cores which they inferred from Fourier transformation of the real space STM spectra [101]. An anisotropy of the pattern gave some indication that this might involve stripe formation. But even more recently, the same group has done a Fourier transformation of zero field data [102]. They find a weaker inhomogeneity in this case, but more interestingly, the Fourier peaks dispersed with energy. Although the interpretation of such Fourier transforms remain controversial (Kapitulnik's group [103] sees similar patterns which they attribute to stripe formation), the latest results [104] are consistent with Friedel oscillations from impurities whose momentum wavevectors can be used to map out the Fermi surface and gap anisotropy. The results are consistent with previous ARPES studies, and have been taken as support of the interpretation of incommensurability in neutron scattering as due to the Fermi surface geometry, as opposed to stripes.

### 1.5. Electron Doped Materials

Electron doped materials have been less studied, mainly due to metallurgical problems. What has been learned, though, is that the magnetic phase extends much further in doping than on the hole doped side [105, 106]. The superconducting phase has a lower  $T_c$  than on the hole doped side, probably for the same reason. A pseudogap phase is observed which appears to be a precursor to the magnetic phase in that they exist over the same doping range [107], though it should be remarked that the pseudogap seen is not the leading edge gap (discussed above in the context of ARPES), but rather the "high energy pseudogap" to be discussed later on in the ARPES section.

The symmetry of the superconducting order parameter is still somewhat controversial in these materials. Earlier penetration depth measurements [108] and point contact tunneling [109] showed behavior expected for s-wave pairing, but more recent penetration depth measurements have found a power law temperature dependence consistent with a disordered d-wave state [110]. Recent ARPES measurements are also consistent with d-wave symmetry [111, 112], but these experiments are near the resolution limit because of the small energy gap. It should be mentioned that the tri-crystal experiments mentioned above in the context of hole doped superconductors have been performed for the electron-doped case as well, and again find a half integral flux quantum in geometries predicted by d-wave symmetry [113]. Based on these developments, it is fairly certain that the pairing symmetry is d-wave in these systems.

More recently, Raman studies by Blumberg and co-workers [114] find evidence that the superconducting gap maximum is displaced away from the Fermi surface crossing along  $(\pi, 0) - (\pi, \pi)$  (as expected for a d-wave gap based on near neighbor pairs) to the “hot spots” (where the Fermi surface crosses the magnetic Brillouin zone boundary). This result is consistent with spin fluctuation mediated pairing if the magnetic correlation length is long (not surprising, given the persistence of long range magnetic order over a larger part of the electron doped phase diagram). It should be noted that ARPES sees an intensity suppression at these “hot spots” [112] associated with the formation of the “high energy pseudogap” [115] mentioned above. In addition, at low dopings, low energy spectral weight is found around the  $(\pi, 0)$  point [116], as opposed to the  $(\pi/2, \pi/2)$  point characteristic of the hole-doped material. This electron-hole asymmetry is what is expected if the chemical potential jumps to the upper Hubbard band upon electron doping.

## 2. Theory

### 2.1. BCS

The first microscopic theory of superconductivity, the much celebrated BCS theory [117], took many years to come about [118]. The reason was that the machinery needed to construct a proper many-body theory of electrons did not emerge until the 1950s. The motivation behind the theory was the isotope experiments of 1950 and their simultaneous prediction by Frohlich based on the electron-phonon interaction. Bardeen also understood the critical role that the concept of an energy gap would play in the ultimate theory. Once Leon Cooper, an expert in many-body theory, joined Bardeen’s group as a postdoc, progress was rapidly made.

What was known by that time was that the electron-phonon interaction could provide attraction among the electrons. The way this works is as follows (left panel, Fig. 11). Positive ions are attracted to an electron because of the Coulomb interaction. But, the ion dynamics are slow because of their heavy mass. Thus, once the electron moves away, another electron can move into this “ionic hole” before the ions have a chance to relax back. This provides attraction at the same point in space which can lead to pair formation. The interaction is retarded in time, though, which is what ultimately puts a limit on the transition temperature (energy, and thus temperature, being conjugate to time).

Such a “pair” theory had been proposed in the past, but the physics of conventional superconductors does not resemble simple Bose condensation, despite the fact that a pair of fermions behaves quantum mechanically like a boson. The key discovery by Cooper was the concept of Cooper pairs. The idea is that one is dealing with a degenerate system, that is, a filled Fermi sea. The problem Cooper considered was two electrons sitting in unoccupied states above the Fermi sea. As the temperature is lowered, the particle-particle response function diverges logarithmically because the

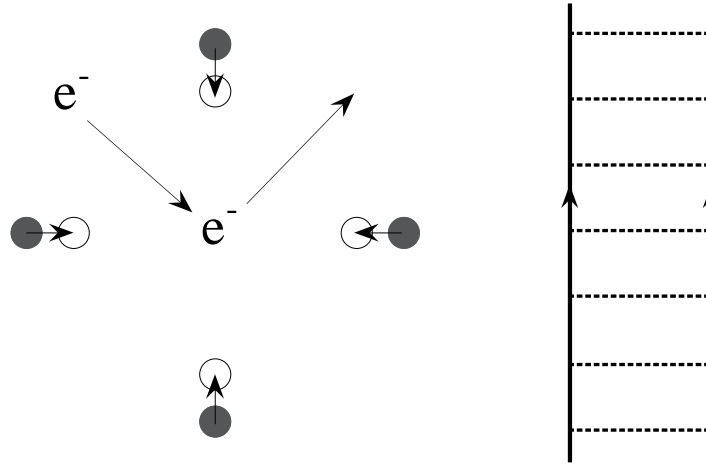


**Figure 11.** Electron-phonon interaction leads to attraction (left panel). Arrows joining circles show displaced ions; the time scale of these ions for relaxation back is slow compared to the electron dynamics. Right panel is the ladder sum for repeated electron-phonon scattering which leads to an electron pairing instability.

Fermi distribution function of the electrons approaches a step function. This divergence is strongest when the two electrons are in time reversed states (that is, a state  $k$  and a state  $-k$ , thus the center of mass momentum of the pair is  $Q=0$ ). Note the difference from the particle-hole response at  $Q=0$ , which simply measures the density of states at the Fermi energy.

This logarithmic divergence is cut-off at some ultraviolet energy scale, which in the electron-phonon problem is the Debye energy,  $\omega_D$ . This leads to a bare response function that goes as  $\chi_0 = N \ln(\omega_D/T)$  where  $N$  is the density of states. Now one sums a ladder series (repeated scattering of the two electrons, right panel, Fig. 11), which leads to an expression for the full response function of  $\chi = \chi_0/(1 - V\chi_0)$  where  $V$  is the interaction. For positive  $V$  (attractive in our sign notation), the denominator will have a pole when  $T_{div} = \omega_D e^{-1/\lambda}$  with  $\lambda = NV$ . This is the famous Cooper pair divergence.

This doesn't answer the question of what the ground state is. This problem was solved by Schrieffer, Bardeen's graduate student (thus BCS). Based on Cooper's solution, he guessed the many-body ground state at  $T=0$  (a rare accomplishment, the other well known example of this was Laughlin's guess for the fractional quantum Hall state). It is of the form  $\prod_k (u_k + v_k c_k^\dagger c_{-k}^\dagger) |0\rangle$ . Here  $|0\rangle$  is the vacuum and  $u, v$  are "coherence" factors (the sum of whose squares equals one). What can be seen here is that the BCS ground state is a superposition of states where the pair  $k, -k$  is either occupied or filled. Solving the variational problem (equivalent to replacing the product of the two creation operators by a c number), BCS found that  $u_k^2, v_k^2 = 1/2(1 \pm \epsilon_k/E_k)$  where  $E_k = \sqrt{\epsilon_k^2 + \Delta_k^2}$  and  $\Delta_k$ , gotten from solving an integral equation (the so-called gap equation), has the same form as  $T_{div}$  above.

Note that the Fermi distribution function has been replaced by  $v_k^2$ , thus leading to particle-hole mixing (Fig. 12). In essence, the BCS instability is a consequence of

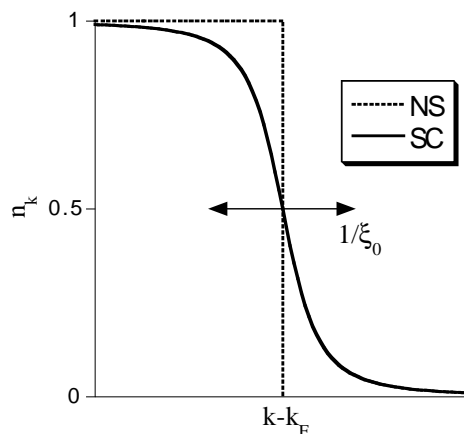


**Figure 12.** Momentum distribution function for the normal state (NS) and superconducting state (SC).  $\xi_0$  is the BCS correlation length.

Nature’s abhorrence of singularities (in this case, the step function behavior of the Fermi function at  $T=0$ ). This distribution is smeared over a momentum range of  $\sim \Delta/v_F$  where  $v_F$  is the Fermi velocity, thus defining the inverse correlation length. Excitations from the ground state can be formed by breaking up a pair. These excitations are of the form  $\gamma_k^\dagger = u_k c_k^\dagger - v_k c_{-k}$  and have an energy  $E_k$ . That is, on the Fermi surface, the quantity  $\Delta$ , which is related to the order parameter, is nothing more than the spectral gap, and thus the energy gap emerges quite naturally from the theory.

What allows this conceptually simple picture to work is Migdal’s theorem [119]. It states that the single particle self-energy can be treated to lowest order, since  $\omega_D/E_F$  is a small expansion parameter (where  $E_F$  is the Fermi energy). Thus, the only diagram series which has to be summed is the particle-particle ladder mentioned above. Such a theorem obviously does not apply if the pairing is due to electron-electron interactions.

## 2.2. Spin Fluctuation Models

As mentioned above, the electron-phonon attraction is local in space and retarded in time. This leads to  $L=0$  pairs. By fermion antisymmetry, this requires that the pair state be a spin singlet. For the case of electron-electron interactions,  $L=0$  pairs are usually not favored (because of the direct Coulomb repulsion between the electrons). In fact, one might wonder how one can ever get an “attractive” interaction in this case.

Let us start with the nearly ferromagnetic case [11]. The particle-particle ladder sum in this case involves exchanging the ends of one of the particle lines, thus representing a particle-hole ladder sum buried inside of a particle-particle one (Fig. 13). Thus, the diverging particle-hole response (representing a ferromagnetic instability) drives a diverging particle-particle response. For  $S=1$  pairs, this is attractive. In essence, the bare triplet interaction is zero (due to the Pauli exclusion principle) and the induced interaction is attractive (representing the tendency for an up spin electron to have another up spin electron nearby). By fermion antisymmetry, the  $L$  state must

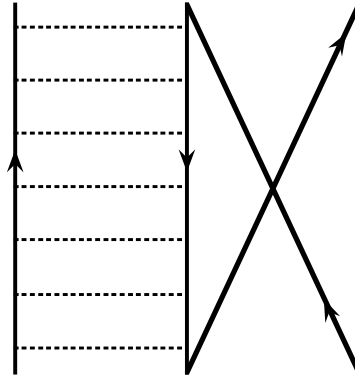


**Figure 13.** Particle-particle diagram for the spin fluctuation case. Note the particle-hole ladder sum buried inside this diagram.

be odd, thus allowing the two electrons in the pair to avoid coming too close to one another (thus minimizing the direct Coulomb repulsion).

For heavy fermions and cuprates, though, the nearly antiferromagnetic case is of more interest. In that case, one again wants to avoid the direct Coulomb repulsion, but now a spin up electron wants to have a spin down electron nearby. In the absence of spin-orbit, this implies  $S=0$ ,  $L=2$  pairs. For strong spin-orbit,  $S = 1$ ,  $S_z = 0$  pairs can be stable as well, which is the basis of the “f-wave” scenario postulated by Norman in the case of heavy fermions [19], but this is not relevant for the cuprate case.

The above considerations on a 2D square lattice leads to a pair state with  $d_{x^2-y^2}$  symmetry [18, 37]. In fact, the theory of this is a bit counterintuitive. Unlike the nearly ferromagnetic case, in the nearly antiferromagnetic case, the interaction is always repulsive (in a momentum space representation, left panel, Fig. 14), and in fact is most repulsive at  $Q = (\pi, \pi)$  where the antiferromagnetic instability would occur. But the d-wave version of  $\Delta_k$  changes sign under translation by  $Q$  (it is of the form  $\cos(k_x) - \cos(k_y)$ ), and this sign change compensates for the repulsive sign of the interaction when solving the integral (gap) equation for  $\Delta_k$ . In real space, the picture is more clear (right panel, Fig. 14) [120]. The on-site interaction is repulsive (which is why the overall interaction is repulsive in momentum space), but this interaction contains Friedel oscillations, with the first (attractive) minimum at a near neighbor separation, representing the tendency of opposite spin electrons to be on neighboring sites.

Note that retardation does not play the central role in the above arguments as in the phonon case. In essence, there is no Migdal’s theorem in this case [121], and so one may question such a theory which does not take into account vertex corrections. The justification that is often given is that if one considers the electrons and spin fluctuations as separate objects (like electrons and phonons), then as the spin fluctuations are “slow” relative to electrons, one gets something like a Migdal’s theorem. But this simple argument usually breaks down [121], though Chubukov has recently made arguments about why an effective Migdal theory would apply in the cuprate case [14]. Regardless, feedback effects definitely have to be considered whenever electron-electron

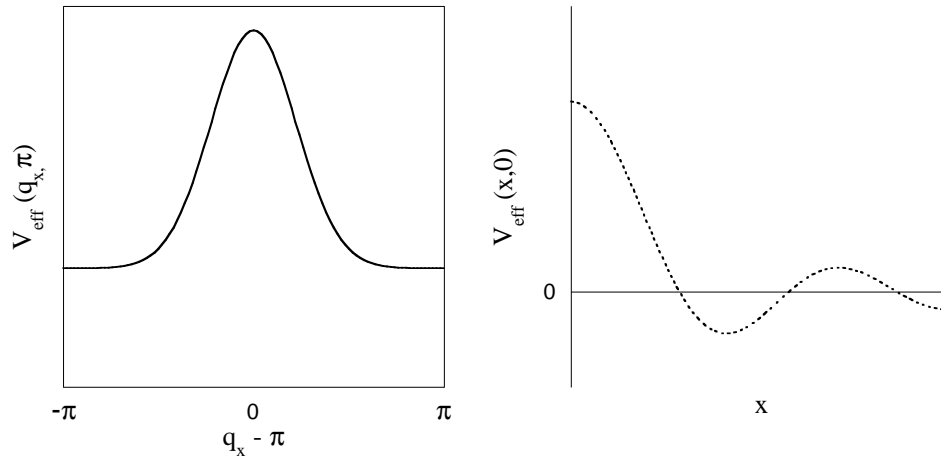


**Figure 14.** Effective interaction for spin fluctuation mediated pairing (AF case). Left panel is for momentum space (overall repulsive, peaked at  $(\pi, \pi)$ ), right panel for real space (repulsive on-site, with first attractive minimum at a near neighbor separation). Adapted from Ref. [120].

interactions are involved, since the spin fluctuation propagator is drastically changed by the introduction of the superconducting gap for the electrons [14]. The classic example of this is the stabilization of the *A* phase relative to the *B* phase in superfluid  $^3\text{He}$  [13].

### 2.3. RVB

The spin fluctuation theory is essentially a weak coupling approach. The RVB picture mentioned in the introduction is the strong coupling version of the spin fluctuation approach [26] (though Anderson differs on this [122]). The amazing thing was how quickly the RVB concept emerged (Anderson first spoke on this before the discovery of YBCO). It has certainly been controversial (one well known scientist, whose name will not be mentioned here, quipped that RVB actually stood for “rather vague bullshit”).

To understand this approach, consider the undoped insulator, where there is one Cu spin per site (the Cu being in a  $d^9$  configuration). The ground state of this system is an antiferromagnet. The reason is that if the spins on each site are parallel, then they cannot virtually hop because of the Pauli exclusion principle, but they can if the spins are antiparallel. In this case, the virtual hopping leads to an energy lowering of  $J = t^2/U$  per bond, where  $t$  is the effective Cu-Cu hopping integral, and  $U$  the Coulomb repulsion for double occupation. Mean field theory would then predict that the arrangement of spins forms a Neel lattice of alternating up and down spins (left panel, Fig. 15).

Anderson, though, suggested that the Cu case was special, since the spin of the single d hole was only  $1/2$ . Because of this, he anticipated that quantum fluctuations would melt the Neel lattice, leading to a spin liquid ground state, a fluid of singlet pairs of spins (right panel, Fig. 15) [26]. The “RVB” notation comes from the fact that a given spin could be taken as paired with any one of its four neighbors, thus each bond fluctuates from being paired to not paired. This is analogous to benzene rings,

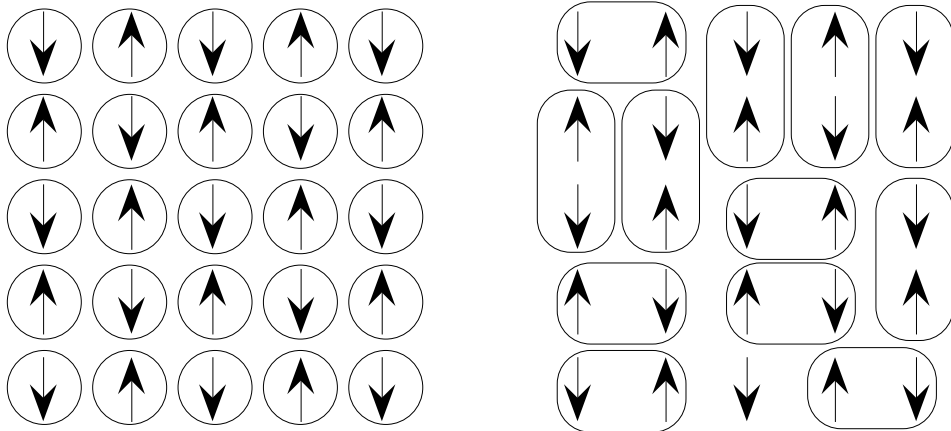


**Figure 15.** Neel lattice (left panel) versus RVB (right panel). The RVB state is a liquid of spin singlets.

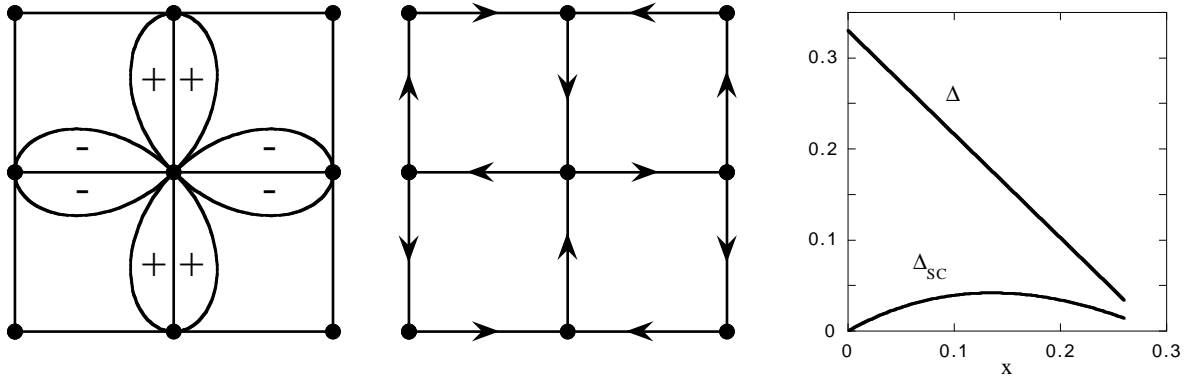


**Figure 16.** Two RVB states which are equivalent at half filling. The left panel is a d-wave pairing of spins, the middle panel a  $\pi$  flux state. Dots are Cu ions, and arrows are bond currents. Right: Variation of the RVB gap parameter,  $\Delta$ , and the superconducting order parameter,  $\Delta_{SC}$ , with doping [39].

where each C-C link fluctuates between a single bond and a double bond. Although it was discovered soon after [33] that the undoped insulator is indeed a Neel lattice, this lattice does indeed “melt” with only a few percent of doped holes. This is rather easy to understand, since the kinetic energy of the doped holes is frustrated in the Neel state.

After Anderson’s original conjecture, it was realized that at the mean field level, there were a number of possible ground states for such a spin fluid. For the undoped case, these states are quantum mechanically equivalent, since the presence of a spin up state is equivalent to the absence of a spin down state, an effective  $SU(2)$  symmetry [123]. That is, various mean field decouplings of the Hamiltonian are equivalent since  $\langle c_{\uparrow}^{\dagger} c_{\downarrow}^{\dagger} \rangle \equiv \langle c_{\uparrow}^{\dagger} c_{\uparrow} \rangle$ . The first decomposition is equivalent to a BCS pairing of spins, the second to a bond current state (left panels, Fig. 16). For the spin pairing case, the d-wave state is favored since it does the best job of localizing the two spins on neighboring sites. Its bond current equivalent is the  $\pi$  flux phase state, where the bond currents flow around an elementary plaquette (square formed from four Cu-Cu bonds), yielding

a net phase of  $\pi$  per plaquette.

Upon doping, this  $SU(2)$  symmetry is broken to  $U(1)$ . At the mean field level, the d-wave state has the lowest energy [38, 39], as it minimizes the kinetic energy of the doped holes. The variational  $\Delta$  associated with the d-wave state is maximal for the undoped case and decreases linearly with doping (right panel, Fig. 16). To understand the implications of this for superconductivity, one should note that the above variational parameter applies to the spins. But only the doped holes carry the current. As their density increases linearly with doping, then the superfluid density of the real electrons (a product of spin and charge) varies linearly with doping, despite the fact that the variational parameter does not. That is, there is a complete decoupling of  $\Delta$  (the excitation gap) from the order parameter (the superfluid density), unlike in BCS theory. These simple mean field considerations have been confirmed by recent variational Monte Carlo calculations of a “projected” d-wave BCS pair state (where double occupied states are projected out) [124]. Such projected states can also be shown to contain orbital current correlations [125].

Although a finite temperature generalization of RVB theory is non-trivial, the overall phase diagram can be easily appreciated by noting that the “pairing” temperature scale,  $T_{RVB}$ , will be proportional to  $\Delta$ , and that the phase coherence temperature of the doped holes will be proportional to the doping. The net result are two crossing lines with doping, with the spin gap phase in the left quadrant, the Fermi liquid phase in the right quadrant, the superconducting phase in the bottom quadrant (below both lines), and the strange metal phase in the upper quadrant (see left panel, Fig. 6) [53].

One of the most important concepts to be introduced by RVB theory is the concept of spin-charge separation [29]. This idea can be most easily appreciated by the RVB explanation of the spin gap phase [126]. Since only the spins are paired, then strong effects are expected for spin probes but only weak effects for charge probes. This is consistent with planar properties of the pseudogap phase, which show a strong spin gap in NMR (left panel, Fig. 7), but only a weak gap-like depression in the in-plane infrared conductivity. In fact, the drop in in-plane resistance in the pseudogap phase is easily understood since when the spins pair up and become gapped, there are less states for the doped holes to scatter off of. On the other hand, spin-charge separation, being a 2D effect, only occurs within a plane. As spins and charges must thus recombine into real physical electrons to tunnel from plane to plane, then large effects are expected in any experiment measuring a c-axis current. This is consistent with experiment, since a hard gap is seen in c-axis infrared conductivity (right panel, Fig. 7), as well as tunneling and photoemission.

Going beyond mean field considerations, though, has proven to be difficult in the RVB scheme. The most promising approach is to use gauge theory to treat the various  $SU(2)$  and  $U(1)$  symmetries of the model [126]. The resulting gauge field fluctuations coupling the “spinons” and “holons”, though, are extremely strong, leading to an uncontrolled theory, as expected given the strong coupling nature of the problem. Still,



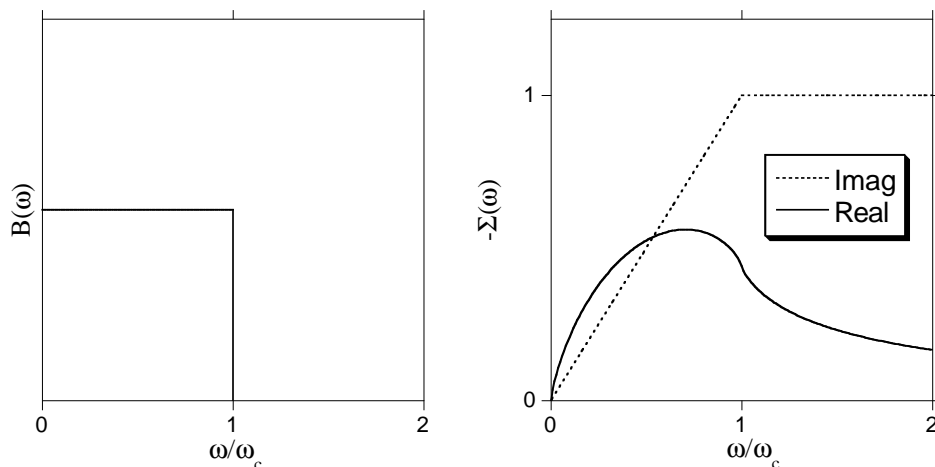


**Figure 17.** Bosonic spectrum which yields a marginal Fermi liquid (left panel). Resulting real and imaginary parts of the electron self-energy (right panel).  $\omega_c$  is the ultraviolet cut-off.  $T=0$ . Adapted from Ref.[55].

these calculations have given a number of important insights into understanding various excited state properties of the cuprates, particularly in the spin gap phase.

#### 2.4. Marginal Fermi Liquid

The striking linear temperature dependence of the in-plane resistivity led Varma and co-workers to propose a marginal Fermi liquid phenomenology [55] to explain many of the anomalous behaviors in cuprates. Their idea was that the electrons are interacting with a spectrum of bosonic excitations which has the following form (left panel, Fig. 17)

$$B(\omega) \propto \min(\omega/T, 1) \quad (1)$$

That is, the bosonic spectrum has no other energy scale present besides the temperature, that is, it exhibits quantum critical scaling. Such a spectrum, though, does not yield a convergent fermion self-energy, necessitating the presence of an ultraviolet cut-off,  $\omega_c$ , in the theory. At zero temperature, the resulting self-energy is (right panel, Fig. 17)

$$\begin{aligned} \text{Im}\Sigma &\propto \omega \\ \text{Re}\Sigma &\propto \omega \ln \frac{\omega}{\omega_c} \end{aligned} \quad (2)$$

This result, obtained by a convolution of  $B$  and  $\text{Im}G$  (where  $G$  is the bare fermion Greens function) can be most easily appreciated by noting that for electrons interacting with an Einstein mode,  $B(\omega) = \delta(\omega - \omega_0)$ ,  $\text{Im}\Sigma$  is a step function, ( $\text{Im}\Sigma = 0, \omega < \omega_0$ ;  $\text{Im}\Sigma \propto 1, \omega > \omega_0$ ). For an array of  $\delta$  functions for  $B$ ,  $\text{Im}\Sigma$  becomes a ramp of steps, which in the limit as the energy spacing of the  $\delta$  functions goes to zero becomes a linear  $\omega$  behavior.

The “marginal” notation comes from the fact that the quantity  $1 - d\text{Re}\Sigma/d\omega$  is logarithmically divergent as  $\omega$  approaches 0. As a result, the momentum distribution function,  $n(k)$ , no longer has a step discontinuity at  $k_F$  as in a Fermi liquid, but rather

an inflection behavior. This logarithm is cut-off by the temperature, and a standard calculation of the longitudinal conductivity leads to a linear temperature dependence of the resistivity [55].

Although an attractive phenomenology for thinking about various properties of the cuprates, the deficiency of the model is that there is no explicit momentum dependence, leading to the question of where d-wave pairing would come from. In later work, Varma has claimed that d-wave pairing could arise from vertex corrections [31], but certainly the underlying microscopics behind this very successful idea remain somewhat unclear at the present time.

These problems have led to a proposal of another phenomenology to explain transport data, the “cold spots” model of Ioffe and Millis [127]. In this picture, there is a Fermi liquid like scattering rate, but it is confined to the vicinity of the d-wave nodes. Such a model can reproduce the linear  $T$  resistivity, but this nice idea now seems to be ruled out by recent photoemission data which find that even at the d-wave node,  $Im\Sigma$  has the linear  $\omega$  behavior [128] predicted by the marginal Fermi liquid phenomenology [55].

The MFL phenomenology can be easily extended to the superconducting state. Since the  $B(\omega)$  spectrum is considered to be electronic in origin, then it will acquire a  $2\Delta$  gap in the superconducting state (see bubble in the left panel, Fig. 5), thus being able to account for the scattering rate gap seen in various measurements [129, 130]. Such a “gapped marginal Fermi liquid”, though, cannot account for all observations, and has to be supplemented by collective effects [131], which we now discuss.

### 2.5. $SO(5)$

Inelastic neutron scattering measurements by the group of Rossat-Mignod [132] revealed the presence of a narrow (in energy) resonance in the superconducting state of YBCO in a small region of momentum centered at the  $(\pi, \pi)$  wavevector [132]. Subsequent polarized measurements by the Oak Ridge group [133] verified that the resonance was magnetic in character. Since the BCS ground state involves  $S=0$  pairs with zero center-of-mass momentum, this implies that this excited state must involve  $S=1$  pairs with center-of-mass momentum  $Q = (\pi, \pi)$ . To see this, note that because of the energy gap, only pair creation processes are present in the particle-hole response at  $T=0$ , these processes being possible because of particle-hole mixing [134]. Since the magnetic signal detected by neutrons involves a spin flip process, then the excited pair must have spin one as the ground state is spin zero [135]. Fermion antisymmetry then implies that the excited pair has odd  $L$ . This is evident as well, since the d-wave gap function  $\cos(k_x) - \cos(k_y)$  translated by  $Q/2$  becomes  $\sin(k_x) - \sin(k_y)$  [135].

At first sight, such a triplet collective mode is a surprise, since they have never been found in classic superconductors. But in the d-wave case, since the order parameter changes sign under translation by  $Q$ , then the BCS coherence factor for the pair creation process takes its maximal value on the Fermi surface, as opposed to the s-wave case where

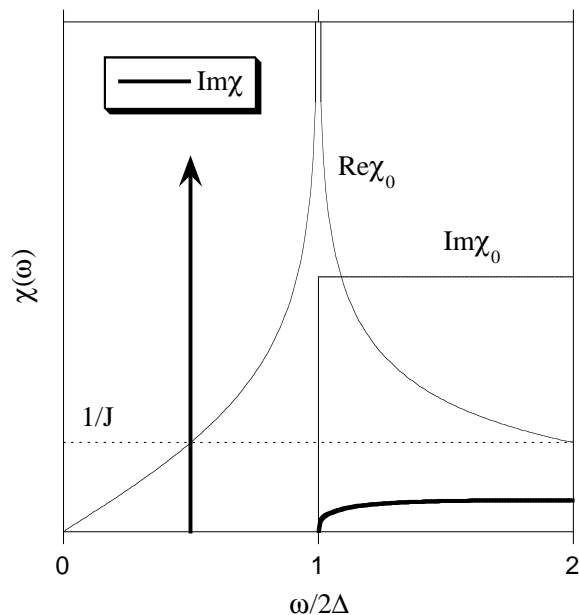


**Figure 18.** Real and imaginary parts of the bare bubble for a d-wave superconductor. Intersection of real part with  $1/J$ , where  $J$  is the superexchange energy, marks the location of the pole in the RPA response function (arrow).

it is zero [136]. The net result (Fig. 18) is that the imaginary part of the bare particle-hole response,  $\chi_0$ , has a step function jump from zero to a finite value at a threshold of  $2\Delta_{hs}$  [97, 14], where  $\Delta_{hs}$  is the value of the superconducting gap at the “hot spots” (points on the Fermi surface connected by  $Q$ ). By Kramers-Kronig,  $Re\chi_0$  will then have a logarithmic divergence at  $2\Delta_{hs}$  because of the step in the imaginary part. Thus, the full response function ( $\chi = \chi_0/(1 - J\chi_0)$ , where  $J$  is the superexchange energy) will always have an undamped pole at some energy less than the threshold energy. That is, linear response theory (RPA) for a d-wave superconductor predicts the presence of a spin triplet collective mode below the  $2\Delta$  continuum edge.

Experiments, though, reveal that the resonance energy does not depend on temperature, and its amplitude scales with the temperature dependence of the d-wave order parameter [137]. This is not easily understood in the “RPA” framework. This led Demler and Zhang to propose that the spin resonance was in fact a particle-particle antibound resonance (antibound, because the triplet interaction is repulsive). In such a picture, the resonance is always present, but can only be detected below  $T_c$  by neutron scattering because of particle-hole mixing, which allows the particle-particle resonance to appear in the particle-hole response [135]. This idea naturally resolves the two puzzles mentioned above. Although this original idea has been put into question on formal grounds by Greiter [138] (in the t-J model, the triplet interaction is formally zero), and on kinematics grounds by Tchernyshyov *et al* [139] (an antibound state is inconsistent with photoemission and tunneling, which indicate that the resonance has an energy lower than the two-particle continuum), the idea led Zhang to propose a very interesting SO(5) phenomenology to explain the cuprate phase diagram [140].

In the SO(5) picture, the “5” stands for the three degrees of freedom of the Neel order ( $N_x, N_y, N_z$ ), and the two degrees of freedom of the superconducting order (real and imaginary parts of  $\Delta$ ). In an imaginary world where these two order parameters were degenerate, then the underlying Hamiltonian would have SO(5) symmetry. This group has ten generators, the three components of the spin operator, the charge operator, and six new generators which rotate the “superspin” between the Neel and superconducting sectors. These new generators are nothing more than the spin resonance discussed above (a spin triplet pair with complex  $\Delta$ ). This idea provides a new framework for thinking about the phase diagram and the various collective excitations of cuprates [140]. Of course, cuprates are doped Mott insulators, and this effect is not present in the theory as stands (that is, charge fluctuations are suppressed strongly at low doping). This has led to the development of a version of the theory known as “projected SO(5)” where double occupation has been projected out [141]. One result of projected SO(5) theory is the claim that it explains the “d-wave-like” dispersion of the valence band seen in the undoped insulator by ARPES [142].

### 2.6. Stripes

A number of models of correlated electron systems predict the presence of phase separation at small doping, with the system bifurcating into hole rich (metallic) and hole poor (magnetic insulating) regions. In some models, these regions form a lamellar pattern, i.e., one dimensional “stripes”.

To connect with experiment, it had been known for some time that inelastic neutron scattering experiments for LSCO indicated the presence of four incommensurate peaks displaced a distance  $\delta$  from the commensurate wavevector  $Q = (\pi, \pi)$  which characterizes the magnetic insulator (right panel, Fig. 10) [94]. The standard way of thinking about these peaks was that they were due to the Fermi surface geometry [143].

An alternate way, though, was to consider having holes residing in 1D stripes, with magnetic domains between these stripes (left panel, Fig. 10). Even if the local ordering within the magnetic domains is commensurate, if the stripes represent an antiphase domain wall, then neutron scattering will see incommensurate magnetic peaks, with  $\delta$  a measure of the spacing between the stripes. Since the hole density is the doping, then this predicts that  $\delta$  will have a linear variation with doping. This is indeed what is seen in LSCO, and is known as the Yamada plot [144]. Associated with these magnetic peaks should be charge peaks at positions of  $2\delta$  relative to the Bragg peaks. These have been observed as well (right panel, Fig. 10) [90].

An attractive feature of the stripes model is its 1D physics [89]. The jury is still out whether Fermi liquids are inherently unstable in 2D [29], but they definitely are in 1D. So, such 1D models naturally contain non Fermi liquid normal states exhibiting spin-charge separation. Moreover, in this picture, the pseudogap is nothing more than the spin gap associated with the magnetic domains. Pairs of holes from the stripes can obtain pairing correlations by virtually hopping into the magnetic

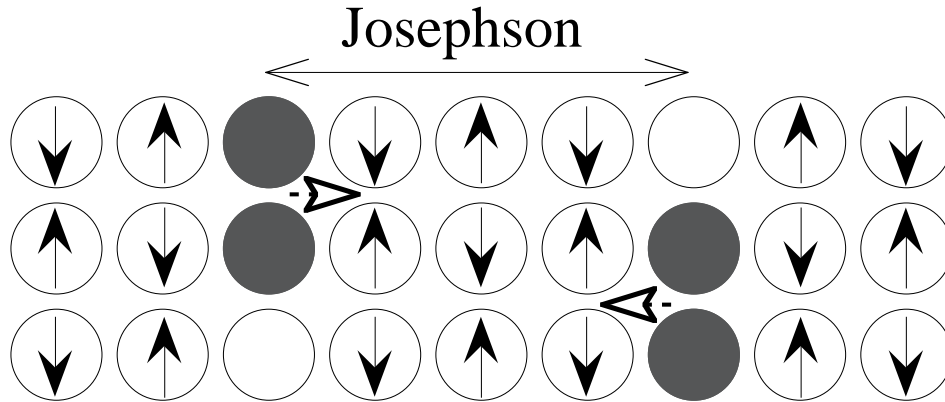


**Figure 19.** Stripes model for cuprates. Pairs of doped holes (dark circles) virtually hop into AF (spin gap) domains, acquiring spin pairing correlations. Josephson coupling of the stripes leads to long range superconducting order. Adapted from Ref. [89].

domains (the fluctuating Neel order in the magnetic domains favors antiparallel spins on neighboring Cu sites). Below some temperature, the stripes phase coherently lock via Josephson coupling, leading to long range (3D) superconducting order (Fig. 19). That is, the system crosses over from a 1D non-Fermi liquid normal state to a 3D coherent superconducting state [89].

### 2.7. Pseudogap

Most authors agree that the superconducting state is isomorphic to a BCS ground state of d-wave pairs. There is no agreement, however, on the nature of the pseudogap phase. The general hope is that once the pseudogap phase is sorted out experimentally, then the number of possible theories for cuprates will be drastically reduced.

One general class of theories is that the pseudogap phase represents preformed pairs [57]. Cuprates are characterized by short superconducting coherence lengths, low carrier densities, and quasi-two dimensionality. All of these conditions favor a suppression of the transition temperature relative to its mean field value due to phase fluctuations. In the intermediate region between these two temperatures, preformed pairs are possible. The cuprates, though, are not in the Bose condensation (local pair) limit, in that photoemission still reveals the presence of a large Fermi surface (in the Bose limit, the chemical potential would actually lie beneath the bottom of the energy band). Still, specific heat data clearly reveal the non-mean-field like character of the superconducting phase transition, particularly for underdoped samples [145].

The “RVB” picture has subtle differences from that of pre-formed pairs. In this case, the pseudogap phase is a spin gap phase (that is, the spins bind into singlets). As an electron is a product of spin and charge, then real electrons acquire an energy gap because of the spin gap, though charge excitations confined to the plane do not. At low enough temperatures, the doped holes become phase coherent, leading to rebinding of

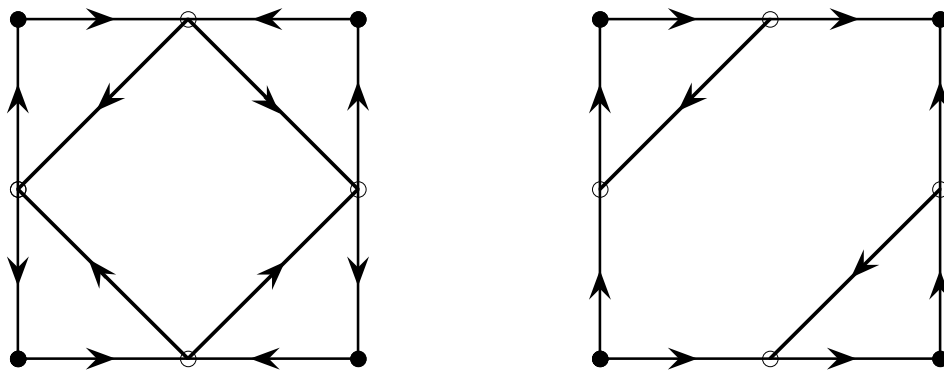


**Figure 20.** Orbital currents states proposed by Varma (Ref. [80]). Solid dots are Cu ions, open dots O ions, and arrows are bond currents. The right panel has a form factor consistent with recent ARPES results [79].

spin and charge, and the formation of a true superconducting ground state. The stripes picture is not unrelated to the RVB picture, in that the pseudogap is due to the spin gap present in the magnetic insulating domains between the stripes.

In the other class of scenarios, the pseudogap is not related to superconductivity per se, but rather is competitive with it. Most of these scenarios involve either a charge density wave or spin density wave, usually without long range order. As the spectral gap associated with the ordering grows with reduced doping, then more and more of the Fermi surface becomes unavailable for pairing, leading to an increasing suppression of the superconducting transition temperature on the underdoped side. This is an old idea, going back to the A15 superconductors where the martensitic phase transition competes with superconductivity [146]. These models have a certain attractiveness, since the basic physics can be appreciated at the mean field level.

The most interesting example of the competitive scenario is that of orbital currents. These involve bond currents either circulating around an elementary plaquette of four coppers (middle panel, Fig. 16) [75, 76, 126, 125, 77] or within a subplaquette involving just the Cu-O bonds (Fig. 20) [31, 80]. So far, only two pieces of experimental evidence point to such a state. Inelastic neutron scattering experiments find small moment magnetism in underdoped YBCO whose form factor drops off more rapidly in momentum space than that associated with Cu spins [78], indicating the presence of a moment extended in real space. And recent circularly polarized ARPES experiments reveal the presence of time reversal symmetry breaking below  $T^*$  [79], whose form factor in momentum space (if interpreted in terms of orbital currents) favors the Varma picture [80].

One of the most interesting aspects of the competitive scenarios is the prediction of a quantum critical point where the pseudogap effect disappears. From experiment, it has been claimed that the  $T^*$  line passes through the  $T_c$  line and vanishes within the superconducting dome at a concentration of 19%, just beyond optimal doping (Fig. 9) [81].

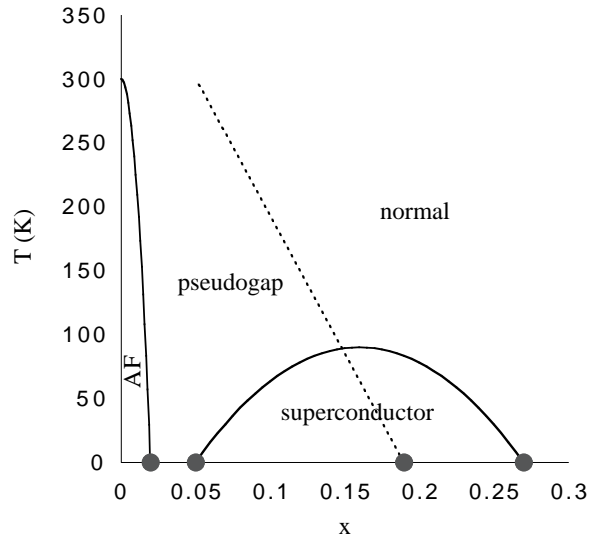


**Figure 21.** Four possible quantum critical points (dark circles) in the cuprate phase diagram. Dotted line is the pseudogap phase line.

In fact, there are several possible quantum critical points in the cuprate phase diagram (Fig. 21). Starting from the undoped material, as the doping progresses, one first finds the point where the Neel temperature vanishes, then the point where superconductivity first occurs, then the critical point mentioned above, and finally at higher doping the point where superconductivity disappears, for a total of four possible quantum critical points. The last point may correspond to where the Fermi surface topology changes from hole-like to electron-like (that is, the saddle point in the dispersion at  $(\pi, 0)$  passes through the Fermi energy), as there is some evidence of this from ARPES.

It remains to be seen whether the “quantum critical paradigm” with its emphasis on competing phases is the proper way of thinking about cuprates [147]. It has certainly led to an enrichment in our understanding of these novel materials [148].

### 3. Photoemission

#### 3.1. General Principles

As emphasized by Anderson, angle resolved photoemission has emerged as one of the most important spectroscopic probes of cuprate superconductors, in some sense playing the role that tunneling spectroscopy played in conventional superconductors [29]. Of course, much has been discovered about cuprates using tunneling, but Anderson’s statement was meant to emphasize the fact that photoemission played no role in the past, and then all of the sudden stepped up to play a major role in the cuprate problem. For those of us working in the “old days”, these developments have been nothing short of amazing.

To understand how this came about, a few comments are in order about

photoemission. This technique has a venerable history; in fact, it was for explaining the photoelectric effect, discovered by Hertz in 1887, that Einstein got his Nobel prize. Although the concept for doing angle resolved experiments had been recognized, the general perception was that not much useful would be learned. This changed in the early 1960s when Spicer developed the three-step model for photoemission, showing that in principle, important information about the electronic structure could be elucidated. Subsequent experiments by a number of groups, including Dean Eastman's, were able to determine the electronic dispersion of transition metals using this technique [149]. For these developments, Spicer and Eastman received the Buckley Prize in 1980.

The technique involves shining photons on a sample with a specific energy. If the photons have an energy larger than the work function of the metal, then electrons will be emitted. In angle resolved mode, an electrostatic detector measures the azimuthal and polar angles of the electrons (relative to the surface normal), as well as their energy. Knowing the energy of the photon, then the initial energy of the electrons in the crystal can be determined, as well as the components of the momentum parallel to the sample surface. In principle, the perpendicular component of the momentum is also determined from the energy-momentum relation (the electrons in vacuum having an energy which is quadratic in momentum), but there are subtleties connected with the breaking of the crystal symmetry by the surface in this direction.

The actual photocurrent is very complicated, since it is formally a three current correlation function (this is the so-called one-step model for photoemission). But in the three-step approximation of Spicer, where the initial electron is photoexcited, this photoelectron transports through the crystal, then out in the vacuum to the detector, the photocurrent (for one band) can be written as

$$I(\mathbf{k}, \omega) = c_{\mathbf{k}} \int_{\delta\mathbf{k}} d\mathbf{k}' \int d\omega' A(\mathbf{k}', \omega') f(\omega') R(\omega, \omega') \quad (3)$$

where  $c_{\mathbf{k}}$  is the modulus squared of the matrix element of the operator  $\mathbf{A} \cdot \mathbf{p}$  between initial and final states ( $\mathbf{A}$  is the vector potential,  $\mathbf{p}$  the momentum operator),  $A$  the single particle spectral function ( $-ImG/\pi$ , where  $G$  is the electron Greens function),  $f$  the Fermi-Dirac function, and  $R$  the energy resolution function (a gaussian). The momentum integration is a window ( $\delta\mathbf{k}$ ) centered about  $\mathbf{k}$  which represents the finite momentum resolution of the spectrometer. This expression assumes the impulse (or sudden) approximation, where the interaction of the photoelectron with the photohole is ignored. Moreover, the expression implicitly assumes the 2D limit, which fortunately is relevant for the cuprate case, where  $k_z$  dispersion effects are weak ("bilayer splitting" is a different matter).

The significance of this expression is obvious. The single particle spectral function is the simplest quantity which emerges from a many-body theory of electrons. We note that  $G^{-1}(\mathbf{k}, \omega) = \omega - \epsilon_{\mathbf{k}} - \Sigma(\mathbf{k}, \omega)$  where  $\epsilon$  is the bare energy and  $\Sigma$  the Dyson self-energy. A simple example of this is BCS theory, where  $\Sigma_{BCS}(\mathbf{k}, \omega) = \Delta_{\mathbf{k}}^2/(\omega + \epsilon_{\mathbf{k}})$ . Since the momentum distribution function (many-body occupation factor) is given by  $n_{\mathbf{k}} = \int d\omega A(\mathbf{k}, \omega) f(\omega)$ , then modulo resolution and dipole matrix elements, the



frequency integral of the ARPES spectrum is  $n_{\mathbf{k}}$  [150].

One problem with photoemission is that it is a surface sensitive probe, particularly for the low energy ( $\sim 20$  eV) photons typically used to achieve high energy and momentum resolution. Even in the quasi-2D cuprates, this can lead to problems unless a natural cleavage plane exists. This is why most measurements have been done on BSCCO, which contains a double BiO spacer layer, with the two BiO layers having the biggest interplanar separation in the cuprates (these layers are at a separation typical of van der Waals interactions). This provides the best possible cleavage in the cuprates. The penalty one pays is that the BiO layers have planar bonds which are longer than the CuO bonds. The material tries to compensate for this by developing a superstructure deformation of the BiO planes. This can lead to “ghost” images of the main CuO signal due to diffraction of the photoelectrons off the BiO surface layer, which have to be taken into account when interpreting ARPES spectra [151].

The advantage of ARPES, though, is now obvious. It is both a momentum and frequency resolved probe. The only other probe comparable to this is inelastic neutron scattering, which measures a more complicated function (the spin part of the particle-hole response). Such a momentum resolved probe was not essential in classic s-wave superconductors where momentum dependent effects are not important, but we know they are essential to consider in the d-wave case. This is an obvious advantage of ARPES over tunneling, though the latter still has much better energy resolution, and has the advantage of being able to see unoccupied states as well. On the other hand, important spatial information can be obtained by STM, which measures the local density of states, which is beyond the scope of this review.

The true impact of ARPES was recently realized by the development of the Scienta detector, which allows collection of data simultaneously as a function of momentum and energy. In angle integrated mode, energy resolutions of order 2 meV become possible, allowing even conventional superconductors to be studied by photoemission [152]. But even though the energy resolution is not as good in angle resolved mode (typically 10-20 meV), it is adequate for the cuprates, and the momentum resolution is quite good, of order 0.005 of a reciprocal lattice vector. This precision in momentum allows fine details of the spectral function to now be resolved. It is certainly a far cry from the pre-cuprate era, when momentum resolutions were typically 0.1 of a reciprocal lattice vector, and energy resolutions were typically 100 meV.

The power of the Scienta detectors can be appreciated by looking at the expression for the spectral function

$$A(\mathbf{k}, \omega) = \frac{1}{\pi} \frac{Im\Sigma(\mathbf{k}, \omega)}{(\omega - \epsilon_{\mathbf{k}} - Re\Sigma(\mathbf{k}, \omega))^2 + (Im\Sigma(\mathbf{k}, \omega))^2} \quad (4)$$

In the past, spectra were typically analyzed at fixed  $\mathbf{k}$  as a function of energy (EDC). This energy lineshape is obviously complicated given the non-trivial  $\omega$  dependence of  $\Sigma$ . But at fixed  $\omega$  as a function of  $\mathbf{k}$  instead, the momentum lineshape (so-called MDC [128]) is considerably simpler. In the normal state near the Fermi energy, we can typically linearize  $\epsilon_{\mathbf{k}}$  in momenta normal to the Fermi surface. As long as  $Re\Sigma$  can also

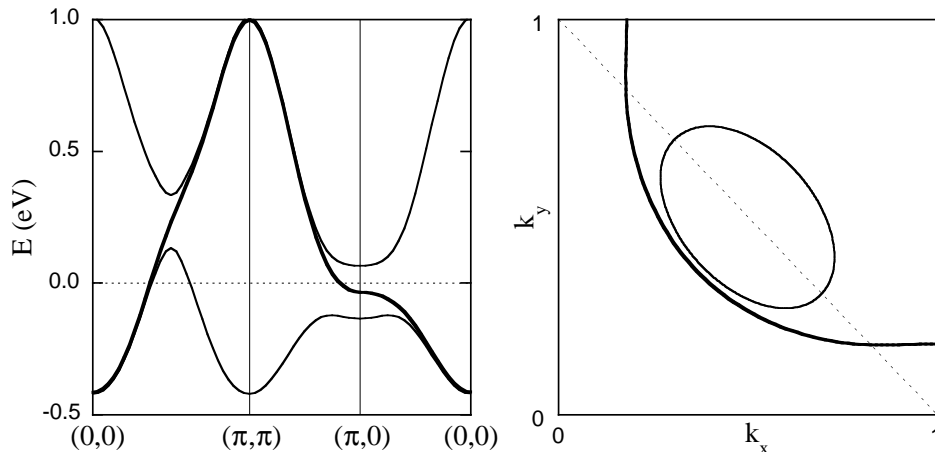


**Figure 22.** Left panel is the dispersion in the non magnetic phase (thick line) and magnetic phase (thin lines), the latter assuming an SDW gap of 200 meV. Resulting Fermi surfaces are shown in the right panel, with the dashed line the magnetic zone boundary.

be linearized, then the MDC reduces to a Lorentzian, with half width  $\Sigma(\omega)/v_{F0}$ , where  $v_{F0}$  is (modulo  $d\text{Re}\Sigma(k)/dk$ ) the bare Fermi velocity (obtained from  $\epsilon_{\mathbf{k}}$ ) [153]. Given an estimate for the bare velocity, then  $\text{Re}\Sigma$  can be read off from the MDC dispersion, and  $\text{Im}\Sigma$  from the MDC width, though it should be noted that the latter is only true if the resolution is accounted for in the analysis.

### 3.2. Normal State

The undoped version of the cuprates is a magnetic insulator. Simple considerations lead one to expect that the valence band maximum is at the  $(\pi/2, \pi/2)$  points of the zone (left panel, Fig. 22). This has been beautifully confirmed by photoemission measurements [85]. When hole doping such a state, then one might expect to form small hole pockets with volume  $x$  centered at these points (right panel, Fig. 22). This would certainly be consistent with transport and optics data, which indicate a carrier density of  $x$ . Somewhat surprisingly, though, this is not what is seen by ARPES [154]. Rather, what is seen is a large hole surface (right panel, Fig. 22) with volume  $1+x$  centered about the  $(\pi, \pi)$  points (remembering the full Brillouin zone corresponds to 2 filled states because of spin degeneracy). This is more or less what is predicted by paramagnetic band theory. To be consistent with transport, this would mean that the spectral weight would have to scale with  $x$ . This was subsequently found to be the case from ARPES, first at the  $(\pi, 0)$  points in Bi2212 [155, 156, 157], then most recently along the nodal direction in LSCO [74]. In some sense, the Fermi surface disappears by losing its spectral weight, much like the Cheshire Cat in Alice in Wonderland.

The energy dispersion seen in the doped case involves the presence of a saddle point at  $(\pi, 0)$  on the occupied side which is relatively close to the Fermi energy (left panel, Fig. 22). This has led to many theories based on van Hove singularities in the

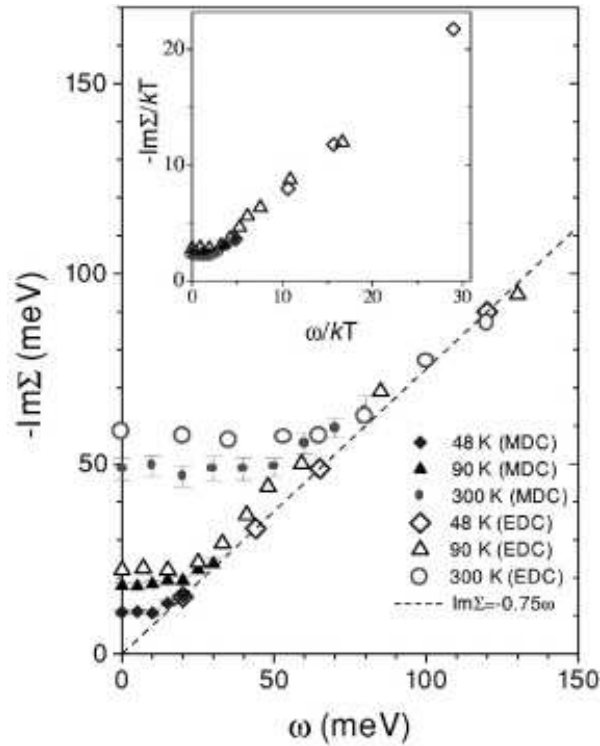


**Figure 23.** Imaginary part of the self-energy determined by ARPES along the nodal direction in Bi2212, demonstrating marginal behavior (quantum critical scaling) as a function of both  $\omega$  and  $T$ . From Ref. [128].

density of states. The dispersion near the saddle point is quite flat, especially in the superconducting state, which has led to the “extended” van Hove singularity concept proposed by Abrikosov [158]. As the hole doping increases, the saddle point approaches the Fermi energy. In the case of Bi2201, which can be heavily overdoped, the saddle point appears to be almost degenerate with the Fermi energy at a concentration where  $T_c$  is essentially zero [159]. Beyond this concentration, the saddle point is expected to pass through the Fermi energy, leading to an electron surface centered at  $(0, 0)$ . There is evidence from ARPES that this occurs in LSCO [160]. This would be consistent with Hall measurements, which see a sign change in the Hall number near this concentration [161].

This dispersion, though, should be taken with a very large grain of salt. In particular, no well defined spectral peaks appear in the normal state, at least for optimal and underdoped samples. That is, the widths of the peaks are of order their energy separation from the Fermi energy. This is why no van Hove singularity in the density of states has been inferred from any experimental measurement.

The momentum and energy dependence of the spectral peaks in the normal state was of great interest from the beginning. The original ARPES analysis of Olson *et al* [162] found the peak width to scale linearly with peak energy. This is the behavior predicted by the marginal Fermi liquid phenomenology [55]. This behavior has been

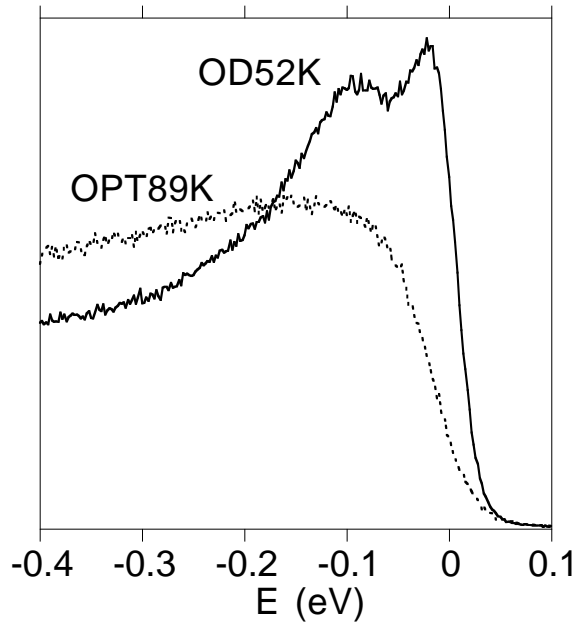


**Figure 24.** ARPES spectrum at  $(\pi, 0)$  for optimal doped and overdoped Bi2212 samples in the normal state. Separate peaks in the overdoped case are due to bilayer splitting. Data from Ref. [167].

confirmed to much better precision with high momentum resolution data along the nodal direction (Fig. 23) [128], which also indicate a linear  $T$  dependence of the linewidth as well.

The momentum anisotropy of the linewidth, though, is still a matter of controversy. Data for optimal doping indicate that the linewidths get broader as the  $(\pi, 0)$  point is approached. This is as opposed to heavily overdoped Bi2201, where the lineshape is relatively isotropic around the Fermi surface. Such momentum anisotropies are not unexpected, given that the d-wave nature of the superconducting order parameter implies momentum dependent interactions. On the other hand, some authors have suggested that the intrinsic lineshape might be fairly isotropic, with the observed anisotropy in Bi2212 a combination of overlap of features due to the “ghost” images associated with the superstructure, along with bilayer splitting of the energy bands [163].

The issue of bilayer splitting has been somewhat controversial, and thus deserves some attention. Most experiments have been done in Bi2212, which has two CuO layers in each formula unit, the two layers being separated by Ca ions. Mixing of the levels on the two planes will lead to an antibonding and bonding combination, thus bilayer splitting (Fig. 24). Band theory predicts that the splitting should be sizable (of order 1/4 eV), with the splitting varying with planar momentum like  $(\cos k_x - \cos k_y)^2$ . Therefore, the effect is largest at  $(\pi, 0)$  [164]. As spectral peaks are broad in the normal state, then it is quite possible that the two overlapping features would smear together into a single feature, making the  $(\pi, 0)$  lineshape look anomalously broad.

Most early reports of bilayer splitting were later attributed to the “ghost” images

associated with the superstructure. The claim was that once this was factored out, no bilayer splitting was apparent in the data, at least for an optimal doped sample [165]. This was of interest, since several theories of cuprates predicted incoherent behavior along the  $c$ -axis in the normal state [29].

Subsequent measurements at high momentum resolution, though, revealed the presence of bilayer splitting in heavily overdoped samples [166]. The  $(\pi, 0)$  spectrum is characterized by a relatively sharp antibonding peak near the Fermi energy (consistent with the more Fermi liquid like character of heavily overdoped samples), plus a broader (bonding) peak at higher binding energy (its width being larger due to its greater binding energy). This leads to a peak-shoulder type spectrum, as opposed to the single broad spectrum seen for optimal and underdoped samples (Fig. 24). The doping dependence of the bilayer splitting, though, is still a controversial issue. Recently, Campuzano's group has presented evidence that bilayer effects disappear in the "strange metal" (quantum critical) phase of Fig. 6 [167].

### 3.3. Superconducting State

There are two remarkable features revealed by ARPES in the superconducting state. First, the opening of an anisotropic superconducting gap in the spectrum. Second, the appearance of a sharp coherent peak below  $T_c$ .

The first observation of a gap was made in 1989 by Yves Baer's group [168], and was considered a tour-de-force at the time. Later, angle resolved, measurements did not detect any gap anisotropy, probably due to the sample qualities at the time. This all changed in 1993 with the observation by Z-X Shen's group of an anisotropic gap consistent with  $d$ -wave symmetry [42].

Not all groups found this behavior, though. It was realized later that the discrepancies were due to complications caused by the "ghost" images associated with the Bi2212 superstructure. Once this was appreciated, then it was evident that the best results could be obtained in the  $Y$  quadrant of the Brillouin zone where these images were well separated from the main image. By fitting the leading edge of the spectrum (taking into account the known resolution), precise values of the energy gap can be obtained. The resultant plot of the gap along the Fermi surface shows a clear V-shaped behavior around the node, as expected for  $d$ -wave symmetry (left panel, Fig. 25) [169]. Moreover, the functional dependence on momentum is precisely of the form  $|\cos k_x - \cos k_y|$  [42, 169] as would be expected for pairs of electrons sitting on near neighbor Cu sites. In fact, along the observed Fermi surface, the functional dependence is essentially  $\cos(2\phi)$ , where  $\phi$  is the angle of the line connecting  $(\pi, \pi)$  to the Fermi surface with the line  $(\pi, 0) - (\pi, \pi)$ . Subsequent measurements have revealed a deviation from this form with increasing underdoping (right panel, Fig. 25) [170], which can be fit by inclusion of the next harmonic in the gap expansion,  $\cos(6\phi)$ , which is related to  $\cos 2k_x - \cos 2k_y$ . This indicates that the pair interaction is becoming longer range in real space as the doping is reduced. The trend is expected, given that the correlation

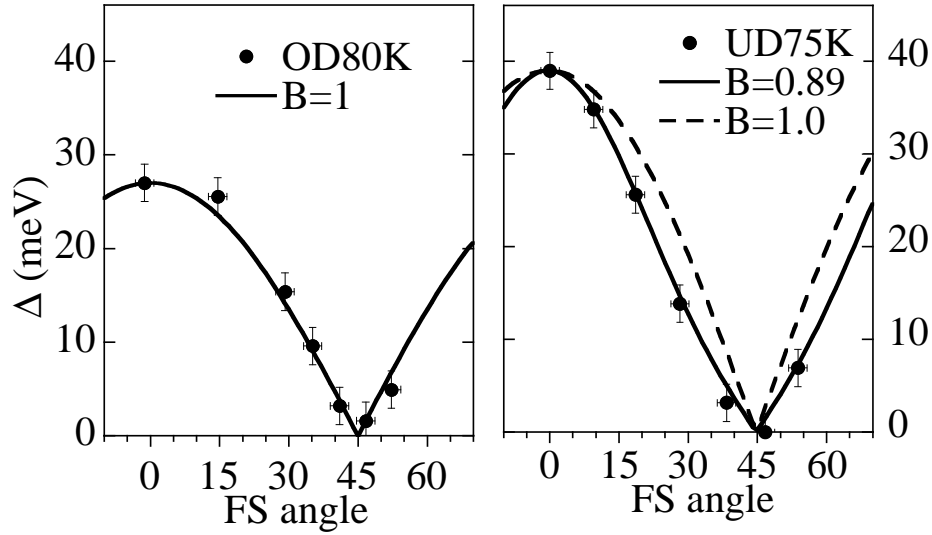


**Figure 25.** Doping dependence of the spectral gap in Bi2212 from ARPES. Left panel for an overdoped sample, right panel for an underdoped one.  $B=1$  is a  $\cos(2\phi)$  dependence of the gap on Fermi surface angle, solid line in the right panel includes a contribution from the next d-wave harmonic,  $\cos(6\phi)$ . From Ref. [170].

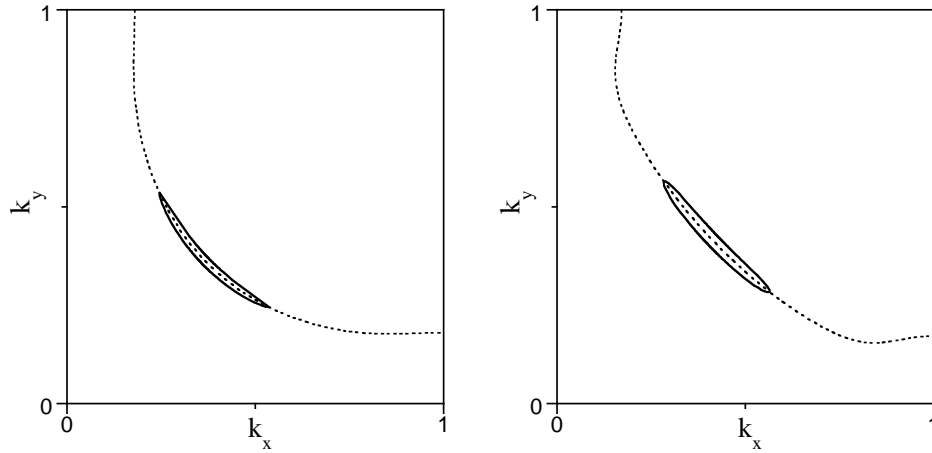


**Figure 26.** Left: Fermi surface (dashed line) and a constant energy contour for quasiparticle excitations in the d-wave superconducting state (solid line) based on ARPES data for Bi2212. Right: Modified version proposed to explain the incommensurability seen in neutron scattering data in YBCO. From Ref. [97].

length associated with magnetic fluctuations increases with underdoping. Recently, the same deviation from the  $\cos(2\phi)$  form has been inferred from Fourier transformation of STM data [104].

One of the most interesting aspects of the superconducting state is that the low energy states have a Dirac-like dispersion, i.e., Dirac cones, whose constant energy contours are centered about the nodes (actually, these contours are banana shaped due to the Fermi surface curvature, Fig. 26). According to ARPES, these cones are quite anisotropic, with the ratio of the velocity normal to the Fermi surface to that along

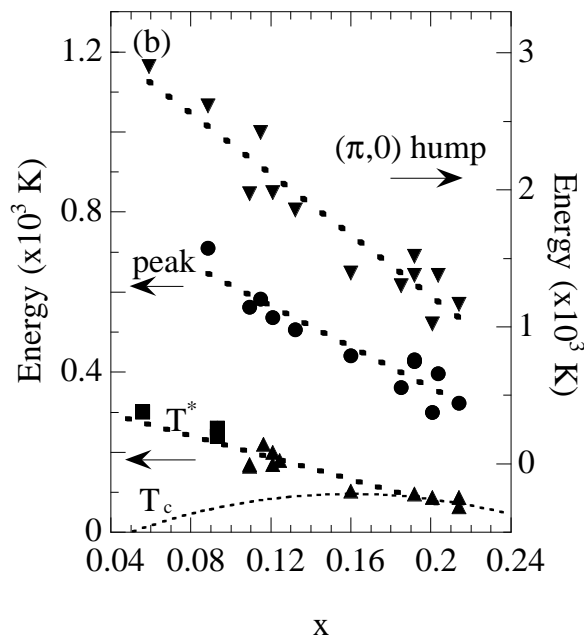


**Figure 27.** Spectral peak energy (maximum superconducting energy gap), energy of the hump, and pseudogap temperature,  $T^*$ , versus doping,  $x$ , from ARPES data on Bi2212. From Ref. [155].

the Fermi surface (the latter the slope of the gap around the node) of 20 [170]. This value has also been inferred from thermal conductivity measurements [171]. In principle, by comparison of this ratio to the value of the linear  $T$  coefficient of the penetration depth, important information can be obtained about the electromagnetic coupling of the quasiparticles. Present results are consistent with a linear doping variation of the particular Landau interaction parameter involved [170], but the associated error bars are quite large. More precise ARPES and penetration depth measurements on Bi2212 would be gratifying in this regard. In particular, the doping variation of the gap slope around the node has not been studied yet with high resolution detectors. It is of some interest to see whether this quantity scales with  $T_c$  on the underdoped side of the phase diagram. Recent thermal conductivity data indicate that this is not the case [172].

What is known, though, is that the maximum superconducting energy gap does not scale with  $T_c$  on the underdoped side (Fig. 27) [173, 155]. Instead, this quantity monotonically increases with underdoping, scaling with the pseudogap temperature,  $T^*$ . The same trend has been seen by tunneling [174]. The observed behavior would be consistent with  $T^*$  representing some mean field transition temperature for pairing. This doping trend was actually predicted many years ago by RVB theory [39], where the spin pairing energy scale is decoupled from the phase stiffness energy associated with the doped holes, since the latter is proportional to  $x$  (see Fig. 16).

The lineshape changes between normal and superconducting states, though, are perhaps the most fascinating aspect of the ARPES data (Fig. 28). The changes are most spectacular near the  $(\pi, 0)$  point for optimal and underdoped samples. As the

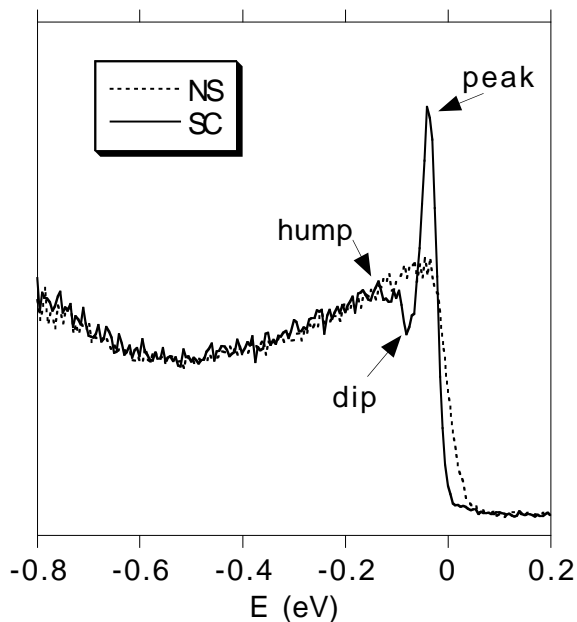


**Figure 28.** ARPES spectra at  $(\pi, 0)$  for an overdoped (87K) Bi2212 sample in the normal state (NS) and superconducting state (SC). Data from Ref. [180].

temperature is lowered, the broad peak in the normal state develops into a sharp coherent peak separated by a spectral dip (near  $(\pi, 0)$ ) or a spectral break (near the  $(\pi, 0) - (\pi\pi)$  Fermi surface crossing) from the higher energy incoherent part [150]. This behavior is consistent with a strong increase in the lifetime of the electrons as the temperature is lowered below  $T_c$ , as has been earlier inferred from microwave conductivity [46] and thermal conductivity [47] experiments. That is, a gap is being opened in the scattering rate, as also derived from infrared conductivity measurements [48]. In ARPES, this can be seen very clearly by “inverting” the data to directly extract the temperature dependence of the electron self-energy [175].

An alternate interpretation has been given to the data, however [176, 156, 157]. In this picture, a gap develops in the incoherent part of the spectrum, with a quasiparticle pole appearing inside the gap. The pole weight monotonically increases with decreasing temperature, and it has been suggested that this behavior tracks the superfluid density [156]. In some sense, this would imply that the quasiparticle weight was equal to the superconducting order parameter. One particular model which is suggestive of this is the Josephson coupling of stripes below  $T_c$  [89].

The remarkable spectral changes near  $(\pi, 0)$  leading to the unusual peak-dip-hump lineshape below  $T_c$  were actually first observed by tunneling [177]. When they were subsequently observed by ARPES, the obvious explanation was that they were due to bilayer splitting (the “hump” representing the bonding band, the “peak” the antibonding band). There are a number of arguments against this (including the fact that tunneling spectroscopy sees this lineshape for single layer materials like Tl2201). What is clear, though, is that bilayer splitting alone is not sufficient to explain the



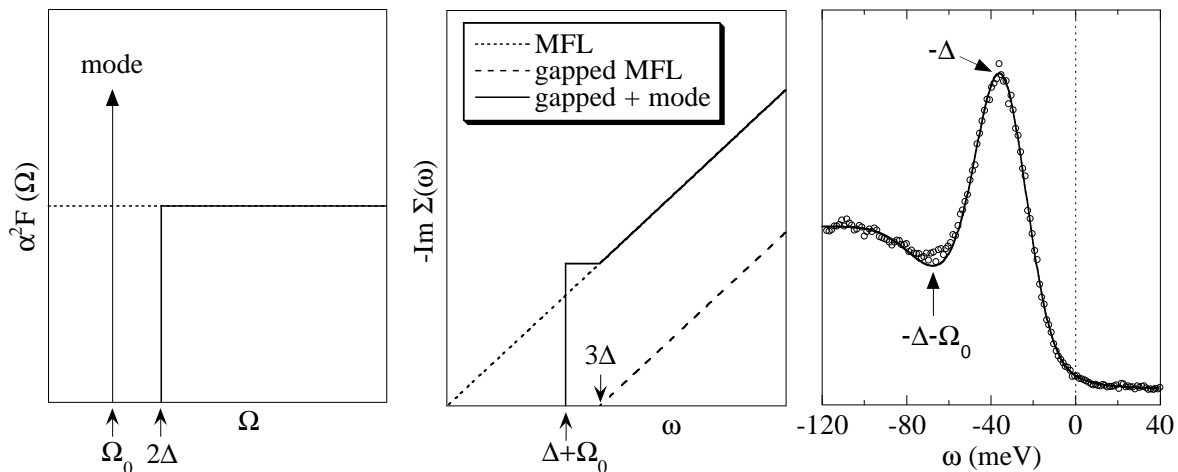


**Figure 29.** Left: boson spectrum (“ $\alpha^2 F$ ”) in the normal state (dashed line, corresponding to a marginal Fermi liquid) and superconducting state (solid line, corresponding to a gapped marginal Fermi liquid). The arrow marks the possibility of a collective mode with energy  $\Omega_0$  inside the continuum gap of  $2\Delta$  (corresponding to a gapped marginal Fermi liquid plus a mode). Middle: Resulting imaginary self-energy for the electrons. Right: Superconducting state spectral function from this model as compared to ARPES data at  $(\pi, 0)$  for slightly overdoped Bi2212. The mode energy,  $\Omega_0$ , equals the spin resonance energy determined independently from neutron scattering. Adapted from Ref. [131].

lineshape. In particular, the spectral dip represents a depletion of states which fills in as the temperature is raised [175]. Moreover, the dip energy scale appears to exist at the same energy throughout the Brillouin zone [153].

These considerations have led to many speculations that the spectral dip represents some sort of many body effect. One of the first treatments of this problem was by Arnold *et al* [178], where they applied the McMillan-Rowell “inversion” procedure [179] to the data to determine the boson spectral function from the frequency dependence of the gap function,  $\Delta(\omega)$ . From this analysis, a sharp bosonic mode was inferred at about 10 meV. The problem with this pioneering analysis was that it assumed the data represent an isotropic density of states proportional to  $\frac{\omega}{\sqrt{\omega^2 - \Delta^2(\omega)}}$ , with the spectral dip corresponding to a strong frequency variation of  $\Delta(\omega)$ . In this case, the “normal” part of the self-energy (diagonal in particle-hole space) drops out, and so all structure in the data can be associated with the pairing self-energy (off-diagonal part). This is not the case if the data represent a spectral function.

The data were later analyzed assuming the primary effects were due to the normal self-energy (the pairing part being treated in a BCS approximation) [131]. In this analysis, the spectral dip can be understood as a sharp threshold for inelastic scattering. To understand this, consider the Feynman diagram for an electron scattering off particle-hole excitations (left panel, Fig. 5). In the superconducting state, the particle-hole continuum will have a gap of order  $2\Delta$  (left panel, Fig. 29). If interactions are strong enough that a bound state (energy  $\Omega_0$ ) emerges inside of this continuum gap, then  $Im\Sigma$

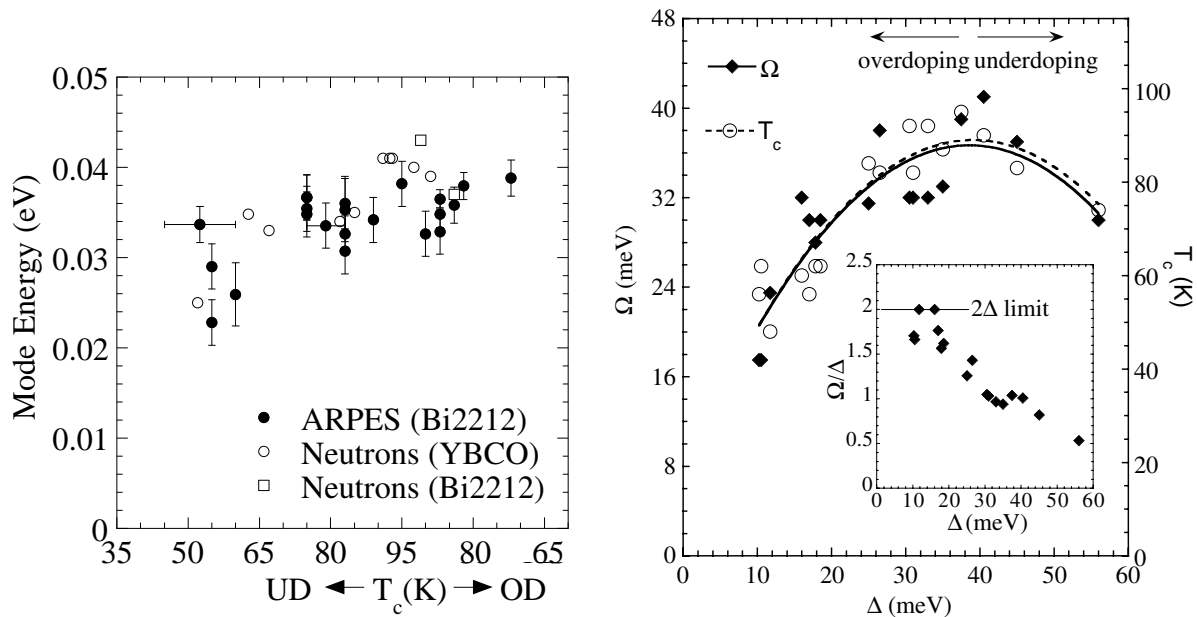


**Figure 30.** Left panel: mode energy inferred from ARPES as compared to that determined directly from neutron data, showing the two data sets agree. From Ref. [155]. Right panel: mode energy inferred from tunneling data, showing scaling with  $T_c$ . Inset demonstrates that the mode energy saturates to  $2\Delta$  in the overdoped limit. From Ref. [174].

will develop a sharp threshold, as implied by the data, at an energy  $\Delta + \Omega_0$  [180] (middle panel, Fig. 29). In this picture, the energy of the bosonic mode will be equal to the energy difference of the dip ( $\Delta + \Omega_0$ ) and the peak ( $\Delta$ ) [131, 181] (right panel, Fig. 29). Moreover, the resulting spectral function will consist of two features: a broad feature at higher binding energy whose dispersion roughly tracks the dispersion of the single feature in the normal state (hump), and a sharp, weakly dispersive feature for smaller binding energies representing the renormalized quasiparticle branch (peak). These two features are separated by the dip energy, which is roughly constant in momentum. This model gives a natural explanation of the unusual dispersions associated with the peak and hump [180].

Moreover, the peak-dip-hump is strongest at the  $(\pi, 0)$  points. As these points are connected by  $(\pi, \pi)$  wavevectors, this would imply that the bosonic excitations involved are associated with this wavevector [182]. This, coupled with the inferred mode energy (40 meV), points to the spin resonance as the boson [180]. At the time of this conjecture, the resonance had only been seen in YBCO, but later experiments found it in Bi2212 at the energy inferred from ARPES [183]. Despite this, a criticism offered against such an interpretation was that all energy scales from ARPES and tunneling appear to increase with underdoping (Fig. 27), but the resonance energy decreases [56]. This was answered later by a doping dependent ARPES study, which found that the mode energy inferred from the data had a doping dependence which indeed tracks the resonance energy (left panel, Fig. 30) [155]. This was confirmed in greater detail by

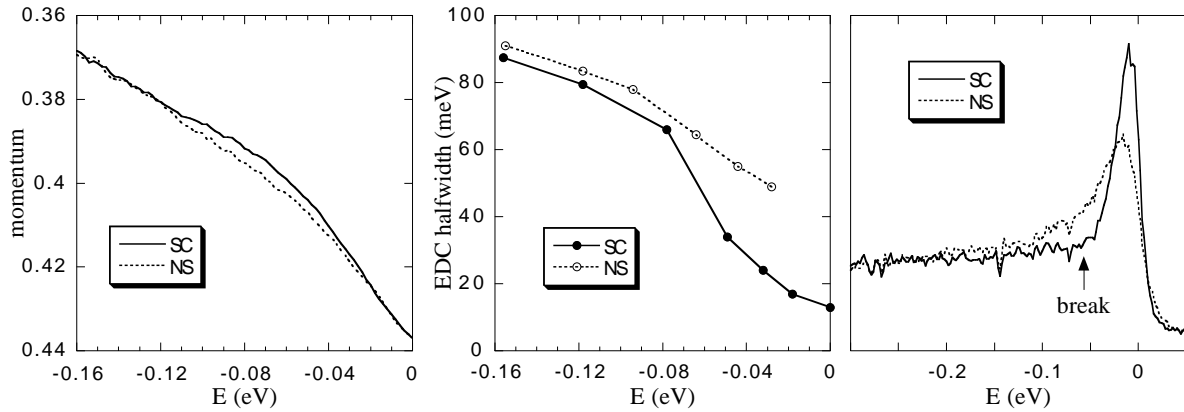


**Figure 31.** Left: Dispersion obtained from ARPES MDCs along the nodal direction for optimal doped (90K) Bi2212. The difference of the superconducting state (SC) as compared to the normal state (NS) gives rise to a kink in the dispersion. Middle: The change in the EDC linewidth, with the drop in the scattering rate in the superconducting state connected to the dispersion kink by Kramers-Kronig relations. Right: EDC at the nodal point. Note the break in the superconducting case marking the separation of the coherent peak from the incoherent part. Adapted from Ref. [153].

tunneling [174], where the energies were tracked over a larger doping range with higher energy resolution (right panel, Fig. 30). Not only were the inferred mode energy the same as the resonance energy, but the mode energy saturated to  $2\Delta$  in the overdoped limit as would be expected for a collective mode inside a continuum gap (inset, right panel, Fig. 30) [174].

There are other things revealed by the doping dependence of the ARPES data as well. Both the peak energy and the hump energy increase strongly with underdoping (Fig. 27), yet the ratio of their energies is roughly constant (3.5-4) as would be expected for a strong-coupling superconductor [155] (a result difficult to explain if their energy separation were simply due to bilayer splitting). Moreover, the hump dispersion (Fig. 36) increasingly begins to resemble that (Fig. 22) expected of a spin density wave insulator as the doping is reduced [155]. That is, as far as the hump dispersion is concerned, the wavevector  $(\pi, \pi)$  begins to look more and more like a reciprocal lattice vector. This is not unexpected, since as the resonance mode energy goes soft with underdoping, the material will be unstable to long range order at this wavevector.

Similar effects to the ARPES ones have been inferred from a generalized Drude analysis of optics data, where the gap in the optical scattering rate has been interpreted in a similar fashion [184]. On the other hand, the optical scattering rate resembles most closely the behavior of the ARPES self-energy at the node, rather than at the  $(\pi, 0)$  point [49] (not surprising, since as  $(\pi, 0)$  is a saddle point, the velocity there is zero, and so it does not contribute to the in-plane optical response).

As mentioned previously, the normal state scattering rate at the node from ARPES resembles that expected for a marginal Fermi liquid [162, 128]. What has been controversial, though, is how this scattering rate changes below  $T_c$ . The latest results

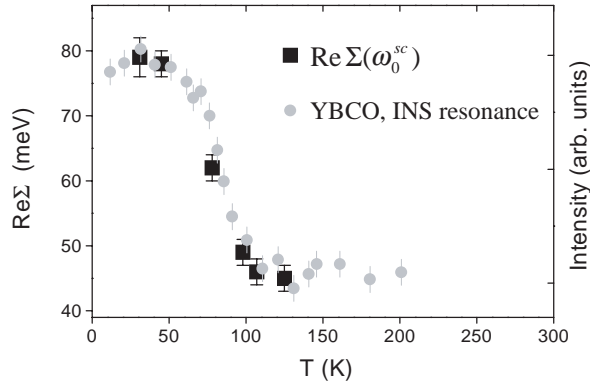


**Figure 32.** Variation of the real part of the self-energy at the kink energy with temperature as determined from ARPES for Bi2212, compared to the intensity of the magnetic resonance for YBCO. From Ref. [187].

are consistent with a strong drop in the scattering rate below some threshold energy (middle panel, Fig. 31) [49], though the expected superlinear behavior this implies with temperature has yet to be positively identified [128]. By Kramers-Kronig, this drop implies a “kink” in the dispersion (left panel, Fig. 31). For binding energies smaller than the “kink”, the spectral peak is sharper and less dispersive, for larger energies, broader and more dispersive. Surprisingly, the kink was not recognized at first (it was later identified by Shen’s group [185]). This kink is present throughout the zone [185], and occurs at the same energy as the “break” in the ARPES lineshape at the Fermi surface separating the quasiparticle peak from the incoherent part (right panel, Fig. 31) [49]. Moreover, it was later shown that this spectral break evolves into the spectral dip as the momentum is swept in the zone from the node to the  $(\pi, 0)$  point [153]. This led to the speculation that the “kink” effect was due to the resonance as suggested earlier for the spectral dip [180]. This was later confirmed by theoretical simulations [186]. Strong support for this conjecture was offered by data from Johnson’s group [187], where the energy scale associated with the kink was found to track in doping with the neutron resonance energy. More importantly, the change in the self-energy with temperature associated with the kink has the same temperature dependence as the resonance intensity (Fig. 32) [187].

This picture has been challenged by Shen’s group [188]. They observed that not only did the kink effect persist above  $T_c$ , it was universally present in all cuprates (Bi2212, Bi2201, LSCO) at roughly the same energy. They argued that this implied the effect was due to a phonon, since the dynamic spin susceptibility of Bi2212 and LSCO look very different. There is some attractiveness to this phonon picture, but one should recognize that (1) most of the “normal” state data were actually taken in the pseudogap phase and (2) the constancy of the energy scale is somewhat surprising in a phonon model as well, since the kink energy, even at the node, should be the sum of the maximum superconducting gap energy plus the mode energy (phonon or otherwise). Also, it is

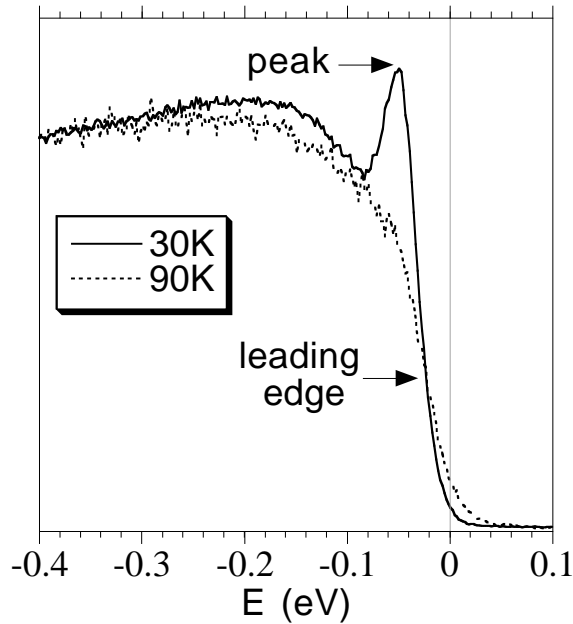


**Figure 33.** ARPES spectrum at  $(\pi, 0)$  for an underdoped Bi2212 sample in the superconducting state (30K) and the pseudogap phase (90K). The sharp peak in the superconducting state is replaced by a leading edge gap in the pseudogap phase. Data courtesy of A. Kaminski and J. C. Campuzano.

somewhat surprising that only a single phonon energy would appear in the data. Still, the arguments being invoked in the Lanzara *et al* paper [188] are quite important, in that they address the fundamental issue of whether the many-body effects in the cuprates should be associated with phonons (as in classic superconductors) or with electron-electron interactions (as has been commonly assumed in the literature).

### 3.4. Pseudogap Phase

ARPES has revealed many unique features connected with the pseudogap phase, and has had a profound influence on our understanding of this unusual state of matter.

We start our discussion by considering states near the  $(\pi, 0)$  point of the zone for underdoped samples. Upon heating above  $T_c$ , the sharp spectral peak disappears, but the leading edge of the spectrum is still pulled back from the chemical potential (leading edge gap, see Fig. 33) [68, 69]. This is quite unusual, in that the spectral function is completely incoherent in nature, but the leading edge is still quite sharp. As the temperature is raised, the leading edge gap appears to go away, with the leading edge becoming degenerate with the Fermi function at a temperature  $T^*$  [69], similar to  $T^*$  inferred from NMR measurements of the spin gap.

One of the more surprising findings, though, was that this leading edge gap has an anisotropy in momentum space quite similar to the d-wave gap in the superconductor (Fig. 8) [68, 69]. This has been taken as strong support for those theories proposing that the pseudogap involves pairs of some kind. In further support of this picture,

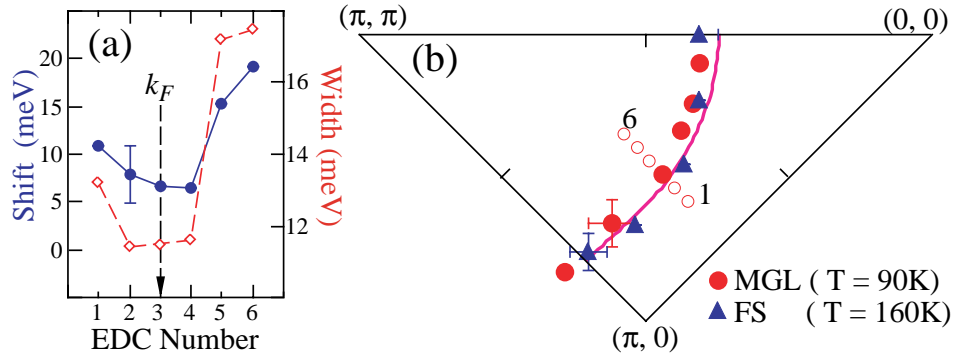


**Figure 34.** Left panel shows the determination of the minimum gap locus along a cut (open circles of right panel) in momentum space from the leading edge shift of ARPES EDCs. The right panel shows that the minimum gap locus (MGL) of the pseudogap phase matches the normal state Fermi surface (FS). From Ref. [71].

it was observed that the minimum gap locus coincided with the normal state Fermi surface (Fig. 34) [71], as occurs for superconductors. This set of points is obtained by taking various cuts in momentum space, and looking for that point along the cut where the leading edge gap is smallest. This behavior can be contrasted with a spin density wave precursor, for instance, where the minimum gap locus would have a new symmetry defined by the magnetic Brillouin zone boundary running from  $(\pi, 0)$  to  $(0, \pi)$  (see Fig. 22).

There are, though, a number of unusual features of the data which are not as easily understood in terms of a precursor pairing scenario. In particular, the pseudogap phase does not have a node like for a d-wave superconductor, instead, it possesses a “Fermi arc” (Fig. 8) centered at the d-wave node [67]. This arc expands in temperature, eventually recovering the full Fermi surface at  $T^*$  [73].

For states near the  $(\pi, 0)$  point, the pseudogap appears to fill in with temperature rather than close [73], much like what is observed in *c*-axis conductivity (Fig. 7) [65]. On the other hand, away from this region, the spectral gap clearly closes [73]. This is most easily visualized (Fig. 35) by “symmetrizing” the data (a way of removing the Fermi function from the data by assuming particle-hole symmetry in the spectral function). This behavior has been further confirmed by data fitting [189], where the spectral gap parameter,  $\Delta$ , at the antinode ( $(\pi, 0) - (\pi, \pi)$  Fermi crossing) is found to be relatively temperature independent. The self-energy has the form  $\Sigma = -i\Gamma_1 + \Delta^2/(\omega + i\Gamma_0)$ .  $\Gamma_1$  is a crude approximation for the normal self-energy (this term becomes strongly reduced in the superconducting state with the onset of coherence), whereas  $\Gamma_0$  is the lifetime of the pair propagator, which is proportional to  $T - T_c$ . Note the contrast with Eliashberg theory, where  $\Gamma_0$  would be equal to  $\Gamma_1$ . An incoherent spectrum with a pseudogap is formed when  $\Gamma_0 \ll \Delta \ll \Gamma_1$ . The strong temperature variation of  $\Gamma_0$  leads to a filling in of the pseudogap ( $\Delta$  being roughly constant in  $T$ ).  $T^*$  is then simply the temperature where  $\Delta = \Gamma_0(T)$ . This behavior can be contrasted with that away from the  $(\pi, 0)$  region, where  $\Delta$  closes with temperature in a BCS like fashion [189].

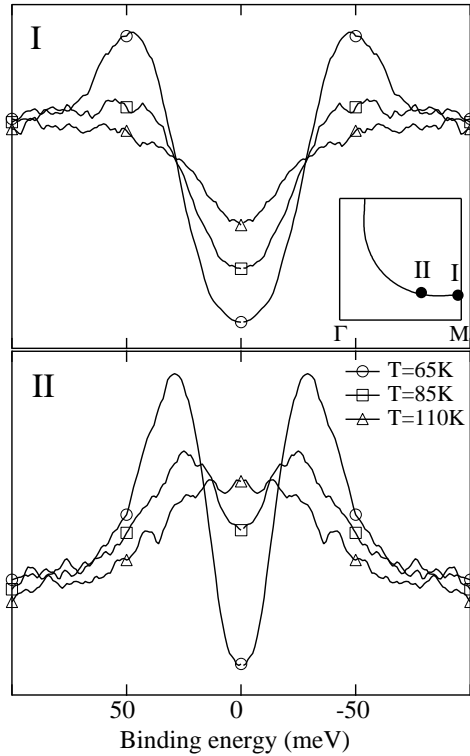


**Figure 35.** Filling in of the spectral gap at the antinode (I,  $(\pi, 0) - (\pi, \pi)$  Fermi crossing) as compared to the closing of the spectral gap about halfway between the antinode and the node (II). Symmetrized ARPES data for underdoped (75K) Bi2212 from Ref. [73].

These findings seem to imply the possibility of two regions in the Brillouin zone, a “pseudogap” region centered at the  $(\pi, 0)$  point and an “arc” region centered at the d-wave node. This picture would be in support of a competitive scenario, where the pseudogap and superconducting gap were different phenomena. On the other hand, newer high resolution data do not necessarily support the picture of two regions of the zone, rather it appears that the gap “closing” and gap “filling in” behaviors smoothly evolve into one another as a function of momentum. In fact, there are several pair precursor calculations [190, 191] which predict the presence of Fermi arcs. In the strong-coupling RVB approaches, these Fermi arcs are also found, and are due to fluctuations in the pseudogap regime between d-wave pairs and the staggered flux phase state, which are nearly degenerate in energy [126]. Arcs are also found in a one loop renormalization group treatment of interacting fermions in 2D [192], and in a high temperature expansion study of the 2D t-J model [193].

The resemblance of the arcs to one side of a hole pocket (Fig. 22) has been noted by a number of authors [67], and as such hole pockets are expected when doping a magnetic insulator, then a magnetic precursor scenario is a possibility. On the other hand, there is no clear evidence from ARPES that the arc deviates from the large Fermi surface and “turns in” so that its normal would be parallel to the magnetic zone boundary

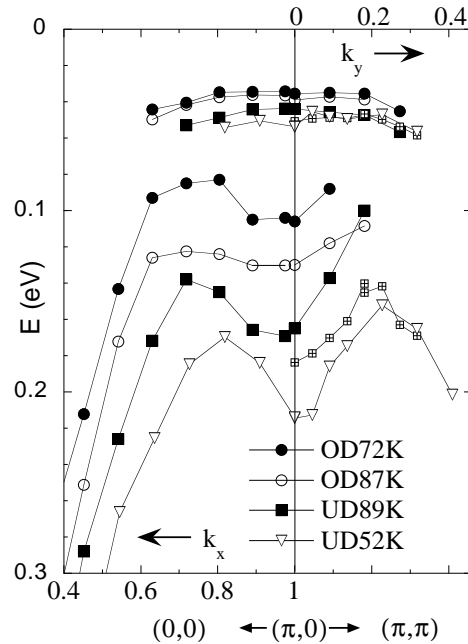


**Figure 36.** Peak (top) and hump (bottom) dispersion from ARPES data of Bi2212 as a function of doping (superconducting state). These quantities become the leading edge (strong) pseudogap and the high energy (weak) pseudogap in the pseudogap phase. The two dispersion directions shown become increasingly similar as the doping is reduced. If magnetic long range order was present, the directions would be equivalent. From Ref. [155].

at the magnetic zone crossing as would be expected in such a scenario (see Fig. 22). And although “shadow” bands have been seen in ARPES [194] (the image of the main band translated by  $Q = (\pi, \pi)$ , which would thus form the back side of this pocket), their intensity seems to scale with  $T_c$  [195], and thus drops off as the doping is reduced, in complete contrast with the expected behavior if the shadows were due to magnetic correlations.

All of the above discussion concerns the leading edge gap, also known as the strong pseudogap. ARPES studies also find a higher energy pseudogap, known as the weak pseudogap. The presence of the latter was evident from the earliest studies [67], but it was not until later that the two effects were clearly differentiated [155]. In contrast to the leading edge gap, which appears to be a precursor to the d-wave superconducting gap, the high energy pseudogap behaves differently. It is simply the continuation of the “hump” from the superconducting state, and has a dispersion which increasingly resembles that of a spin density wave insulator as the doping is reduced (Fig. 36) [155]. In essence, the sharp spectral peak in the superconducting state is replaced by the leading edge gap, the spectral dip is filled in, and the high energy hump becomes the weak pseudogap. This high energy gap is what is commonly observed by ARPES in LSCO and NCCO, as the actual superconducting gaps are difficult to see in these materials because of their small size. This gap strongly increases with underdoping,



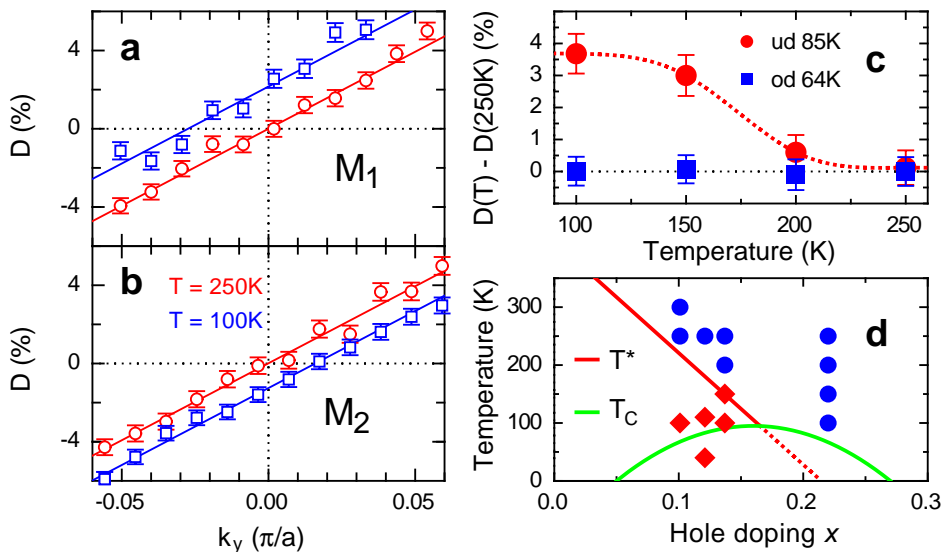


**Figure 37.** Circularly polarized ARPES of underdoped Bi2212. The intensity difference between left and right polarized light normalized to the average is plotted along  $(\pi, 0) - (\pi, \pi)$  in the left panels, with M1 (panel a) and M2 (panel b) indicating orthogonal  $((\pi, 0)$  and  $(0, \pi))$  directions (circles for  $T=250\text{K}$ , squares for  $T=100\text{K}$ ).  $k_y = 0$  is the mirror plane. The shift with temperature at  $k_y = 0$  represents chiral symmetry breaking, and is plotted in panel c versus temperature for an overdoped (squares) and underdoped (circles) sample. Panel d shows that this shift (diamonds) only exists for temperatures below the pseudogap temperature,  $T^*$  (circles indicate no shift). From Ref. [79].

and adiabatically connects to the Mott insulating gap of the undoped phase [196]. The presence of these two gaps may resolve the precursor pair versus competitive scenario debate, in that the leading edge gap seems to be the precursor to the superconducting gap, whereas the high energy gap is the precursor to the magnetic insulating gap. Of course, these two gaps are connected, in that their energies scale together with doping, with a ratio of 3.5-4 (Fig. 27) [155]. This again demonstrates the intimate relation of magnetic and pairing correlations in the cuprates.

None of the spectroscopic data, though, support a picture where the pseudogap phase represents a phase with true long range order, as advocated by a number of theories, in particular those involving a quantum critical point near optimal doping. On the other hand, a recent ARPES experiment does find evidence for broken symmetry in the pseudogap phase (Fig. 37) [79]. In these experiments, circularly polarized light is employed. In general, the signal for left and right polarized light is different, but in a mirror plane, they should be equivalent. This mirror plane effect is seen in overdoped samples along the  $(0, 0) - (\pi, 0)$  ( $\Gamma - M$ ) line. But in underdoped samples, the signals are no longer equivalent in this direction in the pseudogap phase, rather, they become degenerate at some other  $k$  point shifted off this line. Moreover, the size of this shift increases below  $T^*$  as would be expected if an order parameter developed (Fig. 37c). The implication is that time reversal symmetry (or chiral symmetry, depending upon

interpretation), is being broken in the pseudogap phase.

The first worry about such an experiment is that the  $(0,0) - (\pi,0)$  direction is technically not a mirror plane in the Bi2212 crystal structure (due to the orthorhombicity and superstructure). On the other hand, it has been known for some time that the main band signal from ARPES in Bi2212 appears to obey dipole selection rules consistent with tetragonal symmetry [165], and such is the case in these measurements as well. Of course, there could be some structural effect associated with  $T^*$ , but these authors did x-ray scattering on the samples, and found no evidence for a structural change below  $T^*$  [79]. Moreover, the effect of the pseudogap is to shift the overall intensity of the left and right signals relative to one another, as if chiral symmetry was being broken.

A similar effect has not been seen in the  $(0,0) - (\pi,\pi)$  ( $\Gamma - Y$ ) mirror plane, though this has not been studied as extensively yet. If this continues to hold, then it has definite implications. Simple ferromagnetism would cause an effect in both mirror planes. In addition, most orbital current models (the d density wave state, for example) would predict an effect along  $\Gamma - Y$  and not along  $\Gamma - M$  (opposite to experiment). One of the two orbital current patterns discussed by Varma (left panel, Fig. 20) behaves the same way, but the other (right panel, Fig. 20) has a signature similar to experiment [80]. So, it is indeed possible that the data represent an effect which can be attributed to orbital currents, but more experiments would certainly be desirable. What this particular experiment illustrates, though, is the power of photoemission in addressing fundamental issues connected with the cuprates.

#### 4. Inelastic Neutron Scattering

The other momentum resolved probe in the cuprates is inelastic neutron scattering. The part of the signal of interest here is the magnetic part, which is proportional to the imaginary part of the spin-spin response function,  $\chi(\mathbf{q}, \omega)$ , times a Bose population factor. For elastic scattering, one sees Bragg peaks associated with the magnetism if the material is magnetically ordered. (Phonons and structure are measured by neutrons as well, but this takes us beyond the scope of this review).

The first result with neutrons was finding the antiferromagnetic order in the undoped phase [33]. Magnetic moments of  $2/3 \mu_B$  per Cu site are found [197], the reduction from 1 being due to quantum fluctuations associated with the small spin ( $S=1/2$ ) of the Cu ion. The ordering wavevector is  $Q = (\pi, \pi, \pi)$ , which means that successive planes are antiferromagnetically coupled as well.

For bilayer systems like YBCO, there are two branches of the spectrum (Fig. 38), an acoustic branch with form factor  $\sin^2(Q_z d/2)$  and an optic branch with form factor  $\cos^2(Q_z d/2)$ , where  $d$  is the separation of the two CuO layers of the bilayer [198]. The acoustic branch has the classic spin-wave dispersion with respect to  $(\pi, \pi)$ , with the planar exchange energy  $J_{\parallel} \sim 100$  meV determined from the slope. The optic branch has a gap of order 60 meV. As the optic gap is equal to  $2\sqrt{J_{\parallel}J_{\perp}}$ , where  $J_{\perp}$  is the intrabilayer exchange, then  $J_{\perp} \sim 10$  meV [199].

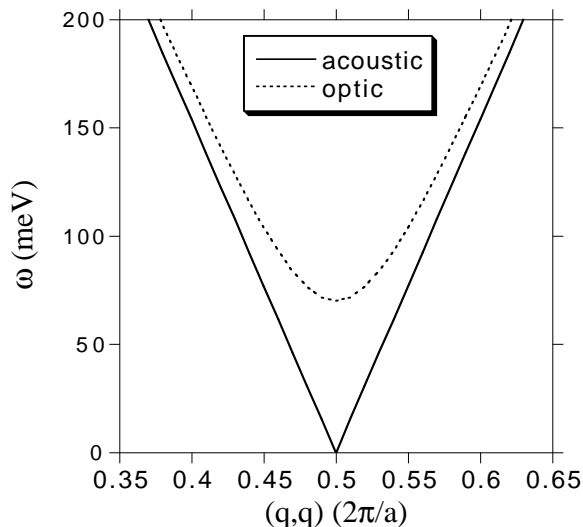


**Figure 38.** Acoustic and optic branches of the spin wave dispersion in the magnetic phase of YBCO as revealed by inelastic neutron scattering. Adapted from Ref. [198].

#### 4.1. LSCO

The first doping dependent studies were done on LSCO. They revealed the presence of four incommensurate peaks (see Fig. 10) at locations  $2\pi(0.5 \pm \delta, 0.5)$  and  $2\pi(0.5, 0.5 \pm \delta)$ , with  $\delta$  scaling with the doping,  $x$  [94]. The original explanation for this incommensurability was related to the Fermi surface geometry. As the doping increases, the Fermi surface hole volume expands, and the predicted incommensurability with doping from RPA calculations more or less agrees with experiment [143].

This view changed, though, with the observation of elastic scattering peaks in the LTT (low temperature tetragonal) phase of Nd doped LSCO [90]. The incommensurate elastic peaks were accompanied by charge ordering peaks (see Fig. 10) at  $2\pi(\pm 2\delta, 0)$  and  $2\pi(0, \pm 2\delta)$ . Tranquada and co-workers interpreted this behavior as due to the formation of stripes of doped holes with commensurate antiferromagnetic domains between the stripes. If the stripes act as antiphase domain walls, then the prediction is that the magnetic signal will be incommensurate, with  $\delta$  proportional to  $x$  (upper panel, Fig. 39). This picture received further support when it was observed in LSCO that for dopings smaller than those where superconductivity occurred, only two spots were present, and they were rotated  $45^\circ$  relative to the previous spots (bottom panel, Fig. 39) [144]. This implies one dimensional behavior, consistent with stripes.

A similar incommensurate pattern was later seen in YBCO [95], and this pattern is also found to be 1D like in detwinned samples (where the CuO chains are all aligned) [200]. This again gives evidence for stripes, though the effect may have a more benign origin due to the influence of the CuO chains. At low dopings, charge ordering peaks are seen in YBCO as well [96].

The effect of superconductivity on LSCO is to lead to a sharpening of the incommensurate peaks, and the formation of a “spin gap” at low energies of  $\sim 6$  meV

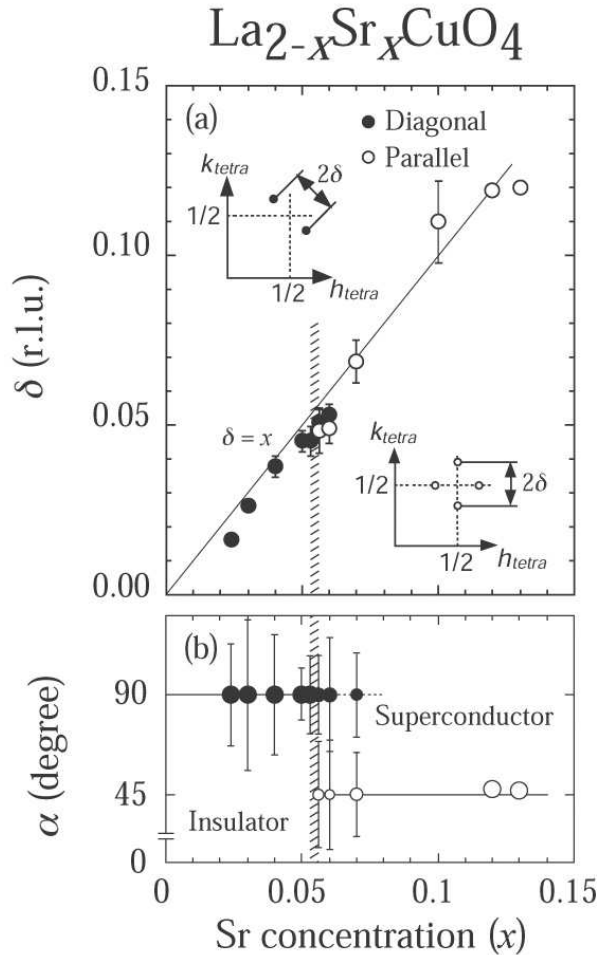


**Figure 39.** Neutron scattering peaks versus doping for LSCO. The spot pattern rotates by  $45^\circ$  at the spin glass/superconducting boundary.  $\delta$  is the incommensurability, and  $\alpha$  the angle of the spots in momentum space relative to the  $(1/2, 1/2)$  wavevector. From Ref. [144].

(Fig. 40). This spin gap is fairly isotropic in momentum space [201], which was taken as evidence against an interpretation of it being the  $2\Delta$  continuum gap since  $\Delta$  is anisotropic for a d-wave superconductor (in particular, there should be a significant continuum gap at  $(\pi, \pi)$ ). This statement should be treated with care, though, since the only low frequency structure is at these incommensurate wavevectors, with the intensity at other wavevectors, like  $(\pi, \pi)$ , due to overlap from these peaks given their finite width in momentum.

Subsequent experiments found that this spin gap filled in at modest values ( $H \ll H_{c2}$ ) of the magnetic field (Fig. 40) [202]. For more underdoped samples, magnetic ordering could even be induced by applying a field [203]. The obvious idea is that some kind of SDW ordering is being stabilized by the vortices [204, 205]. But, the vortex density is quite low at the field values studied, which would imply that there is a very large magnetic polarization cloud around the vortices. This is certainly consistent with

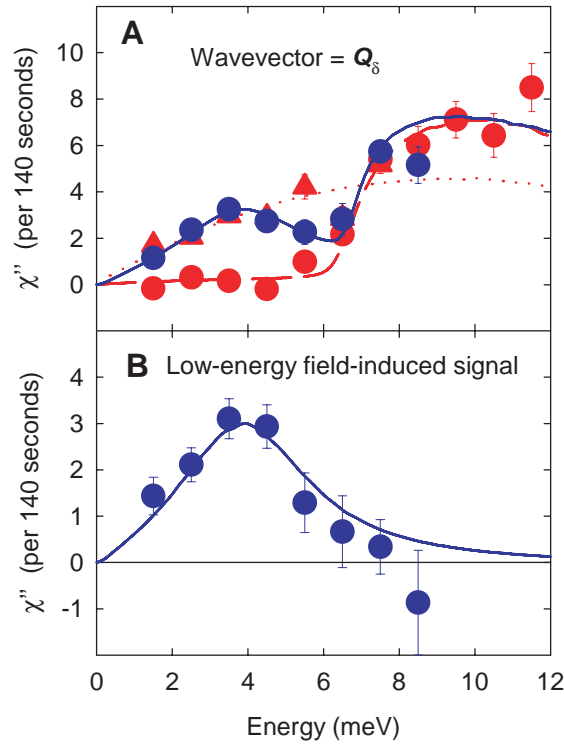


**Figure 40.** Imaginary part of the dynamic susceptibility versus energy (panel A) for the superconducting state of optimal doped ( $x=0.163$ ) LSCO at zero field (lower set of circles), at a field of 7.5 T (upper set of circles), and in the normal state (triangles). The difference of zero and 7.5 T data are plotted in the panel B. From Ref. [202].

the neutron results, in that the magnetic correlation length is quite long in underdoped LSCO samples.

On the other hand, one might interpret these results as a stabilization of stripe formation. In this context, STM experiments on Bi2212 find a charge density wave pattern associated with the vortex cores [101]. The Fourier pattern was anisotropic (factor of 3 intensity difference between orthogonal planar directions), which would argue for 1D behavior, although it is possible that this could be an extrinsic effect due to the STM tip.

#### 4.2. YBCO

Perhaps the most dramatic effect associated with neutron scattering in the superconducting state is the formation of a sharp commensurate resonance at about 40 meV in YBCO (Fig. 41) [132]. The magnetic nature of the resonance was confirmed by later polarized measurements [133]. Subsequently, the resonance was seen in Bi2212 [183]. The resonance has a form factor equivalent to the acoustic branch of the undoped material, and so is centered about the  $(\pi, \pi, \pi)$  wavevector. In particular, the “optic branch” has no resonance, and remains gapped as in the insulator (Fig. 41) [199]. These observations led to speculations that the resonance might be a bilayer effect, since is

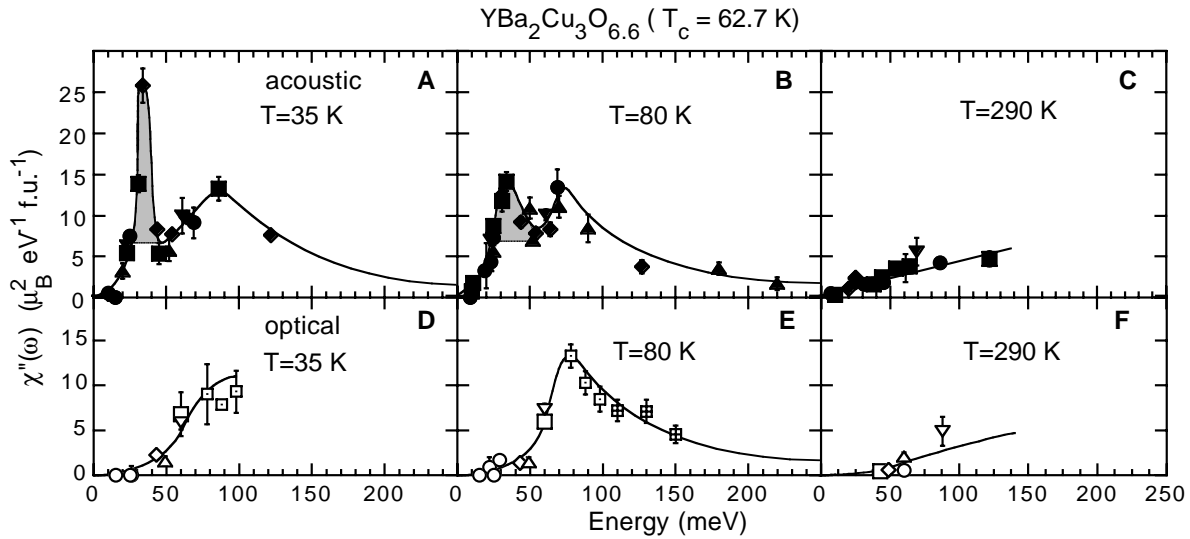


**Figure 41.** Wavevector integrated dynamic susceptibility for underdoped YBCO at 35K (superconducting state), 80K (pseudogap phase), and 290K (normal state) in the acoustic and optic channels. The gray shaded area represents the resonance. From Ref.[209].

it not seen in LSCO, but a new experiment has identified the resonance in single layer Tl2201 [206]. Several theories concerning the resonance were discussed in Section 2, in particular the controversy concerning whether it represents a particle-hole or particle-particle collective mode.

The resonance energy scales with doping like  $5T_c$  [199], and its intensity has a variation with temperature much like that of the superconducting order parameter [137]. Based on previous theoretical work [207], Demler and Zhang made the provocative suggestion that these results implied an equivalence between the exchange energy difference between the normal and superconducting state and the resonance weight [208]; that is, the superconducting condensation energy was related to the formation of the resonance. Their suggestion was tested by measurements on YBCO, which demonstrated a similarity of the specific heat anomaly at  $T_c$  and the temperature derivative of the resonance weight (Fig. 42) [209]. As magnetic fields along the c-axis are known to suppress the specific heat anomaly, this motivated experiments which looked at the field dependence of the resonance. It was found that a field applied perpendicular to the planes did lead to a strong suppression of the resonance in an underdoped YBCO sample [210], as opposed to a parallel field which did not [211]. To understand this result, we note that STM measurements find in underdoped Bi2212 samples that the pseudogap phase is present in the vortex cores, with no coherence peaks [84]. This would imply that the resonance, which is a property of the coherent superconducting state, is suppressed in the cores. On the other hand, an analysis of the neutron data indicates that the effective core radius needed to explain the observed suppression of the resonance is significantly larger than the known superconducting correlation length [212]. This again

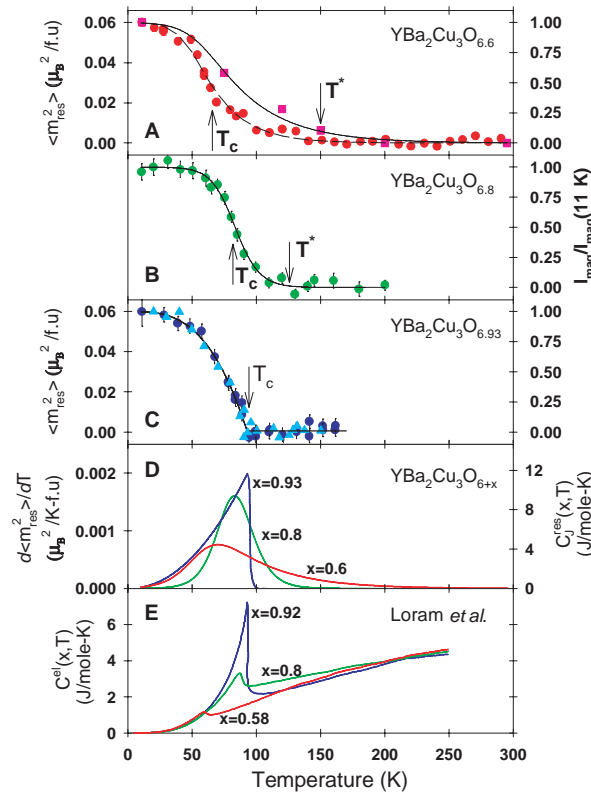


**Figure 42.** Neutron data for YBCO. Panels A-C are the temperature variation of the resonance peak intensity for samples at three different dopings. Panel D is the temperature derivative of the intensity data, in comparison to specific heat data in panel E. From Ref. [209].

demonstrates that for YBCO, like for LSCO, the cores polarize the surrounding medium. This leads to a suppression of the resonance out to a magnetic correlation length about the cores. In that sense, it should be remarked that the YBCO sample studied in the field dependent experiment exhibits an anomalously large magnetic correlation length ( $28 \text{ \AA}$ ) as determined from the resonance width in momentum space [213].

Perhaps the biggest controversy surrounding the resonance is whether it is responsible for structure seen in other spectroscopic probes, like ARPES and tunneling [180]. The smallness of the resonance weight (a few percent of the local moment sum rule) argues against this [214]. On the other hand, phase space considerations can be used as a counterargument [215]. The resonance weight is small because it is localized in momentum space around  $(\pi, \pi)$ . But as electronic states near  $(\pi, 0)$  are connected by these wavevectors, there is no problem for these states to be strongly affected by the resonance despite its overall small weight. These arguments can be extended to states in other regions of the zone as well [186].

One reason this controversy has arisen is the suggestion by certain researchers that the resonance interpretation of ARPES and tunneling implies that the resonance alone is responsible for pairing. Actually, the formation of the resonance, as well as the profound changes in the ARPES lineshape, is a consequence of the onset of superconductivity,

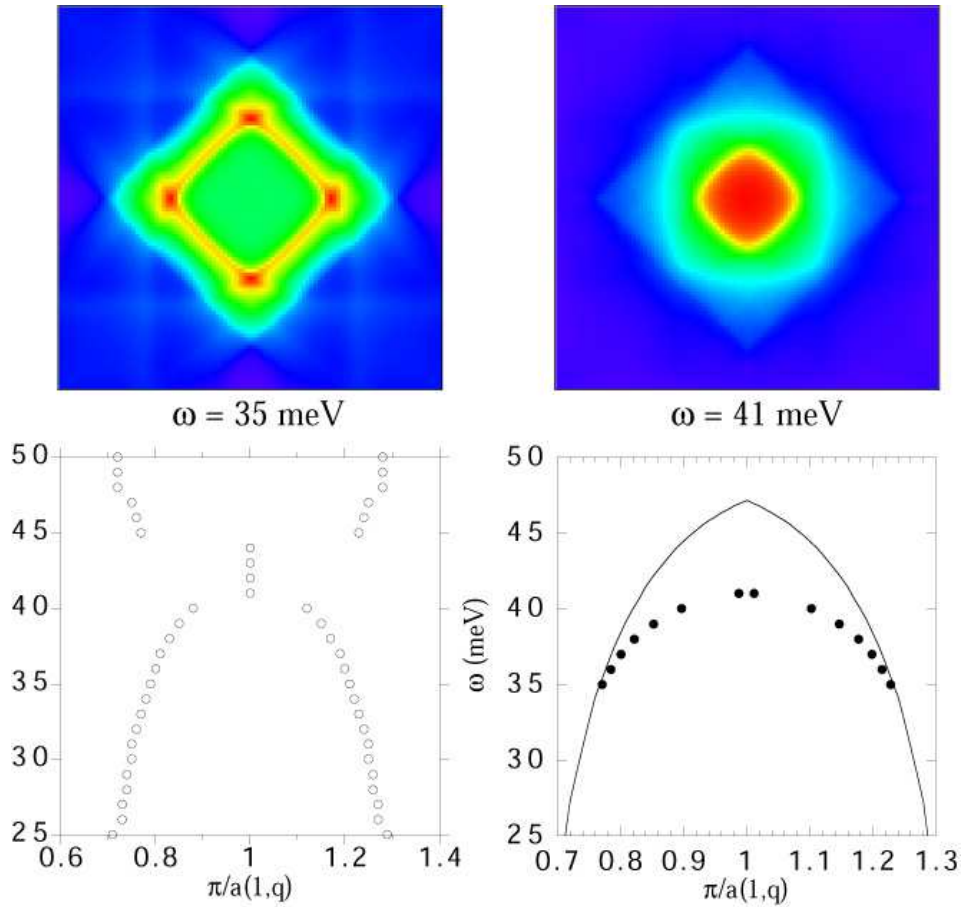


**Figure 43.** RPA calculation of the dynamic susceptibility for YBCO in the superconducting state based on ARPES dispersions. Momentum dependence of the intensity is plotted at resonance in top right panel, and below resonance in top left panel. Note the commensurate pattern at resonance compared to the incommensurate (diamond shaped) pattern below resonance. Resulting  $\omega(q)$  dispersion relation (hourglass shaped) is plotted in the bottom left panel. (The maximum superconducting gap was 29 meV and the superexchange energy 110 meV.) This is further illustrated in the bottom right panel, where the pole of the RPA response function is plotted (circles), with the solid line representing the edge of the continuum. Adapted from Refs. [97] and [219].

rather than the cause of it. Such “feedback” effects are unavoidable in any theory where the pairing is not due to phonons [14]. The classic example is the stabilization of the A phase in  $^3\text{He}$  relative to the B phase due to the feedback of pairing on the spin fluctuations [13].

Below the resonance energy in YBCO, the magnetic response becomes incommensurate (top left panel, Fig. 43) [95]. Detailed studies of the  $\omega(\mathbf{q})$  dispersion relation find an “hourglass” shape (bottom left panel, Fig. 43) [216], with incommensurate “sidebranches” appearing both above and below the resonance energy, though the upper branch is damped (it lies above the two particle continuum). This sidebranch behavior can be understood from linear response calculations for a d-



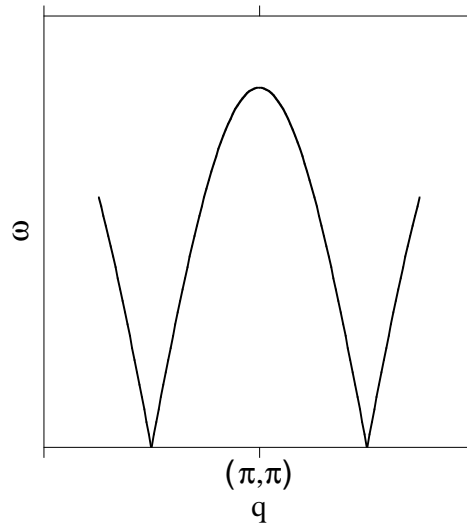


**Figure 44.** Proposed  $\omega(q)$  dispersion relation for the dynamic susceptibility of YBCO based on overlapping spin waves from the AF domains between stripes. Adapted from Ref. [222].

wave superconductor (Fig. 18) [217, 218, 97]. Under certain conditions, the lower incommensurate branch is a collective mode pulled below the two particle continuum, with the commensurate resonance at the top of this lower branch (bottom right panel, Fig. 43) [217, 219]. This is consistent with an interpretation of recent data on slightly underdoped YBCO [220], but differs from an interpretation of more heavily underdoped samples, where the resonance and sidebranches appear to represent separate effects [96]. In the latter case, the incommensurate sidebranches have been interpreted as due to antiphase domain stripes, with the commensurate resonance presumably due in phase domain stripes. It should be remarked that the condition to get pole-like behavior for the lower incommensurate branch is difficult in linear response calculations, and requires reduced curvature of the Fermi surface around the nodes, so that the constant energy contours of the Dirac cones discussed in Section 3 (Fig. 26) are flat instead of banana shaped [221, 97, 219]. For instance, the ARPES Fermi surface of Bi2212 does not indicate such flat contours, and the prediction would be that the incommensurate effects in Bi2212 are weak and unconnected to the resonance [97, 219], as inferred experimentally in heavily underdoped YBCO [96]. Unfortunately, neutron scattering experiments on Bi2212 are difficult due to the small crystals available, and ARPES results for YBCO are controversial because of surface related problems. Still, such studies would be useful to test these ideas.

As discussed by Batista and co-workers [222], differentiation between these various interpretations is not as straightforward as it might seem. The picture they offer is that the lower incommensurate branch is analogous to the spin wave dispersion in an incommensurate antiferromagnet, with the resonance being where the two spin wave branches from  $+Q$  and  $-Q$  intersect (Fig. 44). Actually, the dispersion they plot follows the two particle continuum gap of the linear response calculations. In these

RPA calculations, the incommensurate branch either follows the continuum gap (and thus is not a pole), or is pulled beneath (becoming a pole), depending on how flat the constant energy contours of the Dirac cones are [217, 219]. Presumably, this physics is not unrelated to a stripes interpretation, where quasi 1D behavior would cause the same effects as the flat contours.

Finally, although a lot has been made about the differences between the dynamic susceptibilities of YBCO and LSCO, it should be noted that the most recent data on LSCO find the presence of energy dispersion in the incommensurate response (like in YBCO), with commensurate excitations present beyond 20 meV [223]. Thus, it may be that the central difference between these two materials is that the bulk of the spectral weight sits in the lower incommensurate branch for LSCO, but in the commensurate resonance for YBCO. This difference is probably due to a variety of factors: the smaller energy gap in LSCO, differences in the Fermi surface topology, and the stronger tendency for disorder and inhomogeneous behavior (stripes) in LSCO. In this respect, Bi2212 is probably intermediate between YBCO and LSCO, so more neutron studies of Bi2212 would be desirable.

## 5. Optical Conductivity

Optics measures a two-particle response function as well, the current-current correlation function. Because of the tiny momentum associated with the light used, optics measures the zero  $q$  limit of this function. This can be represented as a particle-hole bubble, like in the previous section, but with the spin operators replaced by current operators at the vertices (the Kubo bubble).

We start with the planar response. The normal state is characterized by a broad, Drude-like response centered at  $\omega = 0$  (Fig. 45). The Drude tail, though, has an anomalous behavior. The data are best appreciated by representing the optical response in a generalized Drude form [224, 48]

$$\sigma(\omega) = \frac{1}{4\pi} \frac{\omega_{pl}^2}{1/\tau(\omega) - i\omega[1 + \lambda(\omega)]} \quad (5)$$

where  $\omega_{pl}$  (the plasma frequency) is given by the sum rule

$$\int_0^\infty d\omega \text{Re}\sigma(\omega) = \omega_{pl}^2/8 \quad (6)$$

(the last integral is usually cut-off at 1 eV or so to avoid interband contributions). In this form,  $1/\tau$  is the scattering rate, and  $1 + \lambda$  the mass renormalization. The two terms are related by a Kramers-Kronig transform. Such an analysis reveals that the scattering rate has the form  $a + b\omega$  (Fig. 46). The  $b$  term is what is expected for a marginal Fermi liquid, but the  $a$  term is not, since it does not appear to be proportional to  $T$ . Abrahams and Varma attribute it to scattering from off planar impurities [225], but more likely, it is a signature of the non-Fermi liquid nature of the normal state. In particular, there is some evidence from ARPES that the  $a$  term is associated with the pseudogap, since it has a similar momentum anisotropy.

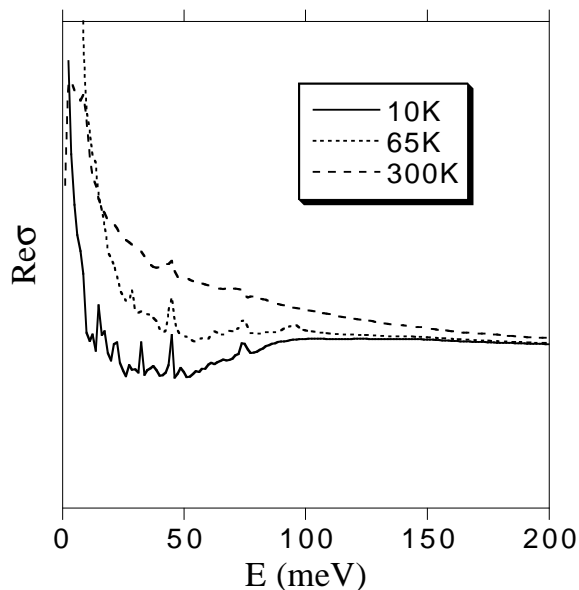


**Figure 45.** Real part of planar infrared conductivity of underdoped YBCO at three temperatures corresponding to the superconducting state (10K), pseudogap phase (65K), and normal state (300K). Note gap-like depression which develops at around 50 meV. From Ref. [48].

When superconductivity sets in,  $Re\sigma$  develops a depression at an energy close to the value  $2\Delta$  expected for a superconductor [60, 224, 226, 61, 48], but a true gap never fully develops. Instead, a narrower Drude peak is present at energies below this depression, representing uncondensed carriers. For a superconductor, one expects the presence of a  $\delta$  function at  $\omega = 0$  due to the dissipationless response of the superfluid, and this is indeed seen as a  $1/\omega$  term in  $Im\sigma$  at low frequencies.

A generalized Drude analysis in the superconducting state [48] reveals that  $1/\tau$  becomes strongly gapped below some threshold energy (Figs. 46 and 47), and the behavior seen is very similar to that inferred from ARPES along the nodal direction (Fig. 46) [49]. The low frequency limit is most easily seen from microwave [46] and thermal conductivity [47] measurements, which find a strong collapse with temperature (see Fig. 5) of the scattering rate below  $T_c$ , with a residual low temperature mean free path of order microns for clean samples of YBCO. It should be remembered that for electron-electron scattering, only Umklapp processes contribute to the electromagnetic response, whereas normal processes contribute to the ARPES and thermal response as well. This has been used to quantitatively account for differences between the microwave and thermal conductivity scattering rates [227]. We should note that although the strong collapse of the scattering rate with temperature below  $T_c$  is consistent with ARPES results near  $(\pi, 0)$  [189], the ARPES results along the nodal direction are still controversial, where a linear T behavior below  $T_c$  has been claimed by one group (Fig. 23) [128] but not by others. All ARPES results are on Bi2212, which is more disordered than YBCO, and in fact terahertz ( $\omega \sim 1$  meV) measurements on Bi2212 claim a linear

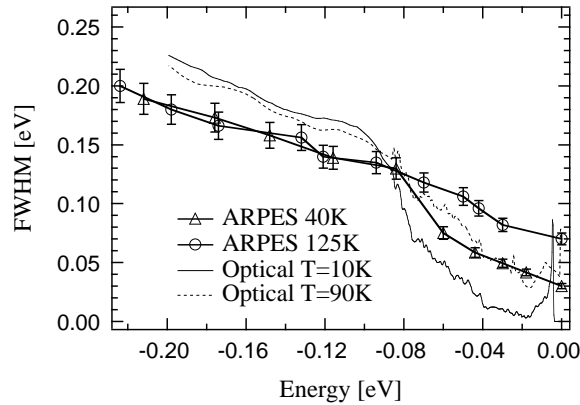


**Figure 46.** Comparison of optical scattering rate,  $1/\tau$ , from Ref. [48] to ARPES nodal linewidth in the superconducting state and pseudogap phase of optimal doped Bi2212. From Ref. [49].

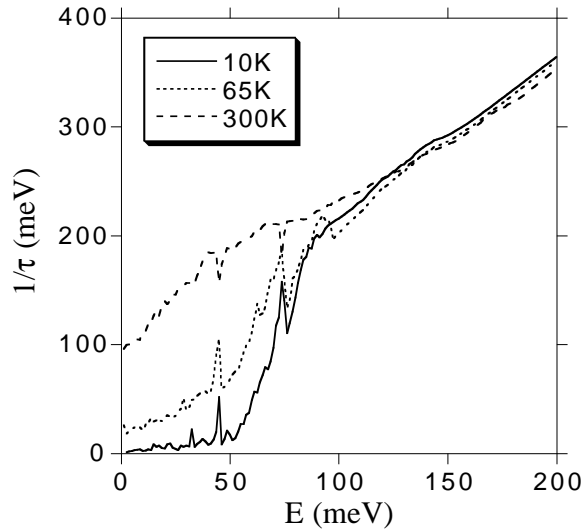


**Figure 47.** Variation of optical scattering rate with energy for underdoped YBCO (10K - superconducting state, 65K - pseudogap phase, 300K - normal state). From Ref. [48].

T scattering rate of the residual carriers as well [228]. The size of this rate is difficult to compare to ARPES, given the fact that the ARPES resolution width greatly exceeds the frequency of this measurement.

The other interesting point is that for underdoped samples, a partial scattering rate gap persists in the pseudogap phase (Fig. 47), likely due to the gapping of electronic states near  $(\pi, 0)$  [48]. In fact, the optics data have a smooth evolution through  $T_c$  for underdoped samples. Even a finite frequency signature of the superfluid response persists above  $T_c$ , as revealed by terahertz measurements of the electrodynamic response [35]. These data have been successfully modeled assuming the superconducting transition is of the Kosterlitz-Thouless type.

All of these behaviors would be difficult to attribute to phonons, in that the latter

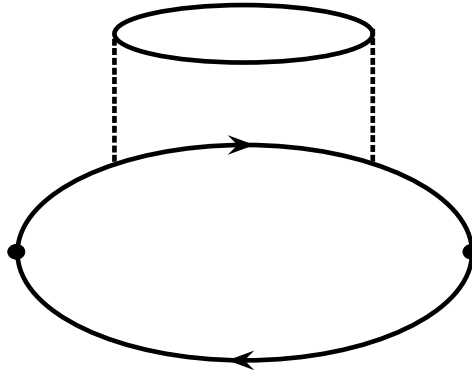


**Figure 48.** Kubo bubble for optical conductivity. Dots represents current vertices. The attached part at the top is the lowest order self-energy insertion to the bubble due to electron-electron scattering.

are not gapped in the superconducting state. There is a drop in the electron-phonon scattering rate, since the electrons themselves are gapped, but the effect is not as dramatic as in the electron-electron case. A Feynman diagram analysis of the Kubo bubble (Fig. 48) would give a scattering rate drop setting in below  $4\Delta$  (analogous to the  $3\Delta$  gap in the single particle scattering rate (Fig. 5) [50]) for the electron-electron scattering case (in the electron-phonon case, the self-energy insertion in Fig. 48 would be replaced by a phonon). The actual optics data, though, show an abrupt onset of the drop at a frequency smaller than this. This implies collective effects, and in fact several researchers [229, 184, 230] have used the same explanation for the optics data as invoked previously to explain the ARPES data [180, 131]. In particular, the scattering rate onset corresponds to  $2\Delta + \Omega_{res}$ , where  $\Omega_{res}$  is the spin resonance energy seen by inelastic neutron scattering.

The c-axis response, though, is quite different (see Fig. 7). Most studies have been done on YBCO, since the electronic part of the c-axis conductivity is small, and non-trivial to separate from the phonons present in the data, particularly for Bi2212 which is more 2D like. The normal state response is non-Drude like in nature,  $Re\sigma$  being more or less flat in frequency [65]. A hard gap begins to open up in this spectrum below  $T_c$  at a frequency near  $2\Delta$  [65]. Beyond this energy, a peak is present in the data whose origin is controversial. It has been identified as the optic plasmon of the bilayer [231], but also appears to be related to the neutron resonance as well [232].

Recent developments in optics have focused on the issue of the condensation energy, which brings us to the topic of the next section.

## 6. Condensation Energy

The condensation energy is defined as the energy difference between the normal and superconducting states at  $T=0$  (at finite temperature, the entropy must be taken into account). Since normal state properties are temperature dependent, then this requires an extrapolation to infer a hypothetical zero temperature normal state. Most estimates

of the condensation energy have been made from specific heat data, which have been recently used to suggest a quantum critical point just beyond optimal doping based in part on the doping dependence of the inferred condensation energy [81], which has a maximum near the suggested critical point (middle panel, Fig. 9).

We begin our story with a piece of pre-BCS history. In 1956, Chester published a paper demonstrating where the condensation energy was coming from in conventional superconductors [233]. What he chose to study was the full Hamiltonian of the solid, which is composed of the kinetic energies of the electrons and ions, and the electron-electron, electron-ion, and ion-ion interactions. Exploiting the dependence of  $T_c$  on ion mass (isotope effect) and the virial theorem, he was able to demonstrate that: (1) the potential energy of the electrons is reduced in the superconducting state, (2) the kinetic energy of the electrons is increased, and (3) the ion kinetic energy is reduced. For the classic value of the isotope coefficient (1/2), the potential and kinetic energy changes of the electrons actually cancel, which means that the entire condensation energy is equivalent to the lowering of the ion kinetic energy.

This is not what occurs in BCS theory, of course. The reason is that it is an effective theory gotten by projecting the full Hamiltonian onto the low energy subspace. In such a theory, the ion kinetic energy term is absorbed into the definition of the potential energy, and so superconductivity is due to a lowering of the effective potential energy of the low energy electrons. Note that the virial theorem does not apply to the projected Hamiltonian, and so cannot be used as a guide.

As for the kinetic energy, in BCS theory, the normal state is taken to be that of non-interacting electrons. Because of this, the effective kinetic energy of the electrons is exactly diagonalized. That is, the momentum distribution function is equal to 1 for  $k < k_F$  and 0 for  $k > k_F$ . In the superconducting state, particle-hole mixing occurs, leading to  $n_k = v_k^2 = \frac{1}{2}(1 - \epsilon_k/\sqrt{\epsilon_k^2 + \Delta_k^2})$  (see Fig. 12). So, the “smearing” of  $n_k$  (Fig. 49) leads to an increase of the kinetic energy.

The potential and kinetic energy differences are straightforward to calculate in BCS theory, and this exercise can be found in Tinkham’s book [234]. Although each term is ultraviolet divergent (and thus cut-off at the Debye energy), the sum is convergent, equal to  $\frac{1}{2}N\Delta^2$  where  $N$  is the density of states. Of course, the normal state of the cuprates is not a Fermi liquid (at least for optimal and underdoped samples), so BCS considerations could be misleading.

In Section 4, we discussed one attempt to get at a piece of the condensation energy. It was noted by Scalapino and White [207] that the difference of the exchange energy between the normal and superconducting states could be obtained from an integral involving the difference of  $Im\chi$  between the normal and superconducting states. Demler and Zhang [208] noted that for optimal doped YBCO, the normal state  $Im\chi$  is small, and so an estimate could be made in that case by simply integrating the neutron resonance (see Figs. 41 and 42). The resulting energy change (the exchange energy is lowered in the superconducting state) is in excess of the known condensation energy, and they suggested this was compensated by an expected increase in the kinetic energy in the

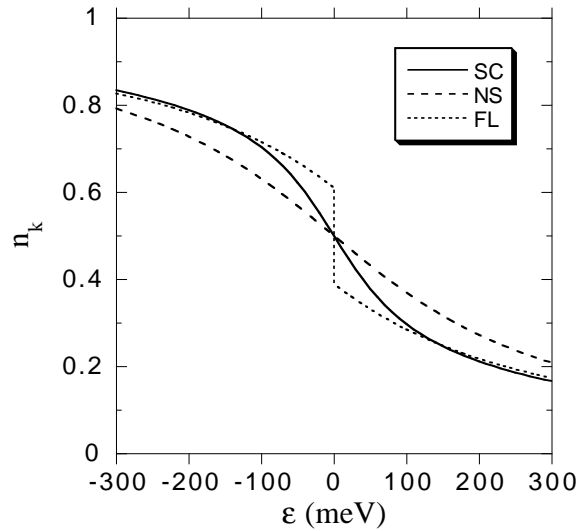


**Figure 49.** Model calculations of the momentum distribution function in the normal state (NS) and the superconducting state (SC) compared to a hypothetical Fermi liquid normal state (FL). From Ref. [248].

superconducting state. Although the latter is true in BCS theory, is it necessarily true in general? Recent optics data give evidence to the contrary, as we now discuss.

### 6.1. Optics

Anderson has noted that several unusual properties of the cuprates could be understood if spectral weight from high energies were transferred to low energies when going from the normal to the superconducting state [235, 29]. Under such conditions, one might anticipate the kinetic energy of the electrons to actually be lowered in the superconducting state rather than raised as in BCS theory. This was also suggested by Hirsch, who predicted a “violation” of the optical sum rule due to this effect [236]. That is, in a conventional superconductor, the weight appearing in the zero frequency condensate peak comes entirely from the weight removed by the  $2\Delta$  gap in the optical response (a result known as the Tinkham-Ferrell-Glover sum rule [234]). But a “violation” would indicate that more weight was present in the condensate peak than expected (Fig. 50) [237].

To understand this, it is necessary to find a relation between the optics and kinetic energy. The optical sum rule of interest is the same one discussed in Section 5

$$\int_0^\infty d\omega \text{Re}\sigma_{jj}(\omega) = \omega_{pl}^2/8 \quad (7)$$

This integral is well known when integrated over all energy bands, and is simply proportional to the bare carrier density,  $n$ , over the bare electron mass,  $m$ . By charge conservation ( $n$  fixed), this integral is always conserved.

On the other hand, what is of interest here is the “single band” sum rule

$$\hat{P} \int_0^\infty d\omega \text{Re}\sigma_{jj}(\omega) = \frac{\pi e^2 a^2}{2\hbar^2 V} E_K \quad (8)$$

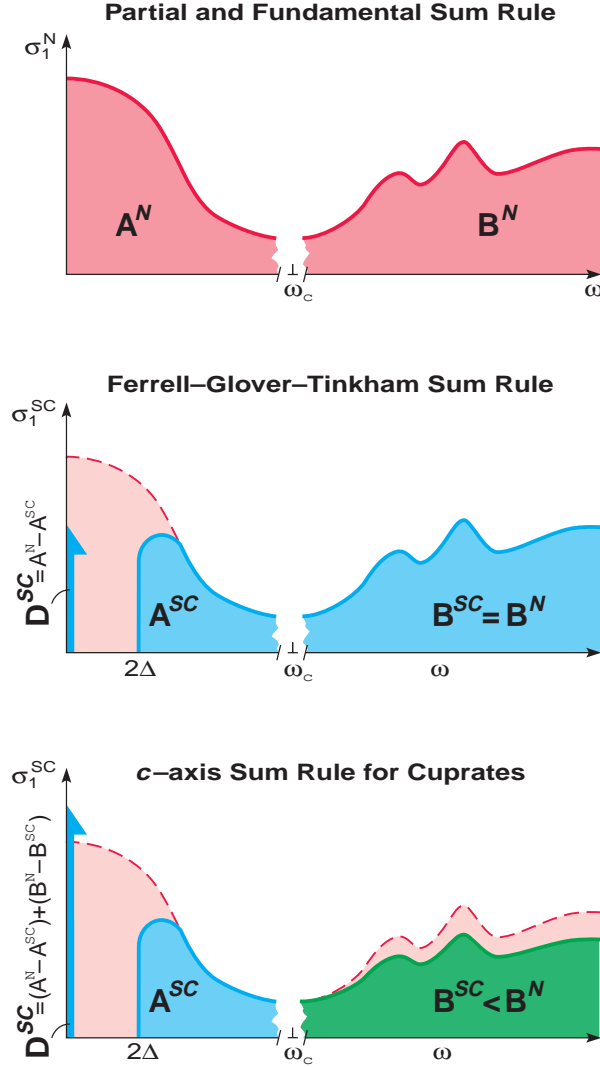


**Figure 50.** Top panel: schematic of optical conductivity (real part) in the normal state (A is low energy, B high energy). Middle panel: Comparison of normal state to superconducting state if the single band sum rule is preserved. Gapped weight appears as a  $\delta$  function at zero energy. Bottom panel: When a sum rule “violation” is present, more weight appears in the  $\delta$  function than is gapped out. This implies that the remaining weight must come from high energies to satisfy the full sum rule. From Ref. [237].

where

$$E_K = \frac{2}{a^2 N} \sum_k \frac{\partial^2 \epsilon_k}{\partial k_j^2} n_k \quad (9)$$

and  $\hat{P}$  projects onto the single band subspace. In these expressions,  $V$  is the unit cell volume,  $a$  the in-plane lattice constant,  $N$  the number of  $k$  vectors,  $\epsilon_k$  the dispersion defined from the kinetic energy part of the effective single band Hamiltonian, and  $n_k$  the momentum distribution function. This was first derived by Kubo [238]. On the other



hand, the kinetic energy for this band is

$$E_{kin} = \frac{2}{N} \sum_k \epsilon_k n_k \quad (10)$$

Thus, the optical integral is of similar form, but not identical, to the kinetic energy [239], except for a near neighbor tight binding form for  $\epsilon_k$ , where  $E_K = -E_{kin}$ . In practice, the optical integral must be cut off at some energy so that interband terms are not included (typically 1 eV in the cuprates).

There have been a number of studies which show anomalous changes in the optical response between normal and superconducting states at energies beyond 1 eV in the cuprates [240, 241, 242]. But matters came to the forefront when Basov and co-workers demonstrated an explicit violation of the single band sum rule for the c-axis optical response of underdoped cuprates [243]. Since a near neighbor tight binding model should be adequate to describe the hopping along the c-axis, this finding gives direct evidence that the c-axis kinetic energy is lowered in the superconducting state, as suggested by Anderson and co-workers [164, 29] and Hirsch as well [236]. There has been an alternate interpretation of this observation, though, from Ioffe and Millis [244]. They claim that a “violation” is possible for the c-axis response if the normal state reference is taken to be a pseudogap phase involving pairs without long range phase order.

Regardless, the c-axis kinetic energy is so small, the energy savings inferred is far below what is needed to account for the actual condensation energy of the cuprates, which is about 3K per CuO plane in optimal doped YBCO [245]. On the other hand, the in-plane kinetic energy is quite large, of order 1 eV. Therefore, if a similar relative violation of the size seen for the c-axis occurs for the in-plane response, then the energy savings could be enough to account for the condensation energy.

Motivated by this, two recent experiments on optimal and underdoped Bi2212 found evidence for a change in the planar optical integral between normal and superconducting states large enough to account for the condensation energy (Fig. 51) [246, 247] (though an earlier study of underdoped YBCO did not [226]). No such violation was found for an overdoped Bi2212 sample [247]. In both experiments, more spectral weight showed up in the zero frequency condensate peak than can be accounted for by the loss of finite frequency weight up to about 1 eV. Integrating up to about 2 eV, though, spectral weight balance is found. This confirms the earlier speculations by Anderson [235, 29] of transfer of spectral weight from high to low energies.

Using the observed form of the scattering rate in the normal state,  $a_k + b\omega$  [225], and assuming both of these terms are gapped below some threshold energy in the superconducting state (left panel, Fig. 52), the optical integral difference was calculated by Norman and Pépin [239] (right panel, Fig. 52) from an  $\epsilon_k$  extracted from ARPES data (more properly, band structure values should be used for  $\epsilon_k$ ). They find that such a calculation gives a good estimate of the optical integral change, including its doping dependence. In these calculations, the sum rule violation is coming from the  $a_k$  term (that is, if the normal state were a pure marginal Fermi liquid, there would be no sum rule violation). This  $a_k$  term, which as stated earlier seems to be associated with the

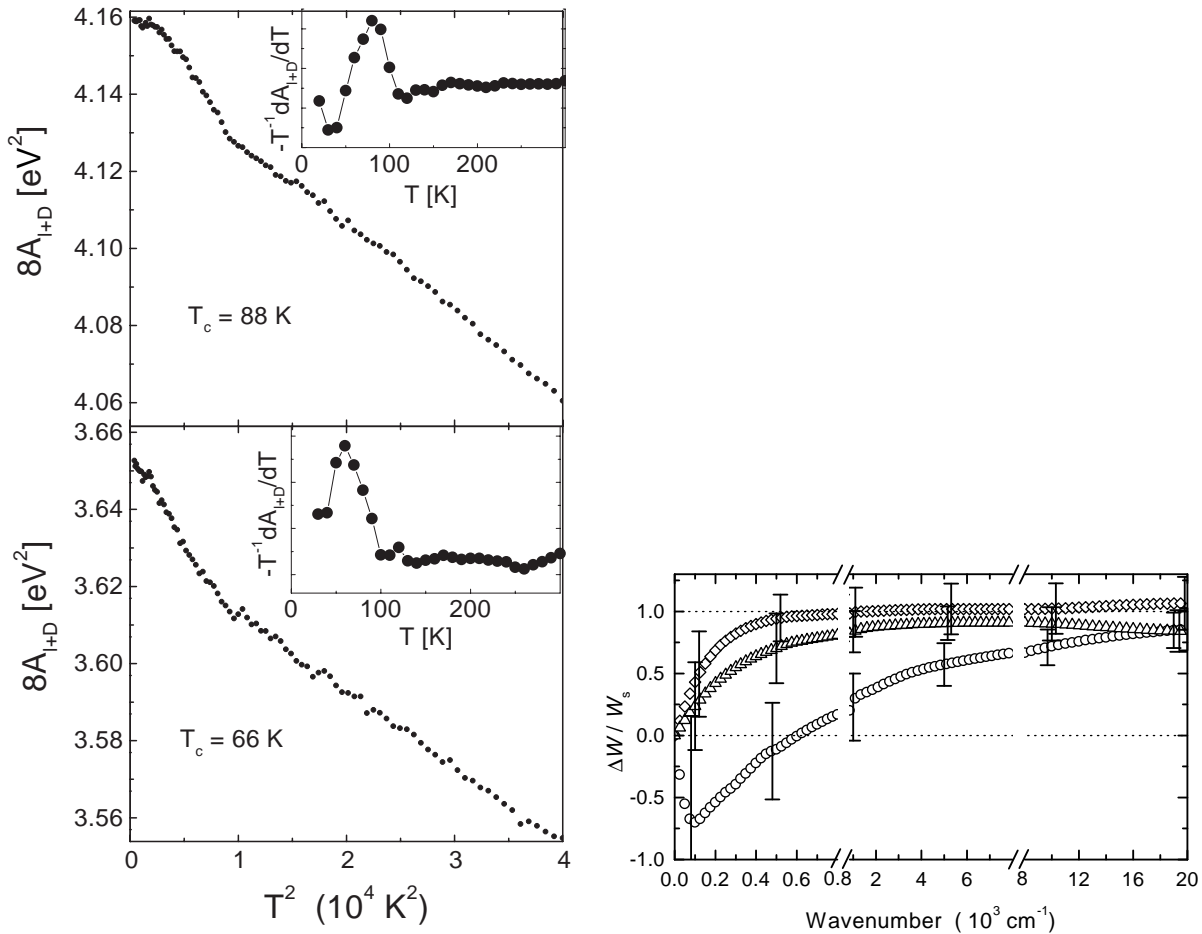


**Figure 51.** Left: Variation of the optical spectral weight (integrated to 1.25 eV) with temperature for an optimal (top left) and an underdoped (bottom left) sample of Bi2212. Anomalous rise below  $T_c$  implies kinetic energy lowering in the superconducting state. From Ref.[246]. Right: Optical spectral weight difference between a temperature above  $T_c$  and 10K integrated to the energy plotted on the x axis normalized to the weight of the superconducting condensate for various samples of Bi2212 (diamonds for overdoped, triangles for optimal doped, and circles for underdoped). Spectral weight balance (sum rule) would correspond to a value of 1. From Ref. [247].

pseudogap, has a strong dependence on doping (left panel, Fig. 52), which explains the large doping dependence of the sum rule violation. The same calculations find that the actual kinetic energy change is about twice that indicated by the optical integral, the difference due to the fact that the inverse mass tensor is not simply the negative of  $\epsilon_k$  as in a near neighbor tight binding model of the energy dispersion. In summary, the origin of the sum rule “violation” and kinetic energy lowering can be traced to the formation of quasiparticle peaks in the superconducting state due to the opening of a scattering rate gap.

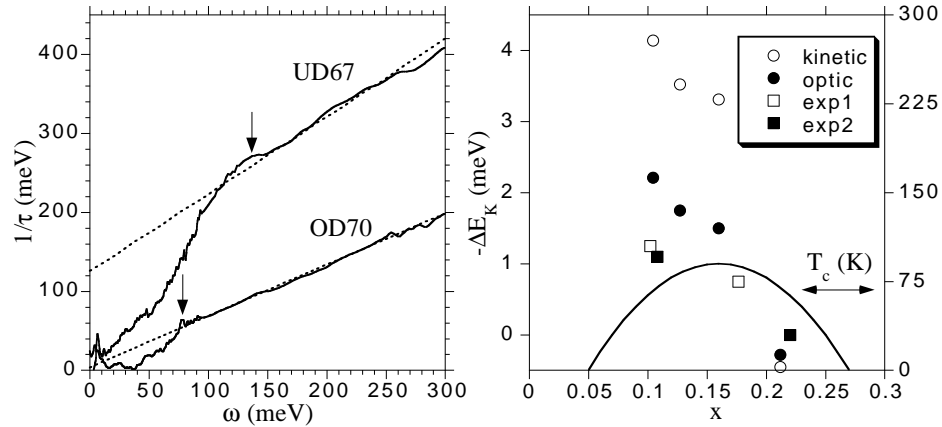


**Figure 52.** Left:  $1/\tau$  vs  $\omega$  in the superconducting state as extracted from optics for an overdoped (OD70) and an underdoped (UD67) sample of Bi2212 [48]. Dotted lines are  $a + b\omega$  fits to normal state data, arrows the locations of the scattering rate gaps. Note the near zero value of  $a$  in the OD case, as contrasted to the large value in the UD case. Right: Calculated change in the kinetic energy (open circles) and optical integral (full circles) versus hole doping,  $x$ , with parameters determined from optics (left panel) and ARPES. The open squares are the data of Ref. [246] and the full squares that of Ref. [247]. Adapted from Ref. [239].

## 6.2. ARPES

These results can be generalized by considering the entire free energy. If only two particle interactions are involved, it is easily shown that the full condensation energy can be written as [248]

$$E_{cond} = \sum_k \int_{-\infty}^{\infty} d\omega (\omega + \epsilon_k) f(\omega) [A_N(k, \omega) - A_S(k, \omega)] \quad (11)$$

where  $A_N$  is the normal state single particle spectral function, and  $A_S$  that of the superconducting state. This expression is the sum of two terms, a kinetic energy term (where  $\omega + \epsilon_k$  is replaced by  $2\epsilon_k$ ) and a potential energy term (where  $\omega + \epsilon_k$  is replaced by  $\omega - \epsilon_k$ ).

This expression can be reduced further by performing some of the integrals and sums

$$E_{cond} = \sum_k \epsilon_k [n_N(k) - n_S(k)] + \int_{-\infty}^{\infty} d\omega \omega f(\omega) [N_N(\omega) - N_S(\omega)] \quad (12)$$

where  $n(k)$  is the momentum distribution function and  $N(\omega)$  the density of states. The first term is related to (but not the same as) the optical integral we just discussed, the second term could be obtained from tunneling spectroscopy. Both terms, though, can in principle be obtained from angle resolved photoemission, since only the occupied states enter. In practice, resolution, normalization, and matrix element effects will be a limiting factor [248].

The above expressions, though, represent a simple conceptual formalism for tackling the condensation energy issue which avoids the problem of considering complicated two

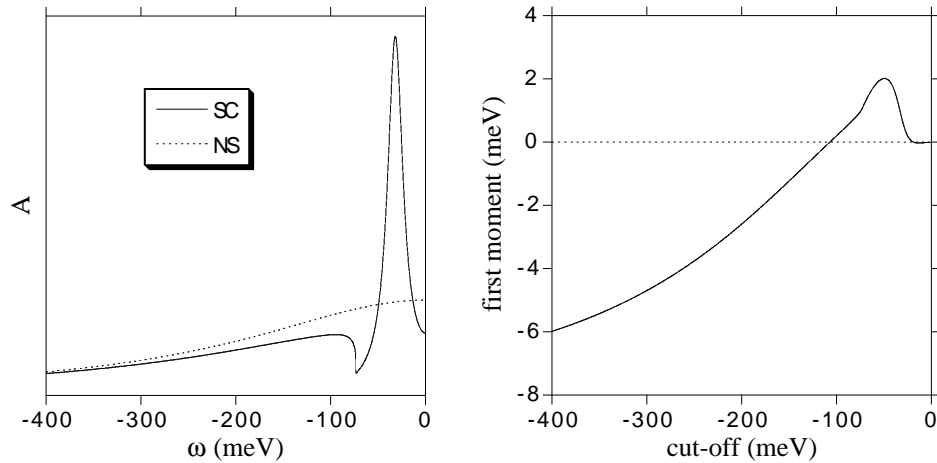


**Figure 53.** Left panel: calculated spectral function in the normal state (NS) and superconducting state (SC). Right panel: resulting difference in first moments of the spectrum versus cut-off energy. Note positive contribution (potential energy decrease in the SC state) from spectral peak, negative contribution (potential energy increase in the SC state) from the difference in the spectral tails. From Ref. [248].

particle correlation functions. This was illustrated by Norman *et al* [248], who evaluated these expressions using the “mode” model of Norman and Ding (Fig. 29) [131] for fitting ARPES spectra (the same model was employed by Ioffe and Millis [244] to analyze the c-axis optical sum rule violation, and Norman and Pépin [239] to analyze the in-plane one). What these authors found was that for small normal state scattering rates, a result similar to BCS theory occurs, which presumably applies on the overdoped side of the phase diagram. For scattering rates much larger than the superconducting energy gap, though, a result opposite to BCS theory was found, in that the kinetic energy was lowered and the potential energy raised in the superconducting state.

The kinetic energy result is rather straightforward to understand (Fig. 49). There is the BCS effect of particle-hole mixing which raises the kinetic energy. Opposed to this is the formation of coherent quasiparticle states from the incoherent normal state, which acts to lower the kinetic energy. For a small scattering rate, the particle-hole mixing effect wins out, and the kinetic energy is raised, but for larger scattering rate, the quasiparticle formation effect wins out, and the kinetic energy is lowered.

The potential energy part is also straightforward to understand (Fig. 53). There is a competition between the formation of a spectral gap (which lowers the potential energy as in BCS theory) and spectral weight transfer from high to low energy to form the coherent peak (which raises the potential energy). For small scattering rate, the spectral gap effect wins out and the potential energy is lowered, whereas for large scattering rate, the weight transfer effect wins out and the potential energy is raised.

What this implies for the phase diagram is that on the overdoped side, one expects more or less BCS like physics. But on the underdoped side, one expects dramatic departures. In particular, the potential energy is lowered across the pseudogap  $T^*$

line due to the formation of a spectral gap, then the kinetic energy lowered across the superconducting  $T_c$  line due to the onset of coherence.

We would like to end with a “cautionary” remark. What one calls kinetic or potential energy depends on what effective Hamiltonian is being employed. The definition of this changes, for instance, if one goes from the three band Hubbard model, to the single band Hubbard model, to the t-J model. The purpose of going through the above exercise is to demonstrate that one’s preconceptions based on BCS theory could well be wrong in pairing models driven by electron-electron interactions, particularly if the normal state reference is non Fermi liquid like.

On that note, we would like to bring this review to a close.

## Acknowledgments

This work was supported by the U.S. Dept. of Energy, Office of Science, under contract W-31-109-ENG-38. This review is based on a series of lectures given at the SPhT in the fall of 2001 by MRN. We would like to thank the staff of the SPhT, in particular Dr. J. P. Blaizot and Dr. G. Misguich, for making these lectures possible.

## References

- [1] Dahl P F 1992 *Superconductivity* (New York: American Institute of Physics)
- [2] Matthias B T 1970 *Comments on Solid State Physics* **3** 93; 1969 *Superconductivity* ed F Chilton (Amsterdam: North-Holland) p 69; 1973 *The Science and Technology of Superconductivity* ed W D Gregory, W N Mathews Jr and E A Edelsack (New York: Plenum Press) p 263
- [3] Cohen M and Anderson P W 1972 *Superconductivity in d- and f-Band Metals* ed D H Douglass (New York: American Institute of Physics) p 17
- [4] Testardi L R 1975 *Rev. Mod. Phys.* **47** 637
- [5] Steglich F, Aarts J, Bredl C D, Lieke W, Meschede D, Franz W and Schafer H 1979 *Phys. Rev. Lett.* **43** 1892
- [6] Stewart G R 1984 *Rev. Mod. Phys.* **56** 755
- [7] Millis A J and Lee P A 1987 *Phys. Rev. B* **35** 3394
- [8] Sigrist M and Ueda K 1991 *Rev. Mod. Phys.* **63** 239
- [9] Joynt R and Taillefer L 2002 *Rev. Mod. Phys.* **74** 235
- [10] Emery V J and Sessler A M 1960 *Phys. Rev.* **119** 43
- [11] Layzer A and Fay D 1971 *Intl. J. Magnetism* **1** 135
- [12] Vollhardt D and Wolfe P 1990 *The Superfluid Phases of Helium 3* (London: Taylor and Francis)
- [13] Anderson P W and Brinkman W F 1973 *Phys. Rev. Lett.* **30** 1108
- [14] Abanov Ar, Chubukov A V and Schmalian J 2001 *J. Elec. Spec.* **117** 129  
Chubukov A V, Pines D and Schmalian J 2002 *Preprint* cond-mat/0201140  
Abanov Ar, Chubukov A V and Schmalian J 2003 *Adv. Phys.* **52** 119
- [15] Aeppli G, Goldman A, Shirane G, Bucher E and Lux-Steiner M-Ch 1987 *Phys. Rev. Lett.* **58** 808
- [16] Saxena S S, Agarwal P, Ahilan K, Grosche F M, Haselwimmer R K W, Steiner M J, Pugh E, Walker I R, Julian S R, Mouthoux P, Lonzarich G G, Huxley A, Sheikin I, Braithwaite D and Flouquet J 2000 *Nature* **406** 587
- [17] Pfeleiderer C, Uhlarz M, Hayden S M, Vollmer R, von Lohneysen H, Bernhoeft N R and Lonzarich G G 2001 *Nature* **412** 58
- [18] Miyake K, Schmitt-Rink S and Varma C M 1986 *Phys. Rev. B* **34** 6554

- Scalapino D J, Loh E Jr and Hirsch J E 1986 *Phys. Rev. B* **34** 8190
- [19] Norman M R 1992 *Physica C* **194** 203
- [20] Sauls J A 1994 *Adv. Phys.* **43** 113
- [21] Bednorz J G and Muller K A 1988 *Rev. Mod. Phys.* **60** 585
- [22] Eagles D M 1969 *Phys. Rev.* **186** 456
- [23] Wu M K, Ashburn J R, Torng C J, Hor P H, Meng R L, Goa L, Huang Z J, Wang Y Q and Chu C W 1987 *Phys. Rev. Lett.* **58** 908
- [24] Feder T 2000 *Physics Today* **53** No 4 p 56
- [25] Hazen R M 1988 *The Breakthrough* (New York: Summit Books)
- [26] Anderson P W 1987 *Science* **235** 1196
- [27] Sawatzky G A and Allen J W 1984 *Phys. Rev. Lett.* **53** 2339
- [28] Pickett W E 1989 *Rev. Mod. Phys.* **61** 433
- [29] Anderson P W 1997 *The Theory of Superconductivity in the High- $T_c$  Cuprates* (Princeton: Princeton Univ. Pr.)
- [30] Hybertsen M S, Stechel E B, Schluter M and Jennison D R 1990 *Phys. Rev. B* **41** 11068
- [31] Varma C M 1997 *Phys. Rev. B* **55** 14554
- [32] Slater J C 1951 *Phys. Rev.* **82** 538
- [33] Vaknin D, Sinha S K, Moncton D E, Johnston D C, Newsam J M, Safinya C R and King H E Jr 1987 *Phys. Rev. Lett.* **58** 2802
- [34] Kleiner R and Muller P 1994 *Phys. Rev. B* **49** 1327
- [35] Corson J, Mallozzi R, Orenstein J, Eckstein J N and Bozovic I 1999 *Nature* **398** 221
- [36] Takigawa M, Hammel P C, Heffner R H and Fisk Z 1989 *Phys. Rev. B* **39** 7371
- [37] Bickers N E, Scalapino D J and Scalettar R T 1987 *Intl. J. Modern Physics B* **1** 687
- [38] Kotliar G 1988 *Phys. Rev. B* **37** 3664  
Kotliar G and Liu J 1988 *Phys. Rev. B* **38** 5142
- [39] Zhang F C, Gros C, Rice T M and Shiba H 1988 *Supercond. Sci. Technol.* **1** 36
- [40] Martindale J A, Barrett S E, O'Hara K E, Slichter C P, Lee W C and Ginsberg D M 1993 *Phys. Rev. B* **47** 9155
- [41] Hardy W N, Bonn D A, Morgan D C, Liang R and Zhang K 1993 *Phys. Rev. Lett.* **70** 3999
- [42] Shen Z-X, Dessau D S, Wells B O, King D M, Spicer W E, Arko A J, Marshall D, Lombardo L W, Kapitulnik A, Dickinson P, Doniach S, DiCarlo J, Loeser A G and Park C H 1993 *Phys. Rev. Lett.* **70** 1553
- [43] Wollman D A, van Harlingen D J, Lee W C, Ginsberg D M and Leggett A J 1993 *Phys. Rev. Lett.* **71** 2134
- [44] Tsuei C C, Kirtley J R, Chi C C, Yu-Jahnes L S, Gupta A, Shaw T, Sun J Z and Ketchen M B 1994 *Phys. Rev. Lett.* **73** 593
- [45] Tsuei C C, Kirtley J R, Rupp M, Sun J Z, Gupta A, Ketchen M B, Wang C A, Ren Z F, Wang J H and Bhushan M 1996 *Science* **271** 329
- [46] Bonn D A, Dosanjh P, Liang R and Hardy W N 1992 *Phys. Rev. Lett.* **68** 2390
- [47] Krishana K, Harris J M and Ong N P 1995 *Phys. Rev. Lett.* **75** 3529
- [48] Puchkov A V, Basov D N and Timusk T 1996 *J. Phys.: Condens. Matter* **8** 10049
- [49] Kaminski A, Mesot J, Fretwell H, Campuzano J C, Norman M R, Randeria M, Ding H, Sato T, Takahashi T, Mochiku T, Kadowaki K and Hoechst H 2000 *Phys. Rev. Lett.* **84** 1788
- [50] Nozieres P 1964 *Theory of Interacting Fermi Systems* (Reading: Addison-Wesley)
- [51] Anderson P W, Baskaran G, Zou Z and Hsu T 1987 *Phys. Rev. Lett.* **58** 2790
- [52] Baskaran G, Zou Z and Anderson P W 1987 *Solid State Commun.* **63** 973
- [53] Nagaosa N and Lee P A 1992 *Phys. Rev. B* **45** 966
- [54] Martin S, Fiory A T, Fleming R M, Schneemeyer L F and Waszczak J V 1990 *Phys. Rev. B* **41** 846
- [55] Varma C M, Littlewood P B, Schmitt-Rink S, Abrahams E and Ruckentstein A E 1989 *Phys. Rev. Lett.* **63** 1996

- [56] Timusk T and Statt B 1999 *Rep. Prog. Phys.* **62** 61
- [57] Randeria M 1999 *Proceedings of the International School of Physics "Enrico Fermi" Course CXXXVI on High Temperature Superconductors* ed G Iadonisi, J R Schrieffer and M L Chialfalo (Amsterdam: IOS Press) p 53 (cond-mat/9710223)
- [58] Warren W W Jr, Walstedt R E, Brennert G F, Cava R J, Tycko R, Bell R and Dabbagh G 1989 *Phys. Rev. Lett.* **62** 1193
- [59] Alloul H, Ohno T and Mendels P 1989 *Phys. Rev. Lett.* **63** 1700
- [60] Cooper S L, Thomas G A, Orenstein J, Rapkine D H, Capizzi M, Timusk T, Millis A J, Schneemeyer L F and Waszczak J V 1989 *Phys. Rev. B* **40** 11358
- [61] Rotter L D, Schlesinger Z, Collins R T, Holtzberg F, Field C, Welp U W, Crabtree G W, Liu J Z, Fang Y, Vandervoort K G and Fleshler S 1991 *Phys. Rev. Lett.* **67** 2741
- [62] Takigawa M, Reyes A P, Hammel P C, Thompson J D, Heffner R H, Fisk Z and Ott K C 1989 *Phys. Rev. B* **43** 247
- [63] Bucher B, Steiner P, Karpinski J, Kaldis E and Wachter P 1993 *Phys. Rev. Lett.* **70** 2012  
Ito T, Takenaka K and Uchida S 1993 *Phys. Rev. Lett.* **70** 3995
- [64] Ishida K, Yoshida K, Mito T, Tokunaga Y, Kitaoka Y, Asayama K, Nakayama Y, Shimoyama J and Kishio K 1998 *Phys. Rev. B* **58** 5960
- [65] Homes C C, Timusk T, Liang R, Bonn D A and Hardy W N 1993 *Phys. Rev. Lett.* **71** 1645; 1995 *Physica C* **254** 265
- [66] Takenaka K, Mizuhashi K, Takagi H and Uchida S 1994 *Phys. Rev. B* **50** 6534
- [67] Marshall D S, Dessau D S, Loeser A G, Park C H, Matsuura A V, Eckstein J N, Bozovic I, Fournier P, Kapitulnik A, Spicer W E and Shen Z-X 1996 *Phys. Rev. Lett.* **76** 4841
- [68] Loeser A G, Shen Z-X, Dessau D S, Marshall D S, Park C H, Fournier P and Kapitulnik A 1996 *Science* **273** 325
- [69] Ding H, Yokoya T, Campuzano J C, Takahashi T, Randeria M, Norman M R, Mochiku T, Kadowaki K and Giapintzakis J 1996 *Nature* **382** 51
- [70] Randeria M, Trivedi N, Moreo A and Scalettar R T 1992 *Phys. Rev. Lett.* **69** 2001
- [71] Ding H, Norman M R, Yokoya T, Takuechi T, Randeria M, Campuzano J C, Takahashi T, Mochiku T and Kadowaki K 1997 *Phys. Rev. Lett.* **78** 2628
- [72] Renner Ch, Revaz B, Genoud J-Y, Kadowaki K and Fischer O 1998 *Phys. Rev. Lett.* **80** 149
- [73] Norman M R, Ding H, Randeria M, Campuzano J C, Yokoya T, Takeuchi T, Takahashi T, Mochiku T, Kadowaki K, Guptasarma P and Hinks D G 1998 *Nature* **392** 157
- [74] Yoshida T, Zhou X J, Sasagawa T, Yang W L, Bogdanov P V, Lanzara A, Hussain Z, Mizokawa T, Fujimori A, Eisaki H, Shen Z-X, Kakeshita T and Uchida S 2002 *Preprint cond-mat/0206469*
- [75] Affleck I and Marston J B 1988 *Phys. Rev. B* **37** 3774
- [76] Schulz H J 1989 *Phys. Rev. B* **39** 2940
- [77] Chakravarty S, Laughlin R B, Morr D K and Nayak C 2001 *Phys. Rev. B* **63** 094503
- [78] Mook H A, Dai P and Dogan F 2001 *Phys. Rev. B* **64** 012502
- [79] Kaminski A, Rosenkranz S, Fretwell H, Campuzano J C, Li Z, Raffy H, Cullen W G, You H, Olson C G, Varma C M and Hoehst H 2002 *Nature* **416** 610
- [80] Simon M E and Varma C M 2002 *Phys. Rev. Lett.* **89** 247003
- [81] Tallon J L, Loram J W, Williams G V M, Cooper J R, Fisher I R, Johnson J D, Staines M P and Bernhard C 1999 *Phys. Stat. Sol. (b)* **215** 531
- [82] Emery V and Kivelson S 1995 *Nature* **374** 434
- [83] Xu Z A, Ong N P, Wang Y, Kakeshita T and Uchida S 2000 *Nature* **406** 486
- [84] Renner Ch, Revaz B, Kadowaki K, Maggio-Aprile I and Fischer O 1998 *Phys. Rev. Lett.* **80** 3606
- [85] Wells B O, Shen Z-X, Matsuura A, King D M, Kastner M A, Greven M and Birgeneau R J 1995 *Phys. Rev. Lett.* **74** 964
- [86] Kohsaka Y, Sasagawa T, Ronning F, Yoshida T, Kim C, Hanaguri T, Azuma M, Takano M, Shen Z-X, and Takagi H 2002 *Preprint cond-mat/0209339*
- [87] Damascelli A, Shen Z-X and Hussain Z 2002 *Preprint cond-mat/0208504 (Rev. Mod. Phys. Apr.*

- 2003)
- [88] Zaanen J and Gunnarsson O 1989 *Phys. Rev. B* **40** 7391
  - [89] Carlson E W, Emery V J, Kivelson S A and Orgad D 2002 *Preprint cond-mat/0206217*
  - [90] Tranquada J M, Sternlieb B J, Axe J D, Nakamura Y and Uchida S 1995 *Nature* **375** 561
  - [91] Axe J D, Moudden A H, Hohlwein D, Cox D E, Mohanty K M, Moodenbaugh A R and Xu Y 1989 *Phys. Rev. Lett.* **62** 2751
  - [92] Zhou X J, Bogdanov P, Kellar S A, Noda T, Eisaki H, Uchida S, Hussain Z and Shen Z-X 1999 *Science* **286** 268
  - [93] Noda T, Eisaki H and Uchida S 1999 *Science* **286** 265
  - [94] Cheong S-W, Aeppli G, Mason T E, Mook H, Hayden S M, Canfield P C, Fisk Z, Clausen K N and Martinez J L 1991 *Phys. Rev. Lett.* **67** 1791
  - [95] Mook H A, Dai P, Hayden S M, Aeppli G, Perring T G and Dogan F 1998 *Nature* **395** 580
  - [96] Mook H A, Dai P and Dogan F 2002 *Phys. Rev. Lett.* **88** 097004
  - [97] Norman M R 2000 *Phys. Rev. B* **61** 14751
  - [98] Pan S H, O'Neal J P, Badzey R L, Chamon C, Ding H, Engelbrecht J R, Wang Z, Eisaki H, Uchida S, Gupta A K, Ng K-W, Hudson E W, Lang K M and Davis J C 2001 *Nature* **413** 282
  - [99] Lang K M, Madhavan V, Hoffman J E, Hudson E W, Eisaki H, Uchida S and Davis J C 2002 *Nature* **415** 412
  - [100] Cren T, Roditchev D, Sacks W, Klein J, Moussy J-B, Deville-Cavellin C and Lagues M 2000 *Phys. Rev. Lett.* **84** 147
  - [101] Hoffman J E, Hudson E W, Lang K M, Madhavan V, Eisaki H, Uchida S and Davis J C 2002 *Science* **295** 466
  - [102] Hoffman J E, McElroy K, Lee D-H, Lang K M, Eisaki H, Uchida S and Davis J C 2002 *Science* **297** 1148
  - [103] Howald C, Eisaki H, Kaneko N, Greven M and Kapitulnik A 2003 *Phys. Rev. B* **67** 014533 (2003)
  - [104] McElroy K, Simmonds, R W, Hoffman J E, Lee D-H, Orenstein J, Eisaki H, Uchida S and Davis J C 2002 *Preprint (Nature Feb. 2003)*
  - [105] Tokura Y, Takagi H and Uchida S 1989 *Nature* **337** 345
  - [106] Luke G M *et al* 1990 *Phys. Rev. B* **42** 7981
  - [107] Onose Y, Taguchi Y, Ishizaka K and Tokura Y 2001 *Phys. Rev. Lett.* **87** 217001
  - [108] Wu D H, Mao J, Mao S N, Peng J L, Xi X X, Venkatesan T, Greene R L and Anlage S M 1993 *Phys. Rev. Lett.* **70** 85
  - [109] Huang Q, Zasadzinski J F, Tralshawala N, Gray K E, Hinks D G, Peng J L and Greene R L 1990 *Nature* **347** 369
  - [110] Kokales D K, Fournier P, Mercaldo L V, Talanov V V, Greene R L and Anlage S M 2000 *Phys. Rev. Lett.* **85** 3696
  - Prozorov R, Giannetta R W, Fournier P and Greene R L 2000 *Phys. Rev. Lett.* **85** 3700
  - [111] Sato T, Kamiyama T, Takahashi T, Kurahashi K and Yamada K 2001 *Science* **291** 1517
  - [112] Armitage N P, Lu D H, Feng D L, Kim C, Damascelli A, Shen K M, Ronning F, Shen Z-X, Onose Y, Taguchi Y and Tokura Y 2001 *Phys. Rev. Lett.* **86** 1126
  - [113] Tsuei C C and Kirtley J R 2000 *Phys. Rev. Lett.* **85** 182
  - [114] Blumberg G, Koitzsch A, Gozar A, Dennis B S, Kendziora C A, Fournier P and Greene R L 2002 *Phys. Rev. Lett.* **88** 107002
  - [115] Armitage N P, Lu D H, Kim C, Damascelli A, Shen K M, Ronning F, Feng D L, Bogdanov P, Shen Z-X, Onose Y, Taguchi Y, Tokura Y, Mang P K, Kaneko N and Greven M 2001 *Phys. Rev. Lett.* **87** 147003
  - [116] Armitage N P, Ronning F, Lu D H, Kim C, Damascelli A, Shen K M, Feng D L, Eisaki H, Shen Z-X, Mang P K, Kaneko N, Greven M, Onose Y, Taguchi Y and Tokura Y 2002 *Phys. Rev. Lett.* **88** 257001
  - [117] Bardeen J, Cooper L N and Schrieffer J R 1957 *Phys. Rev.* **108** 1175
  - [118] Bardeen J 1963 *8th Intl. Conf. on Low Temp.* ed R O Davies (London: Butterworths) p 3



- Cooper L N 1987 *IEEE Trans. on Magnetics* **MAG-23** 376
- [119] Schrieffer J R 1964 *Theory of Superconductivity* (Reading: Benjamin/Cummings)
- [120] Scalapino D J 1994 *Random Magnetism, High Temperature Superconductivity* ed W P Beyermann, N L Huang-Liu and D E MacLaughlin (Singapore: World Scientific) p 155
- [121] Hertz J A, Levin K and Beal-Monod M T 1976 *Solid State Comm.* **18** 803
- [122] Anderson P W 1997 *Adv. Phys.* **46** 3
- [123] Affleck I, Zou Z, Hsu T and Anderson P W 1988 *Phys. Rev. B* **38** 745
- [124] Paramakanti A, Randeria M and Trivedi N 2001 *Phys. Rev. Lett.* **87** 217002
- [125] Ivanov D A, Lee P A and Wen X-G 2000 *Phys. Rev. Lett.* **84** 3958
- [126] Wen X-G and Lee P A 1996 *Phys. Rev. Lett.* **76** 503  
Lee P A, Nagaosa N, Ng T-K and Wen X-G 1998 *Phys. Rev. B* **57** 6003
- [127] Ioffe L B and Millis A J 1998 *Phys. Rev. B* **58** 11631
- [128] Valla T, Fedorov A V, Johnson P D, Wells B O, Hulbert S L, Li Q, Gu G D and Koshizuka N 1999 *Science* **285** 2110
- [129] Kuroda Y and Varma C M 1990 *Phys. Rev. B* **42** 8619
- [130] Littlewood P B and Varma C M 1992 *Phys. Rev. B* **46** 405
- [131] Norman M R and Ding H 1998 *Phys. Rev. B* **57** 11089
- [132] Rossat-Mignod J, Regnault L P, Vettier C, Bourges P, Burlet P, Bossy J, Henry J Y and Lapertot G 1991 *Physica C* **185-189** 86
- [133] Mook H A, Yethraj M, Aeppli G, Mason T E and Armstrong T 1993 *Phys. Rev. Lett.* **70** 3490
- [134] Bulut N and Scalapino D J 1996 *Phys. Rev. B* **53** 5149
- [135] Demler E and Zhang S-C 1995 *Phys. Rev. Lett.* **75** 4126
- [136] Fong H F, Keimer B, Anderson P W, Reznik D, Dogan F and Aksay I A 1995 *Phys. Rev. Lett.* **75** 316
- [137] Fong H F, Keimer B, Reznik D, Milius D L and Aksay I A 1996 *Phys. Rev. B* **54** 6708
- [138] Greiter M 1997 *Phys. Rev. Lett.* **79** 4898
- [139] Tchernyshyov O, Norman M R and Chubukov A V 2001 *Phys. Rev. B* **63** 144507
- [140] Zhang S-C 1997 *Science* **275** 1089
- [141] Zhang S-C, Hu J-P, Arrigoni E, Hanke W and Auerbach A 1999 *Phys. Rev. B* **60** 13070
- [142] Zachar M G, Hanke W, Arrigoni E and Zhang S-C 2000 *Phys. Rev. Lett.* **85** 824
- [143] Si Q, Zha Y, Levin K and Lu J P 1993 *Phys. Rev. B* **47** 9055
- [144] Fujita M, Yamada K, Hiraka H, Gehring P M, Lee S H, Wakimoto S and Shirane G 2002 *Phys. Rev. B* **65** 064505
- [145] Junod A, Erb A and Renner C 1999 *Physica C* **317** 333
- [146] Bilbro G and McMillan W L 1976 *Phys. Rev. B* **14** 1887
- [147] Laughlin R B 1998 *Adv. Phys.* **47** 943
- [148] Sachdev S 2000 *Science* **288** 475
- [149] Hüfner S 1996 *Photoelectron Spectroscopy* (Berlin: Springer-Verlag)
- [150] Randeria M, Ding H, Campuzano J C, Bellman A, Jennings G, Yokoya T, Takahashi T, Katayama-Yoshida H, Mochiku T and Kadowaki K 1995 *Phys. Rev. Lett.* **74** 4951
- [151] Campuzano J C, Norman M R and Randeria M 2002 *Preprint cond-mat/0209476*
- [152] Chainani A, Yokoya T, Kiss T and Shin S 2000 *Phys. Rev. Lett.* **85** 1966
- [153] Kaminski A, Randeria M, Campuzano J C, Norman M R, Fretwell H, Mesot J, Sato T, Takahashi T and Kadowaki K 2001 *Phys. Rev. Lett.* **86** 1070
- [154] Campuzano J C, Jennings G, Faiz M, Beaulaigue L, Veal B W, Liu J Z, Paulikas A P, Vandervoort K and Claus H 1990 *Phys. Rev. Lett.* **64** 2308
- [155] Campuzano J C, Ding H, Norman M R, Fretwell H M, Randeria M, Kaminski A, Mesot J, Takeuchi T, Sato T, Yokoya T, Takahashi T, Kadowaki K, Guptasarma P, Hinks D G, Konstantinovic Z, Li Z Z and Raffy H 1999 *Phys. Rev. Lett.* **83** 3709
- [156] Feng D L, Lu D H, Shen K M, Kim C, Eisaki H, Damascelli A, Yoshizaki R, Shimoyama J-I, Kishio K, Gu G D, Oh S, Andrus A, O'Donell J, Eckstein J N and Shen Z-X 2000 *Science* **289**

277

- [157] Ding H, Engelbrecht J R, Wang Z, Campuzano J C, Wang S-C, Yang H-B, Rogan R, Takahashi T, Kadowaki K and Hinks D G 2001 *Phys. Rev. Lett.* **87** 227001
- [158] Abrikosov A A, Campuzano J C and Gofron K 1993 *Physica C* **214** 73
- [159] Sato T, Kamiyama T, Takahashi T, Mesot J, Kaminski A, Campuzano J C, Fretwell H M, Takeuchi T, Ding H, Chong I, Terashima T and Takano M 2001 *Phys. Rev. B* **64** 054502
- [160] Ino A, Kim C, Nakamura M, Yoshida T, Mizokawa T, Shen Z-X, Fujimori A, Kakeshita T, Eisaki H and Uchida S 2002 *Phys. Rev. B* **65** 094504 (2002)
- [161] Takagi H, Ido T, Ishibashi S, Uota M, Uchida S and Tokura Y 1989 *Phys. Rev. B* **40** 2254
- [162] Olson C G, Liu R, Lynch D W, List R S, Arko A J, Veal B W, Chang Y C, Jiang P Z and Paulikas A P 1990 *Phys. Rev. B* **42** 381
- [163] Bogdanov P V, Lanzara A, Zhou X J, Yang W L, Eisaki H, Hussain Z and Shen Z-X 2002 *Phys. Rev. Lett.* **89** 167002
- [164] Chakravarty S, Sudbo A, Anderson P W and Strong S 1994 *Science* **261** 337
- [165] Ding H, Bellman A F, Campuzano J C, Randeria M, Norman M R, Yokoya T, Takahashi T, Katayama-Yoshida H, Mochiku T, Kadowaki K, Jennings G and Brivio G P 1996 *Phys. Rev. Lett.* **76** 1533
- [166] Feng D L, Armitage N P, Lu D H, Damascelli A, Hu J P, Bogdanov P, Lanzara A, Ronning F, Shen K M, Eisaki H, Kim C and Shen Z-X 2001 *Phys. Rev. Lett.* **86** 5550
- [167] Kaminski A, Rosenkranz S, Fretwell H M, Li Z, Raffy H, Randeria M, Norman M R and Campuzano J C 2002 *Preprint cond-mat/0210531*
- [168] Imer J-M, Patthey F, Dardel B, Schneider W-D, Baer Y, Petroff Y and Zettl A 1989 *Phys. Rev. Lett.* **62** 336
- [169] Ding H, Norman M R, Campuzano J C, Randeria M, Bellman A, Yokoya T, Takahashi T, Mochiku T and Kadowaki K 1996 *Phys. Rev. B* **54** R9678
- [170] Mesot J, Norman M R, Ding H, Randeria M, Campuzano J C, Paramakanti A, Fretwell H M, Kaminski A, Takeuchi T, Yokoya T, Sato T, Takahashi T, Mochiku T and Kadowaki K 1999 *Phys. Rev. Lett.* **83** 840
- [171] Chiao M, Lambert P, Hill R W, Lupien C, Gagnon R, Taillefer L and Fournier P 2000 *Phys. Rev. B* **62** 3554
- [172] Sutherland M, Hawthorn D G, Hill R W, Ronning F, Wakimoto S, Zhang H, Proust C, Boaknin E, Lupien C, Taillefer L, Liang R, Bonn D A, Hardy W N, Gagnon R, Hussey N E, Kimura T, Nohara M and Takagi H 2003 *Preprint cond-mat/0301105*
- [173] Harris J M, Shen Z-X, White P J, Marshall D S, Schabel M C, Eckstein J N and Bozovic I 1996 *Phys. Rev. B* **54** R15665
- [174] Zasadzinski J F, Ozyuzer L, Miyakawa N, Gray K E, Hinks D G and Kendziora C 2001 *Phys. Rev. Lett.* **87** 067005
- [175] Norman M R, Kaminski A, Mesot J and Campuzano J C 2001 *Phys. Rev. B* **63** 140508 (R)
- [176] Federov A V, Valla T, Johnson P D, Li Q, Gu G D and Koshizuka N 1999 *Phys. Rev. Lett.* **82** 2179
- [177] Huang Q, Zasadzinski J F, Gray K E, Liu J Z and Claus H 1989 *Phys. Rev. B* **40** 9366
- [178] Arnold G B, Mueller F M and Swihart J C 1991 *Phys. Rev. Lett.* **67** 2569
- [179] McMillan W L and Rowell J M 1965 *Phys. Rev. Lett.* **14** 108
- [180] Norman M R, Ding H, Campuzano J C, Takeuchi T, Randeria M, Yokoya T, Takahashi T, Mochiku T and Kadowaki K 1997 *Phys. Rev. Lett.* **79** 3506
- [181] Abanov Ar and Chubukov A V 1999 *Phys. Rev. Lett.* **83** 1652
- [182] Shen Z-X and Schrieffer J R 1997 *Phys. Rev. Lett.* **78** 1771
- [183] Fong H F, Bourges P, Sidis Y, Regnault L P, Ivanov A, Gu G D, Koshizuka N and Keimer B 1999 *Nature* **398** 588
- [184] Carbotte J P, Schachinger E and Basov D N 1999 *Nature* **401** 354
- [185] Bogdanov P V, Lanzara A, Kellar S A, Zhou X J, Lu E D, Zheng W J, Gu G, Shimoyama J-I,

- Kishio K, Ikeda H, Yoshizaki R, Hussain Z and Shen Z-X 2000 *Phys. Rev. Lett.* **85** 2581
- [186] Eschrig M and Norman M R 2000 *Phys. Rev. Lett.* **85** 3261; 2002 *Preprint cond-mat/0202083*; 2002 *Phys. Rev. Lett.* **89** 277005
- [187] Johnson P D, Valla T, Fedorov A V, Yusof Z, Wells B O, Li Q, Moodenbaugh A R, Gu G D, Koshizuka N, Kendziora C, Jian S and Hinks D G 2001 *Phys. Rev. Lett.* **87** 177007
- [188] Lanzara A, Bogdanov P V, Zhou X J, Kellar S A, Feng D L, Lu E D, Yoshida T, Eisaki H, Fujimori A, Kishio K, Shimoyama J-I, Noda T, Uchida S, Hussain Z and Shen Z-X 2001 *Nature* **412** 510
- [189] Norman M R, Randeria M, Ding H and Campuzano J C 1998 *Phys. Rev. B* **57** R11093
- [190] Engelbrecht J R, Nazarenko A, Randeria M and Dagotto E 1998 *Phys. Rev. B* **57** 13406
- [191] Preosti G, Vilk Y M and Norman M R 1999 *Phys. Rev. B* **59** 1474
- [192] Furukawa N, Rice T M and Salmhofer M 1998 *Phys. Rev. Lett.* **81** 3195
- [193] Putikka W O, Luchini M U and Singh R R P 1998 *Phys. Rev. Lett.* **81** 2966
- [194] Aebi P, Osterwalder J, Schwaller P, Schlapbach L, Shimoda M, Mochiku T and Kadowaki K 1994 *Phys. Rev. Lett.* **72** 2757
- [195] Kordyuk A A, Borisenko S V, Golden M S, Legner S, Nenkov K A, Knupfer M, Fink J, Berger H, Forro L and Follath R 2002 *Phys. Rev. B* **66** 014502
- [196] Laughlin R B 1997 *Phys. Rev. Lett.* **79** 1726
- [197] Tranquada J M, Moudden A H, Goldman A I, Zolliker P, Cox D E, Shirane G, Sinha S K, Vaknin D, Johnston D C, Alvarez M S, Jacobson A J, Lewandowski J T and Newsam J M 1988 *Phys. Rev. B* **38** 2477
- [198] Reznik D, Bourges P, Fong H F, Regnault L P, Bossy J, Vettier C, Milius D L, Aksay I A and Keimer B 1996 *Phys. Rev. B* **53** 14741
- [199] Fong H F, Bourges P, Sidis Y, Regnault L P, Bossy J, Ivanov A, Milius D L, Aksay I A and Keimer B 2000 *Phys. Rev. B* **61** 14773
- [200] Mook H A, Dai P, Dogan F and Hunt R D 2000 *Nature* **404** 729
- [201] Lake B, Aeppli G, Mason T E, Schroder A, McMorro D F, Lefmann K, Isshiki M, Nohara M, Takagi H and Hayden S M 1999 *Nature* **400** 43
- [202] Lake B, Aeppli G, Clausen K N, McMorro D F, Lefmann K, Hussey N E, Mangkorntong N, Nohara M, Takagi H, Mason T E and Schroder A 2001 *Science* **291** 1759
- [203] Lake B, Ronnow H M, Christensen N B, Aeppli G, Lefmann K, McMorro D F, Vorderwisch P, Smeibidl P, Mangkorntong N, Sasagawa T, Nohara M, Takagi H and Mason T E 2002 *Nature* **415** 299
- [204] Arovas D P, Berlinsky A J, Kallin C and Zhang S-C 1997 *Phys. Rev. Lett.* **79** 2871
- [205] Demler E, Sachdev S and Zhang Y 2001 *Phys. Rev. Lett.* **87** 067202
- [206] He H, Bourges P, Sidis Y, Ulrich C, Regnault L P, Pailhes S, Berzigiarova N S, Kolesnikov N N and Keimer B 2002 *Science* **295** 1045
- [207] Scalapino D J and White S R 1998 *Phys. Rev. B* **58** 8222
- [208] Demler E and Zhang S-C 1998 *Nature* **396** 733
- [209] Dai P, Mook H A, Hayden S M, Aeppli G, Perring T G, Hunt R D and Dogan F 1999 *Nature* **284** 1344
- [210] Dai P, Mook H A, Aeppli G, Hayden S M and Dogan F 2000 *Nature* **406** 965
- [211] Bourges P, Casalta H, Regnault L P, Bossy J, Burlet P, Vettier C, Beaunon E, Gautier-Picard P and Tournier R 1997 *Physica B* **234-236** 830
- [212] Eschrig M, Norman M R and Janko B 2001 *Phys. Rev. B* **64** 134509
- [213] Dai P, Mook H A, Hunt R D and Dogan F 2001 *Phys. Rev. B* **63** 054525
- [214] Kee H-Y, Kivelson S A and Aeppli G 2002 *Phys. Rev. Lett.* **88** 257002
- [215] Abanov Ar, Chubukov A V, Eschrig M, Norman M R and Schmalian J 2002 *Phys. Rev. Lett.* **89** 177002
- [216] Arai M, Nishijima T, Endoh Y, Egami T, Tajima S, Tomimoto K, Shiohara Y, Takahashi M, Garrett A and Bennington S M 1999 *Phys. Rev. Lett.* **83** 608
- [217] Onufrieva F and Pfeuty P 1999 *Preprint cond-mat/9903097*; 2002 *Phys. Rev. B* **65** 054515

- [218] Kao Y-J, Si Q and Levin K 2000 *Phys. Rev. B* **61** R11898
- [219] Norman M R 2001 *Phys. Rev. B* **63** 092509
- [220] Bourges P, Sidis Y, Fong H F, Regnault L P, Bossy J, Ivanov A and Keimer B 2000 *Science* **288** 1234
- [221] Brinkmann J and Lee P A 1999 *Phys. Rev. Lett.* **82** 2915; 2002 *Phys. Rev. B* **65** 014502
- [222] Batista C D, Ortiz G and Balatsky A V 2001 *Phys. Rev. B* **64** 172508
- [223] Hiraka H, Endoh Y, Fujita M, Lee Y S, Kulda J, Ivanov A and Birgenau R J 2001 *J. Phys. Soc. Japan* **70** 853
- [224] Schlessinger Z, Collins R T, Holtzberg F, Feild C, Koren G and Gupta A 1990 *Phys. Rev. B* **41** 11237
- [225] Abrahams E and Varma C M 2000 *Proc. Natl. Acad. Sci.* **97** 5714
- [226] Orenstein J, Thomas G A, Millis A J, Cooper S L, Rapkine D H, Timusk T, Schneemeyer L F and Waszczak J V 1990 *Phys. Rev. B* **42** 6342
- [227] Duffy D, Hirschfeld P J and Scalapino D J 2001 *Phys. Rev. B* **64** 224522
- [228] Corson J, Orenstein J and Eckstein J N 2000 *Phys. Rev. Lett.* **85** 2569
- [229] Munzar D, Bernhard C and Cardona M 1999 *Physica C* **312** 121
- [230] Abanov Ar, Chubukov A V and Schmalian J 2001 *Phys. Rev. B* **63** 180510
- [231] Gruninger M, van der Marel D, Tsvetkov A A and Erb A 2000 *Phys. Rev. Lett.* **84** 1575
- [232] Timusk T and Homes C C 2002 *Preprint cond-mat/0209371*
- [233] Chester G V 1956 *Phys. Rev.* **103** 1693
- [234] Tinkham M 1975 *Introduction to Superconductivity* (New York: McGraw Hill)
- [235] Anderson P W 1990 *Phys. Rev. B* **42** 2624
- [236] Hirsch J E 1992 *Physica C* **201** 347  
Hirsch J E and Marsiglio F 2000 *Physica C* **331** 150; 2000 *Phys. Rev. B* **62** 15131  
Hirsch J E 2002 *Science* **295** 2226
- [237] Klein M V and Blumberg G 1999 *Science* **283** 42
- [238] Kubo R 1957 *J. Phys. Soc. Japan* **12** 570
- [239] Norman M R and Pépin C 2002 *Phys. Rev. B* **66** 100506 (R)
- [240] Fugol I, Samovarov V, Ratner A, Zhuravlev V, Saemann-Ischenko G, Holzapfel B and Meyer O 1993 *Solid State Commun.* **86** 385
- [241] Holcomb M J, Collman J P and Little W A 1994 *Phys. Rev. Lett.* **73** 2360
- [242] Rubhausen M, Gozar A, Klein M V, Guptasarma P and Hinks D G 2001 *Phys. Rev. B* **63** 224514
- [243] Basov D N, Woods S I, Katz A S, Singley E J, Dynes R C, Xu M, Hinks D G, Homes C C and Strongin M 1999 *Science* **283** 49
- [244] Ioffe L B and Millis A J 1999 *Science* **285** 1241; 2000 *Phys. Rev. B* **61** 9077
- [245] Loram J W, Mirza K A and Freeman P F 1990 *Physica C* **171** 243
- [246] Molegraaf H J A, Presura C, van der Marel D, Kes P H and Li M 2002 *Science* **295** 2239  
van der Marel D 2003 *Preprint cond-mat/0301506*
- [247] Santander-Syro A F, Lobo R P S M, Bontemps N, Konstantinovic Z, Li Z Z and Raffy H 2001 *Preprint cond-mat/0111539*
- [248] Norman M R, Randeria M, Janko B and Campuzano J C 2000 *Phys. Rev. B* **61** 14742